EFFICIENT COMPUTATIONAL MODELS AND METHODS FOR INVESTIGATING LOCAL POLYMER DYNAMICS

by

CANAN BAYSAL

B.S. in Ch.E., Boğaziçi University, 1991

Submitted to the Institute for Graduate Studies in
Science and Engineering in partial fulfillment of
the requirements for the degree of
Doctor
of
Philosophy

Boğaziçi University

1996

EFFICIENT COMPUTATIONAL MODELS AND METHODS FOR INVESTIGATING LOCAL POLYMER DYNAMICS

APPROVED BY:

Prof. Dr. İvet Bahar .....
(Thesis Supervisor)

Prof. Dr. Burak Erman .....
(Thesis Supervisor)

Prof. Dr. Zeynep İlsen Önsan .....

Prof. Dr. Önder Pekcan .....

Prof. Dr. Ersin Yurtsever .....

DATE OF APPROVAL: 4/1/1996

ACKNOWLEDGMENTS

I thank Prof. İvet Bahar and Prof. Burak Erman for generously offering so much of their knowledge and for creating the environment which makes one realize her limits.

Very special thanks to Ali Rana Atılgan: His great affection for science and the many stimulating discussions we had together made me see things from a different perspective. It is great pleasure to work with him.

Prof. Zeynep İlsen Önsan made her patience and guidance available at all times. I feel that it is the delight of the ChE students to have such a considerate Chairman.

I would like to express my gratitude to Prof. Önder Pekcan and Prof. Ersin Yurtsever who devoted their valuable time to reading and commenting on the thesis.

Surely I am much indebted to all my friends at ChE and PRC who were always there to share the good days and the bad ones. Please excuse me for mentioning only some of you: Mine Kaplan, Zeynep Saraç, and Toprak Serhatkulu made the hard (and cold) working days more than enjoyable. Özlem Keskin, Erhan Aksoylu, and Seza Orçun, gave lots of moral support during the writing of this thesis.

Thank you Mom and Dad: You always let me do things my way. I know that you are proud of me and I wish to be half as good a parent...

I hope I knew a better way to thank my husband Nihat. He gave so much of himself during the past years, I *know* there would be no thesis without him. I do not dedicate this thesis to him because it is *his* as much as it is mine.

ABSTRACT

Local phenomena related to the isomerization of torsional angles in polymers are studied using computational tools with emphasis on the problem of efficiency. Brownian and molecular dynamics (BD and MD) methods reproduce the time evolved coordinates of the particles in the system. An efficient algorithm to incorporate the effect of side-groups into these dynamic simulation methods is proposed. BD is demonstrated to give results that are in agreement with experimental findings. Other methods which are suitable for the solution of more specific problems are also used: Dynamic Rotational Isomeric States (DRIS) method is utilized to probe local dynamics of chain molecules in solution. Cooperative Kinematics (CK), on the other hand, is a computationally inexpensive method for observing dynamic behavior in the bulk state. The results from DRIS and CK are shown to compare well with those from BD and MD, respectively. These are also in agreement with experimental findings.

MD, BD, DRIS, and CK are used to study various aspects of local dynamics. The results provide a clear picture of local phenomena: Disturbances along the chain are accommodated by local motion confined to a segment of ten bonds approximately. Mainly, large and small amplitude torsions in neighboring bonds, spatial reorientation of bonds, and translational motion of chain atoms occur. The exact mechanism of relaxation behavior is dictated by the geometry of the backbone bonds. The state of the environment, on the other hand, alters the amplitudes of motion only. All of the mentioned mechanisms are composed of the combined effect of rotameric jumps and librational motions. Coupling between the two is particularly enhanced during the passage over the rotation barrier. It is now known that librational motions which are generally assumed to be decoupled from the slow relaxation processes in polymer chains in many studies in literature are not random. On the contrary, they are highly directed so that local chain direction is preserved and the reorientations induced by isomeric jumps are accommodated without significant distortion of chain conformation on a large scale.

ÖZET

Polimerlerin dönme açılarının izomerleşmesine bağlı yerel olaylar hesaplama yöntemlerinde verimliliğe önem verilerek araştırılmıştır. Brownian ve moleküler dinamik (BD ve MD) yöntemleri sistemdeki parçacıkların bir zaman dilimi boyunca koordinatlarını verir. Yan grupların etkisini bu dinamik simülasyon yöntemlerine verimli şekilde uyarlayan bir algoritma geliştirilmiştir. BD'nin deneysel yöntemlerde elde edilen sonuçlara uygun olduğu gösterilmiştir. Daha belirgin problemleri çözmek amacıyla ortaya atılmış hesap yöntemleri de kullanılmıştır: Dinamik dönme izomerleri (DRIS) modeli çözünmüş haldeki zincirlerin yerel dinamiğini incelemek için kullanılmaktadır. Kooperatif kinematik (CK) ise polimerlerin yoğun ortamdaki dinamik davranışını gözlemlemek için kullanılan bir hesaplama yöntemidir. DRIS ve CK sonuçlarının BD ve MD yöntemleri ve deneylerle benzer olduğu gösterilmiştir.

MD, BD, DRIS ve CK yerel dinamiği çeşitli yönleriyle araştırmak üzere kullanılmıştır. Sonuçlar, yerel olayları genel bir bakış açısından açıklamaktadır: Zincir boyunca oluşan büyük ölçekli hareketler, yaklaşık on bağa sıkışmış yerel hareketlere yol açar. Buna bağlı olarak, komşu bağlarda büyük ve küçük ölçekli dönme hareketleri, bağların uzayda yön değiştirmesi, ve atomların uzayda hareketi oluşan başlıca mekanizmalardır. Bu rahatlama mekanizmaları zincirin geometrisince kontrol edilmektedir. Öte yandan zincirin içinde bulunduğu ortam hareketin karakterini değil büyüklüğünü belirlemektedir. Belirtilen tüm mekanizmalar minimumlar arasındaki atlamalar ve titreşimlerin etkileşmesiyle oluşmaktadır. Bunlar arasındaki iletişim özellikle konformasyonlar arasındaki atlama anında öne çıkmaktadır. Literatürdeki birçok çalışmada yavaş rahatlama hareketlerinden bağımsız kabul edilen titreşimlerin aslında raslantısal olmadığı görülmüştür. Aksine, bunlar yerel zincir yönünü sabit kılacak şekilde çalışmaktadır. Böylece izomerleşme anında ortaya çıkan yön değiştirmeler büyük ölçekte zincir konformasyonunu fazlaca bozmadan sabitleştirilmektedir.

TABLE OF CONTENTS

Page

Page

Page

LIST OF FIGURES

Page

Page

LIST OF TABLES

LIST OF SYMBOLS

a	Hydrodynamic radius
$\mathbf{a}_i$	Acceleration of the ith particle
$\mathbf{A}$	Transition rate matrix
A_o	Front factor related to the mobility of the system
$\mathbf{A}_i$	Gaussianly distributed random force
$A^{\pm}$	anticlinal$^+$ and anticlinal$^-$ conformers of dihedral angles
$A(t)$	Trajectory of interest
$\mathbf{B}$	Matrix of eigenvectors of $\mathbf{A}$
c	cis conformer of dihedral angles
C	Carbon
$\mathbf{C}(t)$	Time delayed conditional probability
d_1, d_2, d_3	Distance between couples g_1, g_2, g_3
$\mathbf{e}_1, \mathbf{e}_2, \mathbf{e}_3$	Base vectors of the laboratory fixed coordinate system
$E_k(t)$	Kinetic energy trajectory
E_ω	Energy difference between two distinct torsional states
f	Force exerted at a point
$F(\nu)$	Filter function
$\mathbf{F}_i$	Force exerted on ith particle
g_1, g_2, g_3	Couples resulting from the moment $\mathbf{m}$
$g^{\pm}$	gauche$^+$ and gauche$^-$ conformers of dihedral angles
$\mathbf{G}_i$	Cumulative force exerted on ith particle together with that transmitted from side groups
H	Hydrogen
k_o	Dimensionless ratio relating the frictional resistance to internal rotation barriers
k_B	Boltzmann constant
k_{ij}	Rate constant of passage from jth isomeric state to ith
k_φ	Barrier height for single bond rotation

l_o	Equilibrium bond length
$\mathbf{l}_i$	Bond vector adjoining atoms i and i-1
L	Lagrangian
m	Mass
$\mathbf{m}$	Moment
m_x, m_y, m_z	Components of moment $\mathbf{m}$ along the local frame
$\mathbf{m}(t)$	Unit vector affixed to the bond vector of interest at time t
M_2	Second orientational autocorrelation function
$M[l(\tau)]$	OACF
$M[\varphi(\tau)]$	CACF
n	Number of bonds
$\mathbf{P}$, p	Probability
$\mathbf{q}$	Set of generalized coordinates
$\mathbf{Q}_i$	Operator for passage from the set of position vectors to the set of generalized coordinates
r	Rate constant in **A**
r_{cut}	Cutoff radius for the application of LJ potential
$\mathbf{r}_i$	Position vector of the ith atom relative to a laboratory fixed frame
$\mathbf{R}$	Gas contant
t	trans conformer of dihedral angles
t^*	Total duration of simulation
$\mathbf{T}$	Temperature
$\mathbf{V}$	Total potential
V_l	Bond stretching potential
V_{LJ}	Lennard-Jones potential
V_θ	Bond bending potential
V_φ	Torsional potential
$\mathbf{W}$	Energy spent against the environment
x_i, y_i, z_i	Components of $\mathbf{r}_i$ along the respective base vectors $\mathbf{e}_1$, $\mathbf{e}_2$, $\mathbf{e}_3$.
α	sp^3 - sp^2 bonds in PIP and PBD
β	sp^3 - sp^3 bonds in PIP and PBD
δ	Kronecker delta

$\delta(t-t')$	Dirac delta function
δ_{ij}	Length parameter in LJ potential
$\delta_x, \delta_y, \delta_z$	Unit vectors along the laboratory fixed frame
δR_i	Incremental displacement in chain units
δW_ξ	Differential work done by the chain against friction
Δt	Time step size
ε_{ij}	Energy parameter in LJ potential
η	Solvent viscosity
θ_o	Equilibrium bond angle
θ_i	Bond angle between bonds i and i+1
θ_s	Bond angle between side groups
Λ	Diagonal matrix of eigenvectors of **A**
ν	Frequency
ξ	Friction coefficient
τ	Time delay
τ_C	Correlation time
φ_i	Torsional angle of the ith bond
Φ, Ψ, χ	Euler angles
$\Phi(\nu_i, \nu_j, l, \tau)$	Symmetric part of the modal correlation function
$\chi(\nu_i, \nu_j, l, \tau)$	Modal correlation function
$\Psi(\nu_i, \nu_j, l, \tau)$	Antisymmetric part of the modal correlation function
∇_r	Gradient with respect to $\mathbf{r}_i$
Å	Angstroms
$\mathscr{F}$	Rayleigh's dissipation function

ABBREVIATIONS

BD	Brownian Dynamics
CACF	Conformational Autocorrelation Function
CK	Cooperative Kinematics
DRIS	Dynamic Rotational Isomeric States
FFT	Fast Fourier Transform
fs	Femtosecond
FT	Fourier Transform
IR	Infrared
MD	Molecular Dynamics
NM	Normal Mode
NMR	Nuclear Magnetic Resonance
ns	Nanosecond
OACF	Orientational Autocorrelation Function
PBD	Polybutadiene
PE	Polyethylene
PIP	Polyisoprene
ps	Picosecond

1. INTRODUCTION

Polymers constitute an integral part of our everyday life. Since the beginning of the century, human beings have been using more and more synthetic polymers. Biopolymers, on the other hand, have been around since the beginning of life on Earth. For the chemist, biologist and the material scientist it is extremely important to determine the structure/function relationship in these molecules. Their study is also challenging for the physicist in that the multi-body structure and collective motions of macromolecules lead to a class of dynamics that is nonexistent in other complex systems. Thus, investigation of polymer dynamics invites attention to many scientists from numerous disciplines.

The dynamics of polymer chains results from the coordinated motions of its atoms. Depending on the length and time scale of observations, the dynamics may be analyzed in two broad regimes: (i) The Rouse-Zimm regime[1,2] involves the cooperative reorganization of individual Gaussian subchains, and cover time scales of 10^{-7} s or slower in solution; (ii) local dynamics regime encompasses the faster motions contributing to the local rearrangements within subunits of the chain[3-7]. The former dictates the long-range motions of the polymer and the chemical identity is not realized. On the other hand, many of the properties that are of interest for the experimentalist take place in a much shorter time and length scale. Local dynamics refers to motions on this scale where the chemical identity of each chain becomes significant.

The mechanism and rate of conformational changes in polymer chains are controlled by chain connectivity, intramolecular conformational potential and interactions with the environment. These factors set the polymer in motion which is subdivided into two groups consisting of high-frequency motions such as bond angle bending, bond stretching and small amplitude oscillations about rotational energy minima, and bond rotameric transitions in the form of discrete jumps from one isomeric state to another. Comprehension of local phenomena will provide an understanding of the mechanism and basic factors controlling the stochastic process of local relaxation in specific polymers. The ultimate goal is to explore the structure/property relationship in polymers so as to interpret the macroscopic behavior.

Within the last two decades, due to the vast amount of improvements made in the speed of computers, a new area of research has emerged in the study of polymers. It is now possible to simulate the static and dynamic behavior of a given polymer in the computer

environment and use the output to interpret experimental results and theoretical propositions. In fact, these studies are suitably called computer experiments.

In the original computer simulation studies of polymers, simple models of bistable oscillators[8] and linked rigid bodies[9,10] have been used. More realistic model chains involving three-fold symmetric rotation barriers for backbone bonds have then been adopted to study stress, dielectric, mode and conformational relaxation of chains[11,12]. When the prediction of real polymer behavior is aimed at, adopting more complicated models is inevitable. At this point, a compromise between realistic molecular models and efficient computation algorithms is necessary in order to search the enormous configuration space of macromolecular systems. Molecular models with different levels of complexity have been employed depending on the nature of the problem at hand. For example, for simulating polyethylene (PE) several models have been proposed which contributed to the understanding of the mechanism of various processes, such as orientational and translational motions in solution[13-16] and in the bulk state[17-19], glass transition phenomena[20,21], and conformational transitions in uniaxially deformed state[22,23]. The "united atom" approximation has been commonly adopted in simulations, by collapsing the hydrogen atoms onto the backbone carbon atoms. This is a computationally efficient approach due to the fact that the total simulation duration scales roughly with the square of the number of units explicitly considered. Furthermore, elimination of the highest frequency motions associated with hydrogen atoms allows the use of larger size time steps in the numerical integration algorithms. Likewise, a highly simplified model of polyisoprene has been adopted by Adolf and Ediger[24], in which the $CH = CCH_3$ group was treated as a united group. The differences in the orientational correlation times of different C-H vectors observed in NMR experiments were successfully reproduced by this method. However, the united atom approximation is not, in general, adequate for investigating properties which are affected by the intrinsic conformational features of the chains. A full atomic description, in which side groups are explicitly considered, becomes indispensable for the examination of local phenomena, and in particular, when dealing with polymers having large side groups.

When large systems such as polymers in the bulk state and biopolymers are explored, or when properties effective on time scales longer than those attainable by available computer systems are investigated, numerical solution of particle motion becomes too costly. For example, it is reported in the bulk PIP simulation of Moe and Ediger that it takes 50 days of CPU time to reproduce a nanosecond trajectory for the system of 3562 atoms on an IBM RS6000/325[25]. In this case, analytical models are developed[26-28]. Among such models is the dynamic rotational isomeric state (DRIS) formalism whereby the classical

rotational isomeric state theory of chain statistics is recapitulated to interpret local phenomena[29-37]. In DRIS, successive transitions of bond torsional angles from one isomeric minimum to another is assumed to be the only dynamic process governing local motions. Thus, short-range conformational statistics are emphasized. In this respect, DRIS is more appropriate for dilute polymer systems in which environmental effects are negligibly small compared to internal barriers to bond rotations. In contrast, Cooperative Kinematics (CK) model[38-41] systematically accounts for the restrictions imposed by the long-range connectivity of the chain and by the frictional resistance of the environment. CK therefore applies to the investigation of chain dynamics in dense media.

A group of methods have been developed in the present thesis, and applied to different model chains with the purpose of improving the efficiency of the computer simulation of polymers, and understanding the basics of local chain dynamics using these computationally efficient approaches. In Section 2, the methods and models are outlined in detail with a sample application to polyisoprene (PIP). In particular, a computationally efficient method developed for incorporating the effect of side group motions to the backbone dynamics is illustrated. In Section 3, the applications to model chains of PE, *cis*- and *trans*-polybutadiene (PBD) and their copolymers are presented. Mainly, overall mechanisms underlying local motions, the specific types of torsional coupling between neighboring bonds, the consequences of simplifications intrinsic in the model used on the nature of torsional coupling, the effect of backbone geometry, the range and character of orientational correlations, and communication between motions operating at different frequencies are investigated. The conclusions of the study are presented in Section 4, together with recommendations on possible future applications.

2. COMPUTATIONAL METHODS AND MOLECULAR MODELS

The prerequisite for effective simulation is the utilization of an appropriate model which is complete enough to represent the true dynamics of the polymer but simple enough to extract information in reasonable computational time. A compromise between realistic models and efficient computation algorithms is necessary in order to search the configurational space of macromolecular systems. The simulation techniques utilized in this study are broadly classified as (i) those solving the real-time motion of a system of particles in space, (MD and BD); and (ii) those employing analytical models (DRIS and CK) to generate the most probable motion without intensive simulations.

2.1. Molecular and Brownian Dynamics Methods

Both MD and BD rest on the idea of solving the equations of motion of particles so as to find the time evolution of their coordinates. In principle, any quantity of interest may be calculated provided that the so-called "trajectory" of the system is available. In both methods, a chain of n+1 backbone units, indexed from 0 to n, is considered. The notation of Flory[42] is adopted for defining bond vectors ($\mathbf{l}_i$), bond angles (θ_i), and torsional angles (φ_i). A portion of a polymer chain designating the Flory convention is presented in Figure 2.1. The position vector of the ith backbone atom relative to the laboratory-fixed system is given by

$$\mathbf{r}_i = x_i\,\mathbf{e}_1 + y_i\,\mathbf{e}_2 + z_i\,\mathbf{e}_3 \qquad 0 \le i \le n \qquad (2.1)$$

where x_i, y_i, z_i are the components of $\mathbf{r}_i$ along the respective base vectors $\mathbf{e}_1$, $\mathbf{e}_2$, and $\mathbf{e}_3$ of the coordinate system.

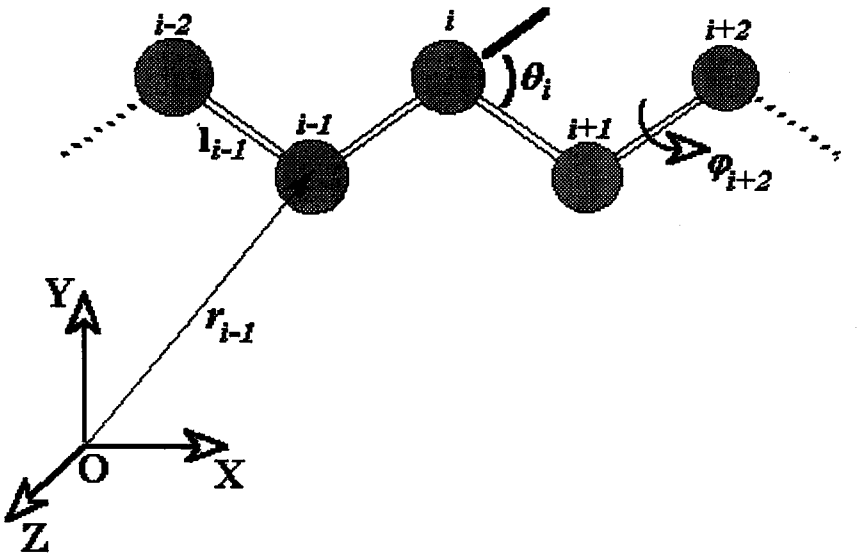

FIGURE 2.1. Part of a polymer chain, showing the definition of internal coordinates.

In MD, the potentials governing the motion of every particle within the system is incorporated into the model. The equation of motion of the *i*th particle is

$$\mathbf{F}_i = m_i a_i = -\nabla_r V \tag{2.2}$$

where m_i is the mass of *i*th particle, $\mathbf{F}_i$ is the force exerted on the particle, a_i is its acceleration. $-\nabla_r V$ denotes the gradient of the total potential experienced by the *i*th particle with respect to r_i. The potential, V, governing the motion of the particle i is the sum of all the effective potentials and are explained in detail in Appendix A. The velocity Verlet algorithm[43] is used to integrate Equation 2.2. The time steps by which the motion of the particles is propagated is dictated by the fastest motions and is on the scale of femtoseconds. The time evolved coordinates of the atoms are recorded at time intervals appropriate for the property to be investigated. The velocity rescaling procedure proposed by Berendsen *et al.*[44] is adopted to keep the temperature of the system constant at the desired value.

One of the greatest problems in MD is encountered when one form of motion in the

system is much faster than another. This is called time scale separation. The short time steps needed to handle the fast motion and the long runs needed to allow evolution of the slower modes make the simulations very expensive. This is especially a problem if the fast motions are not of great interest in themselves. A full MD simulation is very expensive, since the motion of the solvent molecules is of little interest but cannot be discarded as it effects the dynamics. In such a case, an approximate approach is adopted: The solvent particles are omitted from the simulation, and their effects upon the solute is represented by a combination of random forces and frictional terms. Newton's equations of motion are thus replaced by the Langevin equation:

$$m\frac{d^2\mathbf{r}_i}{dt^2} = -\xi\frac{d\mathbf{r}_i}{dt} - \nabla_r V + m\mathbf{A}_i(t) \qquad 0 \le i \le n \qquad (2.3)$$

In the high friction limit where the acceleration of the particles is negligible, Equation 2.3 reduces to the Brownian equation of motion:

$$\frac{d\mathbf{r}_i}{dt} = -\frac{1}{\xi}\nabla_r V + \mathbf{A}_i(t) \qquad 0 \le i \le n \qquad (2.4)$$

In Equations 2.3 and 2.4, ξ is the friction coefficient of solvent and Stokes equation, $\xi = 6\pi a\eta$, is utilized to generate the friction coefficient of a solvent at the given temperatures. η is the viscosity of the solvent and a is the hydrodynamic radius of the group interacting with the solvent, which is usually taken as half the bond length[45]. $\mathbf{A}_i(t)$ is a Gaussianly distributed random force with mean zero and covariance characterized by the correlation

$$\left\langle \mathbf{A}_i(t)\cdot\mathbf{A}_j(t')\right\rangle = \frac{2k_BT}{\xi}\delta_{ij}\delta(t-t') \qquad (2.5)$$

Here, k_B is the Boltzmann constant, T is the absolute temperature, δ_{ij} is the Kronecker delta, and $\delta(t\text{-}t')$ is the Dirac delta function. In BD simulations, the temperature is maintained during the simulations through the random noise whose covariance obeys a temperature dependent Gaussian distribution, according to Equation 2.5. Thus, fixed temperature is a consequence of the application of white noise, which acts as a constant temperature heat bath. No further temperature control is implemented in the simulation algorithm. The numerical method developed by Helfand[46] is applied to integrate Equation 2.4. An extensive review on BD simulation technique has recently been presented by Ediger and Adolf[47].

At this point, it is convenient to provide specific examples for (i) demonstrating the applicability of the presented techniques to real systems, and (ii) increasing the efficiency of the methods. These cases will be taken up in the next two subsections.

2.1.1. An Illustrative Example: Application of the BD Technique to *cis*-PIP

As an illustration of the simulation techniques, the application of BD to *cis*-PIP is presented with comparisons to experimental data. The motivation is to test the predictive capabilities of BD simulation technique with its inherent approximations for a dynamically flexible polymer.

In many of the BD studies, because of its simple structure, the PE chain has conveniently been utilized; a simplified model of *cis*-PIP has also been studied. Unlike PE which lacks experimental findings describing its dynamics in solution, *cis*-PIP provides a good example for understanding the applicability of the BD method to real systems, since it has been studied extensively in a variety of solvents by many experimental techniques such as ^{13}C NMR[48,49] or transient holographic grating[50].

In the following, BD simulations of *cis*-PIP in solvents at different viscosities and at different temperatures are presented. The structure of *cis*-PIP repeat unit is given in Figure 2.2.

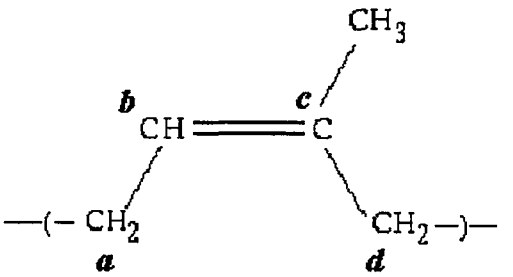

FIGURE 2.2. Structure of *cis*-PIP repeat unit.

Simulation results are compared with those of experimental observables to see the extent of a reasonably realistic description of the local dynamics by the technique. The model is an extension of that used in the BD simulation of local motions in PIP by Adolf and Ediger[24,51]. There, the doubly bonded carbon atom along with the attached hydrogen atoms and the CH_3 group has been considered as one unit with the argument that this group is rigid enough to suppress all the internal degrees of freedom. Here, the simple representation has been elaborated by incorporating this unit more explicitly; the double bond is given a limited freedom to rotate about its own axis and the CH_3 side group is explicitly included. The hydrogen atoms are kept collapsed onto the carbon atom they are bonded to. Short-range interactions between atom pairs separated by four bonds are also included in the effective potential since the local dynamics might be considerably affected by such interactions. The details of the operating potentials are given in Appendix B.

Simulations are performed for a set of viscosity-temperature combinations describing the dynamic environment of the following solvents: chloroform, cyclohexane, tetrachloroethane and Aroclor 1248. These are chosen from the set of solvents used in reference 48 so as to compare the NMR results therein with those from BD in this study. Of these, chloroform, cyclohexane and tetrachloroethane are good solvents for *cis*-PIP; *i.e.* the polymer-solvent contacts are preferred over polymer-polymer contacts. Aroclor 1248, which will be referred to as Aroclor from this point on, is a highly viscous mixture of polychlorinated biphenyls. The equations giving the temperature dependence of solvent viscosities and the associated temperature dependent viscosity relations are also taken from reference 48 and are given explicitly in Appendix B.

The simulated polymer chain consists of 20 repeat units, *i.e.* 80 backbone atoms. The backbone carbon atoms are labeled a-d in Figure 2.2. Depending on the C-H vector

utilized for a particular calculation, the notation C-H^a or C-H^b is used in reference to positions *a* or *b* in Figure 2.2.

Time steps of 0.1 - 0.8 fs are used depending on the viscosity of the solvent and the temperature of the system. The suitable time step corresponding to a particular viscosity-temperature combination is determined so that the equilibrium properties of the system are maintained. A minimum number of three runs with independent starting configurations are performed at each viscosity-temperature set to obtain statistically reliable results.

The trajectories are analyzed in comparison to ^{13}C NMR results. The correlation times, τ_C, measured by these experiments correspond to the integral of the decay of the second orientational auto-correlation function, M_2, given as

$$M_2(\tau) = \frac{1}{2}\left\langle 3\left[\mathbf{m}(t)\cdot\mathbf{m}(t+\tau)\right]^2 - 1\right\rangle \qquad (2.6)$$

Here, $\mathbf{m}(t)$ is the unit vector affixed to C-H bond vector of interest at time t. The τ_C values obtained from the simulations are compared to those from ^{13}C NMR experiments[48,49] at different viscosities for the temperature range of 230 - 330 K in Figure 2.3 for C-H^a bonds.

At moderate viscosities, exemplified by the solvents chloroform, cyclohexane and tetrachloroethane, the BD results exhibit satisfactory agreement with experiment. Simulations reproduce average deviation of τ_C in a particular solvent as 10 - 75 per cent for either C-H vector. At higher viscosities, represented by the uppermost curve of solvent Aroclor, there is a marked difference between the τ_C values predicted by BD simulations and measured experimentally, indicating that the technique fails in this high viscosity regime. This result suggests that in polymers with fast dynamics such as *cis*-PIP, the motion of the polymer might involve time scales comparable to that of the solvent and thus be coupled to that of the solvent. Equation 2.5 is not applicable under these conditions. In contrast, slow polymers have time-scales well separated from that of the solvent. For the former type of polymers, at high viscosities, both the motion of the solvent and the solute slow down appreciably so that their motion becomes coupled.

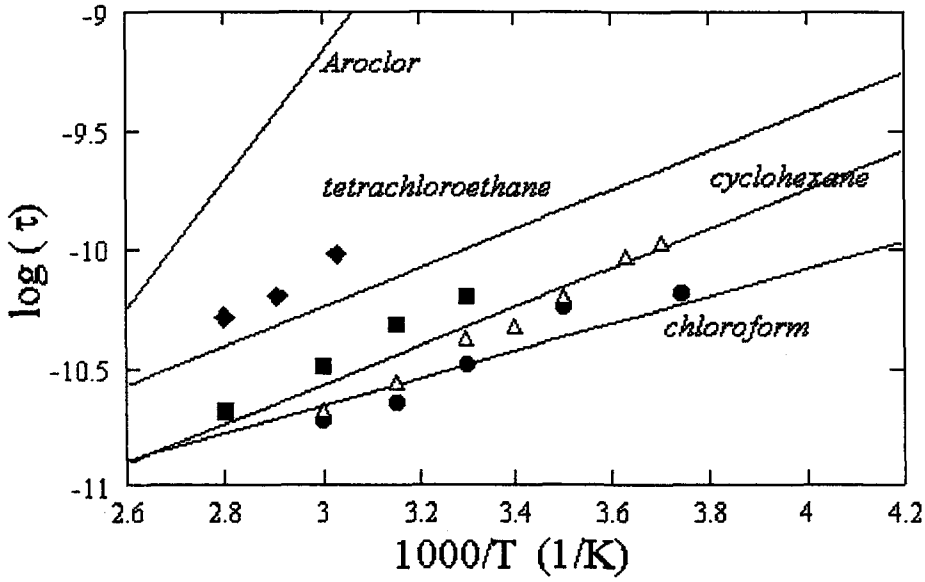

FIGURE 2.3. Comparison of experimental and simulation results for the correlation times of *cis*-PIP CH^a vectors in various solvents.

In summary, BD simulation technique proves to be a powerful tool to study local phenomena in dilute solution, provided that a cautious choice of polymer-solvent system is made within the frame of approximations of the technique. The rigorous approach used here leads to define a domain of applicability insofar as the viscosity of the solvent and temperature is concerned.

2.1.2. A Computationally Efficient Method for Incorporating Side Group Effects into Polymer Dynamic Simulations

The full atomic description of the molecule being investigated has the disadvantages of (i) necessitating the use of relatively small time steps in the integration algorithm due to the inclusion of the high frequency motions of side groups, and (ii) increasing the computation time cost of each step due to the presence of larger number of interacting

atoms. In order to circumvent the step size limitation associated with high frequency vibrations, models with holonomic constraints have been invoked. In fact, the so-called SHAKE method[52], based on the iterative solution of equations constraining bond lengths and angles has been widely employed in MD simulations. In general, constraining bond lengths decreases the computing time by a factor of 2 - 4[53]. On the other hand, the imposition of constraints on bond angles has been pointed out to alter the mechanism of molecular motion[54]. It is also possible to freeze the high frequency motions of only the side groups by using an appropriate set of constraint equations[55,56].

The problem of achieving computational efficiency in realistic chain models has led to devising a method accounting for the contribution of the side group interactions on the dynamics of the chain backbone, without explicit consideration of the fast vibrational motions associated with the side groups. The proposed method can be conveniently implemented in various simulation algorithms and allows the use of relatively large time steps. The basic approach relies on the transfer of the forces exerted on the side groups onto the backbone atoms by an appropriate choice of equivalent forces and couples. A couple is defined here as two parallel forces which are equal in magnitude, and opposite in direction. These forces impart a rotational motion, without translation, to the object on which they act.

2.1.2.1. Basic Approach. A portion of a polymer chain is presented in Figure 2.4. The side groups are shown as empty spheres and the backbone atoms as filled ones. A chain of n bonds with bond vectors $\mathbf{l}_i$, indexed as $0 \leq i \leq n$, $\mathbf{l}_i$ extending from atom i-1 to i, is considered. Side groups affixed to the ith atom are connected by bond vectors $\mathbf{l}_{i1}$ and $\mathbf{l}_{i2}$ originating from the ith atom. The position vector of the ith backbone atom with respect to the laboratory fixed frame OXYZ is indicated by the position vector $\mathbf{r}_i$. Local chain-embedded coordinate frames $x_iy_iz_i$ with origin affixed to the ith backbone atom, C_i, are defined for each backbone atom, i. The x_i-axis is normal to the plane formed by atoms C_{i-1} - C_i - C_{i+1}, and points outward. The z_i-axis bisects the angle formed by the bond vectors $\mathbf{l}_{i1}$ and $\mathbf{l}_{i2}$. The y_i-axis completes a right handed coordinate system. The side group atoms are denoted by H_{i1} and H_{i2}, pointing in the $+x_i$ and $-x_i$ directions of the local frame, respectively.

The unit vectors δ_x, δ_y and δ_z along the axes of the frame $x_iy_iz_i$ are expressed as

$$\left.\begin{aligned} \delta_x &= \frac{\mathbf{l}_{i+1} \times \mathbf{l}_i}{|\mathbf{l}_{i+1} \times \mathbf{l}_i|} \\ \delta_y &= \frac{\mathbf{l}_{i2} \times \mathbf{l}_{i1}}{|\mathbf{l}_{i2} \times \mathbf{l}_{i1}|} \\ \delta_z &= \delta_x \times \delta_y \end{aligned}\right\} \qquad (2.7)$$

Here, × denotes the vector product and the magnitude of a vector is shown by two vertical bars.

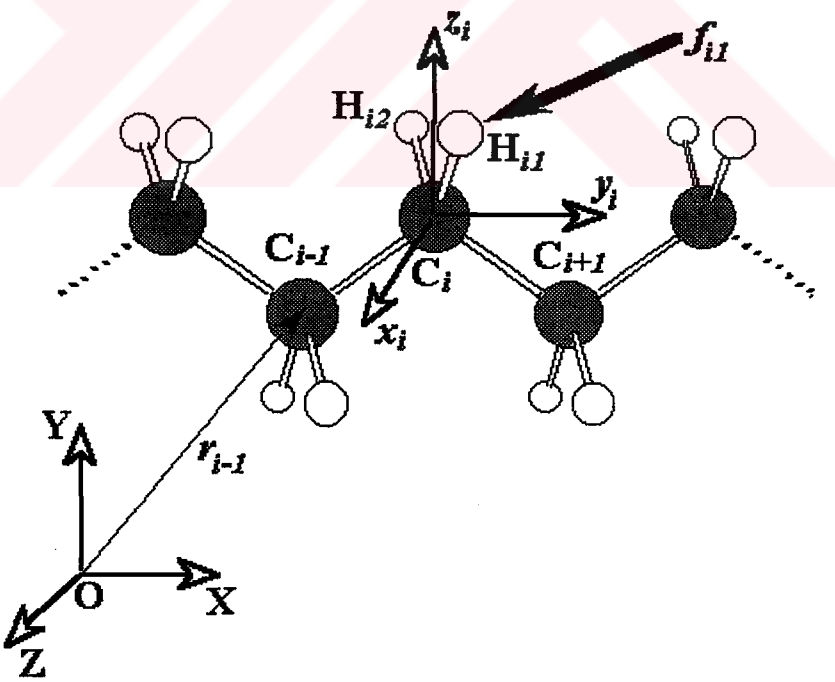

FIGURE 2.4. Segment of the polymer chain showing the general coordinate system OXYZ and the local frame $x_iy_iz_i$.

The side group atoms are subject to forces exerted either by the environment or by other atoms of the chain in close neighborhood. One such force, $\boldsymbol{f}_{i1}$ acting on H_{i1} is shown in Figure 2.4. In the united atom model, the side group is collapsed on the backbone and the force $\boldsymbol{f}_{i1}$ is applied directly to the backbone. In that approximation, the eccentricity present due to the finite distance of the side group from the backbone is ignored. In the presence of eccentricity the force on the side group imparts a torque to the backbone which is absent in the united atom approximation. In this work such effects resulting from the finite separation of the side groups from the backbone are incorporated. This is achieved through the following steps:

(1) The force $\boldsymbol{f}_{i1}$ is translated from H_{i1} to C_i and a moment $\mathbf{m} = \mathbf{l}_{i1} \times \boldsymbol{f}_{i1}$ is added. In order to accomplish this transformation we assume that the bond C_i-H_{i1} is rigid and is rigidly embedded to the backbone. The transformation is based on the principle that in a rigid body, a force $\boldsymbol{f}$ exerted at a point $\boldsymbol{P}$ may be translated to another point $\boldsymbol{P'}$ provided that a moment equating to $\boldsymbol{PP'} \times \boldsymbol{f}$ is added. As a result of this step, the side group is removed but a moment $\mathbf{m}$ acting on the backbone is introduced that is absent in the united atom model.

(2) The moment $\mathbf{m}$ introduced in step 1 imparts a rotational effect to the backbone. At this step we replace $\mathbf{m}$ by equivalent couples (pairs of parallel, equal magnitude and opposite sense forces) acting on the three backbone atoms, C_{i-1}, C_i and C_{i+1}. To achieve this, the C_{i-1} - C_i - C_{i+1} unit is assumed to be momentarily rigid. It is to be noted that this assumption is adopted only during the distribution of the effect of $\mathbf{m}$ to the three backbone atoms. For this replacement, $\mathbf{m}$ is expressed as the sum of three components along the local x_i-, y_i- and z_i-axes as

$$\mathbf{m} = m_x \boldsymbol{\delta}_x + m_y \boldsymbol{\delta}_y + m_z \boldsymbol{\delta}_z \tag{2.8}$$

The three components of $\mathbf{m}$ are obtained from

$$\left.\begin{aligned} m_x &= \left[\mathbf{l}_{i1} \times \boldsymbol{f}_{i1}\right] \cdot \delta_x \\ m_y &= \left[\mathbf{l}_{i1} \times \boldsymbol{f}_{i1}\right] \cdot \delta_y \\ m_z &= \left[\mathbf{l}_{i1} \times \boldsymbol{f}_{i1}\right] \cdot \delta_z \end{aligned}\right\} \qquad (2.9)$$

Now these three components of **m** are replaced by couples acting on the atoms C_{i-1}, C_i and C_{i+1}. The couples are chosen according to the following procedure: m_x is assumed to be the result of a couple composed of a pair of forces of magnitude g_1 acting on atom C_{i+1} along the $+z_i$ direction and on atom C_{i-1} along the $-z_i$ direction as shown in Figure 2.5(a).

Thus, m_x imparts a right handed rotation and defines g_1 as

$$g_1 = m_x / d_1 \qquad (2.10)$$

where d_1 is the distance between the couple, given by

$$d_1 = 2\, l_{i1} \sin(\theta/2) \qquad (2.11)$$

Here, θ is the bond angle defined by atoms C_{i-1}, C_i and C_{i+1} and l_{i1} is the magnitude of the bond vector $\mathbf{l}_{i1}$. The component m_y results from three forces; a force of magnitude g_2 acting on atom C_i along the $+x_i$ direction and two forces of magnitude g_2 /2, acting on atoms C_{i-1} and C_{i+1} along the $-x_i$ direction as shown in Figure 2.5(b). g_2 is expressed in terms of m_y as

$$g_2 = \mathrm{m}_y / d_2 \tag{2.12}$$

where d_2 is

$$d_2 = l_{i1} \cos(\theta/2) \tag{2.13}$$

m_z results from two forces each of magnitude g_3 , acting on atom C_{i+1} along the $-x_i$ direction and the other on atom C_{i-1} along $-x_i$ direction as shown in Figure 2.4(c). g_3 is evaluated from

$$g_3 = \mathrm{m}_z / d_1 \tag{2.14}$$

The couples chosen in this manner form a system equivalent to **m**. The choice of these components is not unique, however, and different couples acting on the three backbone atoms may be chosen with the same resultant moment **m**. Combining the results of Equations 2.8 - 2.14, the forces $\mathbf{F}_{i-1}$, $\mathbf{F}_i$ and $\mathbf{F}_{i+1}$ exerted on the respective backbone C_{i-1}, C_i and C_{i+1}, as a result of the external forces applied on atom H_{i1} become equal to

$$\left.\begin{aligned} \mathbf{F}_{i-1} &= (g_3 - g_2/2)\delta_x - g_1\delta_z \\ \mathbf{F}_i &= g_2\delta_x + f_{i1} \\ \mathbf{F}_{i+1} &= -(g_3 + g_2/2)\delta_x + g_1\delta_z \end{aligned}\right\} \tag{2.15}$$

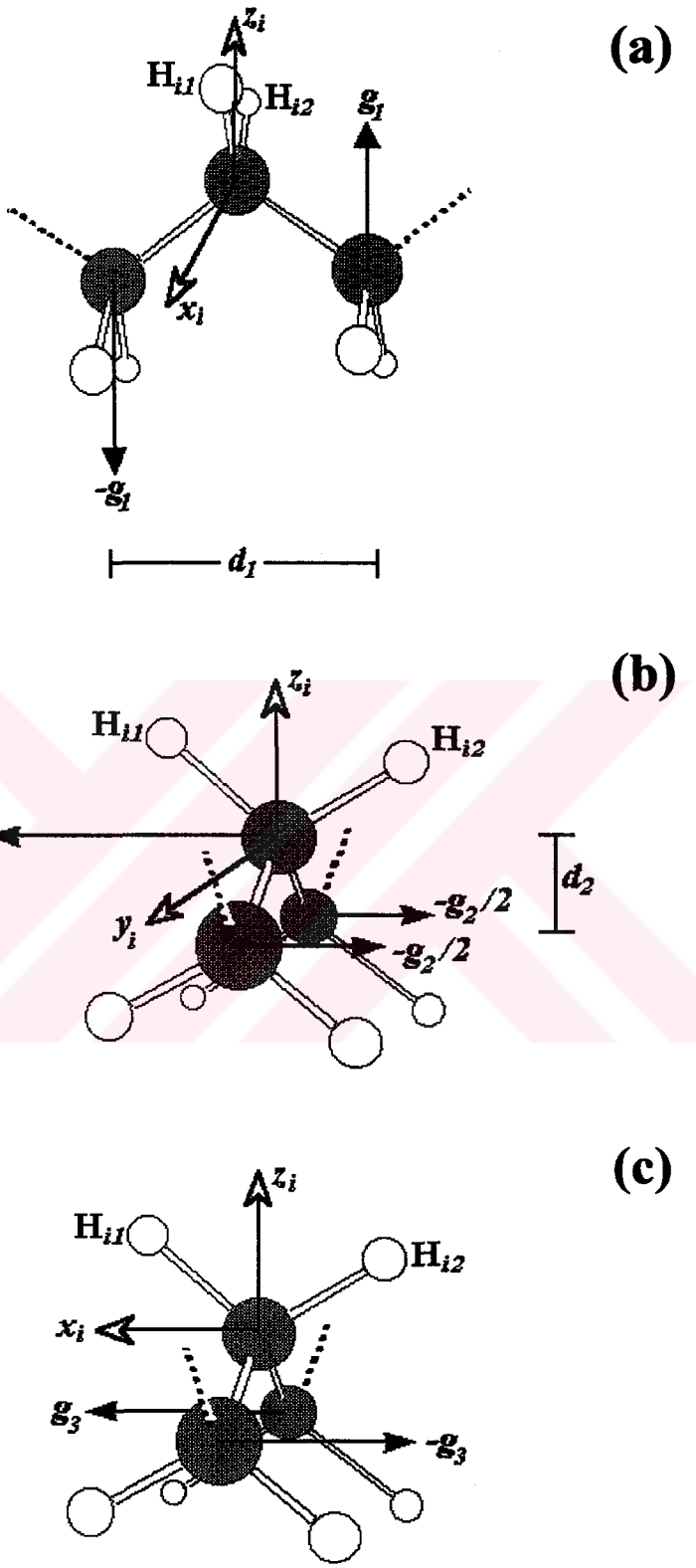

FIGURE 2.5. Selected couples giving rotations about the local axes.

The procedure described above is repeated for all side chain atoms. Thus, forces acting on side groups are transmitted to the backbone atoms, and the problem reduces to that of the simulation of backbone dynamics using common integration algorithms.

2.1.2.2. Calculations. The application of the above scheme to BD simulations of PE is presented. Comparison of the results is made with those from a model in which the full atomic description of the same chain is adopted. The two approaches will be referred to as Model I and Model II, respectively.

A polyethylene chain of $n = 30$ bonds, each of length $l_i = 1.53$ Å, is considered. Following Model I described above, the hydrogen atoms are assumed to be rigidly affixed to carbon atoms. C-H bonds are of fixed length $l_{i1} = l_{i2} = 1.10$ Å, and make an angle $\theta_s = 109.5°$ with each other. The constraints on bond lengths and angles of side groups are relaxed in Model II, in which the forces on H atoms are not transferred to backbone but are considered explicitly. In Model I, the vectors $\mathbf{l}_{i1}$ and $\mathbf{l}_{i2}$ of C-H bonds are determined at each step from the backbone geometry using

$$\mathbf{l}_{ij} = \left[\frac{\mathbf{l}_i - \mathbf{l}_{i+1}}{|\mathbf{l}_i - \mathbf{l}_{i+1}|} \cos\frac{\theta_s}{2} + \frac{\mathbf{l}_{i+1} \times \mathbf{l}_i}{|\mathbf{l}_{i+1} \times \mathbf{l}_i|} \sin\frac{\theta_s}{2} \right] l_{ij} \qquad (2.16)$$

The second term on the right-hand side of Equation 2.16 is positive for $j = 1$ and negative for $j = 2$.

The total conformational potential of the chains results from (i) the intrinsic threefold symmetric torsional potentials of each backbone bond, characteristic of sp^3 bonds, (ii) the Lennard-Jones (LJ) interactions between non-bonded pairs of atoms, including both backbone and side groups, and (iii) the harmonic potentials controlling the stretching and angle distortion of backbone bonds. Model II, on the other hand, comprises the harmonic potentials associated with the stretching and angle distortion of the bonds of the side groups in addition to the potentials of Model I. Appendix A summarizes the potential energy functions and Appendix B gives parameters, as well as other simulation and geometry parameters used in these models.

The position vector $\mathbf{r}_i(t+\delta t)$ of backbone atom i at time $t+\delta t$ is computed from that of the preceding step by applying the following numerical integration algorithm[57]:

$$\mathbf{r}_i(t+\delta t) = \mathbf{r}_i(t) + \frac{\delta t\ \mathbf{G}_i(t)}{\xi_i} + \delta \mathbf{A} \qquad (2.17)$$

Here δt is the size of an integration time step and ξ_i is the friction coefficient corresponding to the ith atom. $\delta \mathbf{A}$ is related to the Gaussianly distributed stochastic force acting on the backbone carbon atoms, given by Equation 2.5. In Model I, the force $\mathbf{G}_i(t)$ comprises the force exerted on atom i due to the gradient of potential energy and the force $\mathbf{F}_i(t)$ transmitted to atom i from the attached side groups. After the evaluation of the new configuration of the backbone, the position of the side groups are readily calculated in Model I by using Equation 2.16. On the other hand, in Model II, the position vectors of side groups are updated by direct application of the integration algorithm given by Equation 2.17. In all simulations, the ratio of the atomic radius of hydrogen to that of carbon is taken as $r_H / r_C = \xi_H / \xi_c = 2 / 3$ and $\xi_c = 1400$ kg mol^{-1} ns^{-1} at a temperature of 300 K.

2.1.2.3. Comparison of Models I and II. First, simulation time and efficiency is tested. For each model, a trajectory of duration 4.25 ns is generated. The efficiency of a simulation method is measured by the real-time it takes to generate a trajectory of a given duration. In the present study, the simulations are carried out on Silicon Graphics, Challenge L Networked Resource Server System, with 2 x 150 MHz CPUs. It turns out that the computation time is 1.25 times faster with Model I compared to Model II, provided that integration time steps δt of the same size are adopted in both models. However, a larger time step may be employed in Model I, since the high frequency modes associated with side group motions are eliminated, as discussed above. Note that, it is trivial in MD to determine the largest δt which reproduces the same trajectories as those of smaller size; whereas, in BD, the trajectory is not unique since the effect of the surroundings is included via a random term, and the sequence of random numbers generated changes with different δt. This problem is resolved by examining the consistency of the general conformational features of runs, such as the extent of bond stretching and bond angle distortions, obtained at various δt's. Model I can take on about three times larger time steps. Thus, the computing time of the program is improved by a factor of about 3.75 upon using Model I.

Next, the proposed algorithm is tested for reproducibility of the general equilibrium conformational features of PE chains. The analysis of the results from the two models demonstrates that the amplitudes of the highest frequency motions, which are associated with bond stretching and bond angle distortion, are of comparable magnitudes in the two models. In fact, the rms fluctuations of bond lengths are observed to be 9.9 x 10^{-3} nm for Model I and 9.1 x 10^{-3} nm for Model II. Similarly, the respective rms fluctuations in the bond angles are found to be 8.2° and 10.6°, which are within acceptable proximity of each other. The conformational statistics predicted by Model I also exhibit the characteristics of real PE chains, in agreement with Model II. The backbone bonds have three rotational minima at 0° (*trans, t*), and ±120° (*gauche*±, *g*±), with probabilities closely conforming with real PE chains. A distinguishing property is the severe suppression of the g^+g^- (or g^-g^+) state. Furthermore, a rigorous examination of the probability surface obtained as a function of two consecutive dihedral angles reveals in both models the splitting of the minimum at g^+g^- into two, those being slightly distorted from the (±120°, ∓120°) location towards (±110°, ∓130°), similar to the well established behavior of PE bonds[42,58]. Thus, although in Model I, the repulsive interactions between hydrogen atoms separated by a pair of g^+g^- (or g^-g^+) bonds are not directly accounted for, but only transmitted to the backbone atoms, the detailed features of the rotameric probability distributions of real PE chains are satisfactorily reproduced.

The new model should also reproduce the dynamic, *i.e.* time dependent, properties. As a sample dynamic property, distributions of bond torsion and reorientation angles are utilized. A mean isomerization time of 11 ps is obtained with Model I, by taking into account the total number of rotational transitions occurring throughout the 4.25 ns trajectories of four independent runs. Similarly, Model II yields a mean isomerization time of 12 ps. A more detailed description of the time evolution of relaxation processes associated with isomerization mechanisms may be obtained by considering time-dependent probability distribution functions[22,23]. In Figure 2.6, the probability, $P(|\Delta\phi|, \Delta t)$, of having an absolute change $|\Delta\phi|$ in bond dihedral angles occurring within the time interval Δt is presented. The solid curves are obtained from Model I and the dotted curves from Model II for Δt = 0.005 and 1.0 ns, as indicated in the figure. In each case, the probability values are recorded in 3° intervals of $\Delta\phi$; the displayed curves are normalized so as to make the area under the curve equal to one radian. Since the curves evolve from a Dirac delta function at Δt = 0 ns, the probability distribution curves are confined to a small range of angles at short times (Δt = 0.005 ns). After a sufficiently long time interval, on the other hand, a second peak in the 120° region is observed due to the occurrence of conformational jumps with a mean isomerization time of 11 - 12 ps as mentioned above. $P(|\Delta\phi|, \Delta t)$ values for Model II

in the range $|\Delta\varphi| < 10°$ are slightly lower than those for Model I, indicating faster torsional librations of small amplitudes in the full atomic Model II. However, this increased rate does not affect features related to the behavior of the bond torsional motions such as the isomerization rates or the distribution of consecutive bond torsional angles since the region where it is effective is associated with the fluctuations of bond torsional angles about their equilibrium values. The close similarity between the curves from the two models at a given time demonstrates that the bond torsional motion, which represents the most important degree of freedom in polymers, is adequately represented by the new model.

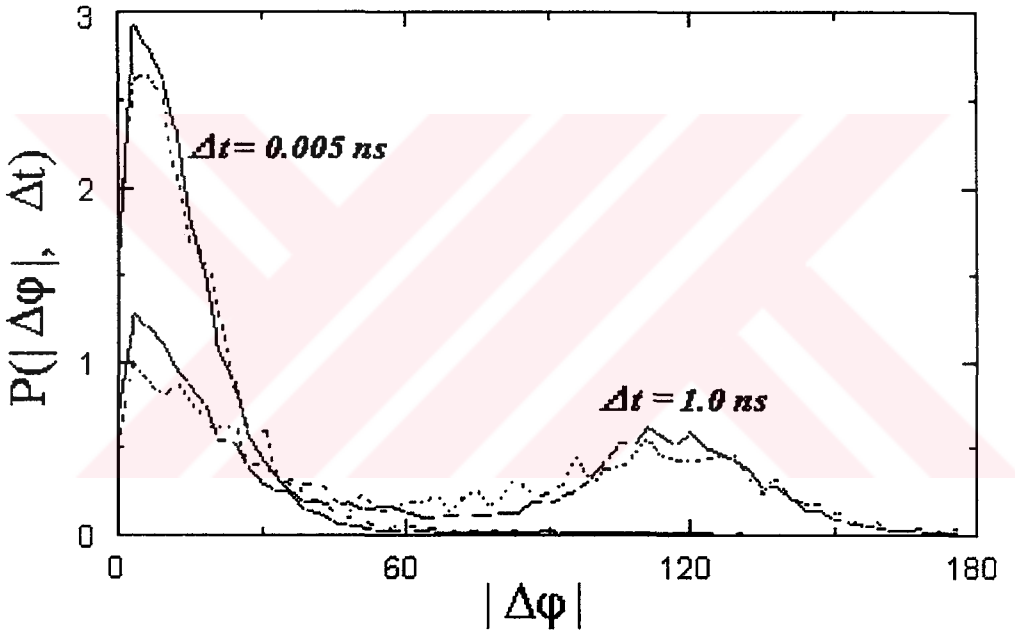

FIGURE 2.6. Comparison of Models I and II: Time dependent distribution function of bond torsional motions.

Information similar to that for bond torsional angles may be obtained for the bond vectors from distributions of C-C and C-H bond reorientation angles. The probabilities $P(|\Delta\alpha|, \Delta t)$ of the reorientation angles, $|\Delta\alpha|$, experienced by the bond vectors C-C and C-H are shown in Figures 2.7 and 2.8, respectively. The recording of the probability values and the normalization of the curves are carried out as in Figure 2.6. At short times, the C-C bonds display a somewhat faster dynamics in Model I (Figure 2.7, $\Delta t = 0.005$ ns). However,

the correspondence between the two models is quickly achieved as can be observed in the Δt = 0.01 ns curves, and is maintained until the equilibrium distribution (Δt = 1 ns) is reached. Hence, the proposed model correctly describes the orientational dynamics of the backbone bonds.

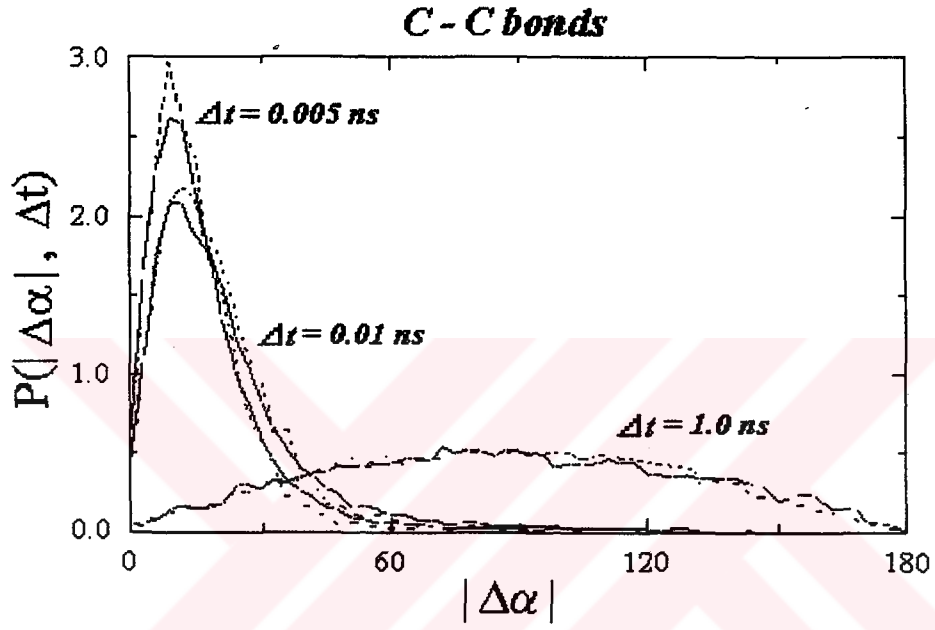

FIGURE 2.7. Comparison of Models I and II: Time dependent distribution function of the reorientation of C-C bond vectors.

On the other hand, in the case of the reorientation of C-H vectors, the departure between the two models which appears at small Δt (Figure 2.8, Δt = 0.005 ns) persists even at long time intervals (Figure 2.8, Δt = 0.1 ns) until the equilibrium distributions are obtained. Here, Model I predicts a slower reorientation for the C-H bonds indicating a loss in their mobility which should be expected due to the suppression of the flexibility of bond angles and bond lengths of the side groups in this model. The probability distributions at large Δt (Figure 2.8, inset), are identical in the two models, which shows that the equilibrium properties of the polymer are not altered by the conditions imposed in Model I.

In summary, the introduced method includes the role of the side groups into dynamic

simulations without their explicit incorporation into the integration algorithm. Such an approach eliminates the uninteresting degrees of freedom e.g. the high frequency motions of the side groups, and thereby increases the efficiency of simulations. The main assumptions of the proposed method are valid in that they bring about no major changes in the static and dynamic properties of the chain. It should be noted that although the model presented here has been used in BD simulations of PE, it is readily applicable to MD simulations of more complex macromolecules bearing bulky side groups.

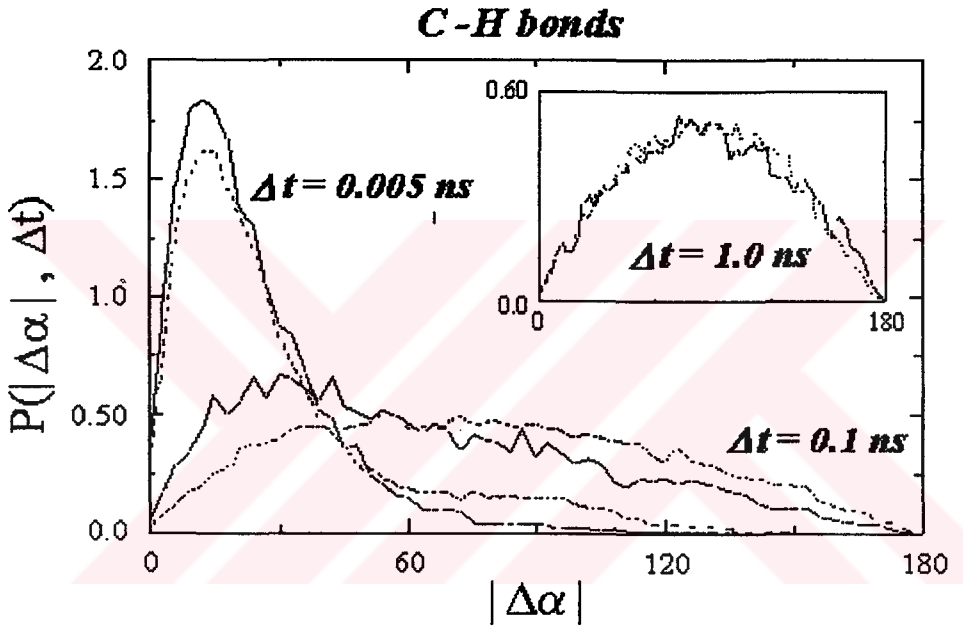

FIGURE 2.8. Comparison of Models I and II: Time dependent distribution function of the reorientation of C-H bond vectors.

2.2. Other Computational Methods

As mentioned previously, some computational methods do not reproduce the trajectories of the polymeric system. Instead, the goal of efficiency is achieved by

developing special models that are suitable for solving the problem at hand. Two such models will be presented in this section: The DRIS scheme is an efficient method for studying local dynamics of chains of a given detailed chemical structure up to several nanoseconds in solution whereas CK is applicable to the local dynamics of polymers in dense environment[26,29].

2.2.1. Dynamic Rotational Isomeric States Model

The DRIS model developed for investigating local chain dynamics has been applied to segments of polymer chains like polyethylene[29], poly(ethyleneoxide)[33], poly(dialkyl siloxanes)[59] and PIP[37]. The model is based on the master equation

$$\mathbf{dP}(t)/dt = \mathbf{A}\,\mathbf{P}(t) \qquad (2.18)$$

where $\mathbf{P}(t)$ is the vector of time-dependent probabilities of all possible configurations and $\mathbf{A}$ is the transition rate matrix of the rate constants for the passage between configurations. Sequences of bond torsional states characterize a given configuration. Bond angles and lengths are assumed to be fixed at their equilibrium values. In general, the dynamic behavior of a given segment of n bonds with ν rotational isomeric states accessible to each bond is characterized by the set of eigenvalues λ_j of $\mathbf{A}$, with j=1 to ν^N. For stationary processes, the elements of $\mathbf{P}(t)$ are independent of time and equal to the equilibrium probabilities of the ν^N configurations.

Precise determination of $\mathbf{A}$ is critically important for a realistic estimation of the conformational dynamics of polymers. In the simplest case of bonds subject to independent conformational energetics $\mathbf{A}$ is readily evaluated from the direct product of the transition rate matrices for independent bonds, and closed form expressions for the frequencies and distributions of isomerization modes are obtainable[60]. However, in most cases, consideration of the interdependence of neighboring bonds rotational states is a basic

requirement for establishing the connection between theory and experiments. Interdependence of bonds may be extended beyond first neighbors by considering simultaneous and/or coupled transitions of groups of bonds of size $n > 2$. Previous DRIS study of polyisoprene is an example in which coupled rotational dynamics of groups of three or more bonds were considered for the interpretation of dielectric relaxation behavior[37]. Here, the discussion is confined to the stochastics of pairwise interdependent bonds.

The types and activation energies of passages between pairs of rotameric states are found from conformational energy maps constructed as a function adjacent torsional angles. For the case of bond pairs with $\nu = 3$ rotational states accessible to each bond, the operating transition rate matrix, denoted as $\mathbf{A}^{(2)}$, is given by a 9x9 matrix. The superscript in $\mathbf{A}^{(2)}$ refers to the number of interdependent bonds. The explicit form of $\mathbf{A}^{(2)}$ for bonds in PE reads

$$\mathbf{A}^{(2)} = \begin{bmatrix} A_{11} & r_{-1} & r_{-1} & r_{-1} & 0 & 0 & r_{-1} & 0 & 0 \\ r_1 & A_{22} & 0 & 0 & r_{-2} & 0 & 0 & r_{-3} & 0 \\ r_1 & 0 & A_{33} & 0 & 0 & r_{-3} & 0 & 0 & r_{-2} \\ r_1 & 0 & 0 & A_{44} & r_{-2} & r_{-3} & 0 & 0 & 0 \\ 0 & r_2 & 0 & r_2 & A_{55} & 0 & 0 & 0 & 0 \\ 0 & 0 & r_3 & r_3 & 0 & A_{66} & 0 & 0 & 0 \\ r_1 & 0 & 0 & 0 & 0 & 0 & A_{77} & r_{-3} & r_{-2} \\ 0 & r_3 & 0 & 0 & 0 & 0 & r_3 & A_{88} & 0 \\ 0 & 0 & r_2 & 0 & 0 & 0 & r_2 & 0 & A_{99} \end{bmatrix} \qquad (2.19)$$

where the diagonal elements are evaluated from the negative sum of the remaining elements in the corresponding column, and r_i ($i = \pm 1 - 3$) refer the rate constants of the transitions shown in Figure 2.9. In general, the off-diagonal element $A_{ij}^{(2)}$ of $\mathbf{A}^{(2)}$ is the rate constant, k_{ij}, of passage from the jth isomeric state $\zeta\eta$ of the bond pair to the ith state $\zeta'\eta'$. k_{ij} is given by the Arrhenius-type expression $k_{ij} = A_o \exp\{-E_{a,ij}/RT\}$ where R is the gas constant, T is the absolute temperature and $E_{a,ij}$ is the activation energy for the particular transition $\zeta\eta \rightarrow \zeta'\eta'$. A_o is the front factor related to the mobility of the system, which may be constructed to include the frictional resistance of the environment depending on the specific transition.

The master equation 2.18 is solved by using the transformation $\mathbf{A} = \mathbf{B}\,\Lambda\,\mathbf{B}^{-1}$ where Λ is the diagonal matrix of the eigenvalues of **A**, and **B** is the matrix of the eigenvectors of **A**, and $\mathbf{B}^{-1}$ is the inverse of **B**. The solution is written as

$$\mathbf{P}(t) = \mathbf{C}(t)\,\mathbf{P}(t=0) = \mathbf{B}\,e^{\Lambda t}\,\mathbf{B}^{-1}\,\mathbf{P}(t=0) \tag{2.20}$$

where $\mathbf{P}(t = 0)$ is the vector of the original probabilities of all configurations, $\mathbf{C}(t)$ is the time-dependent conditional probability defined by the second equality in Equation 2.20. The ijth element $C(\zeta'\eta',t\,|\zeta\eta,0)$ of $\mathbf{C}(t)$ represents the time-delayed conditional probability of occurrence of state $\zeta'\eta'$ at time t, provided that the given pair of bonds assumes the state $\zeta\eta$ at t=0.

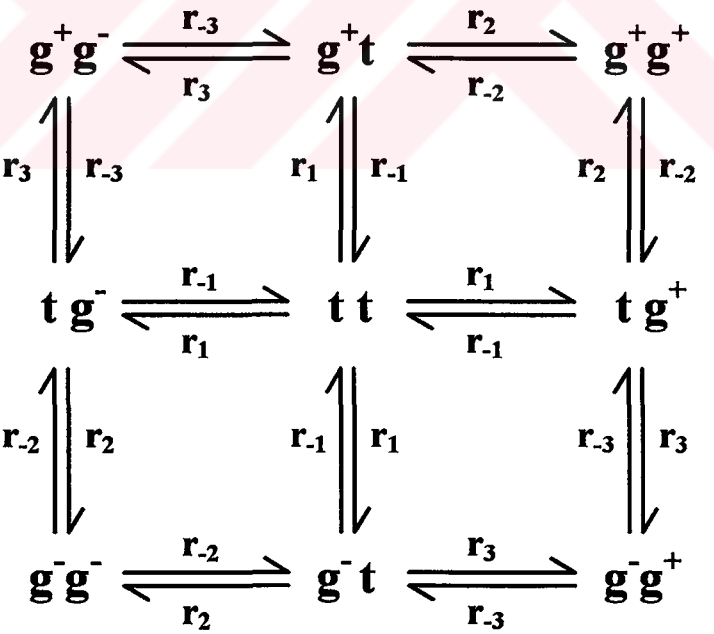

FIGURE 2.9. Kinetic scheme of PE with bond interdependence.

The transition probability $C(\zeta'\eta',t\,|\zeta\eta,0)$ may also be calculated by BD since for a stationary process, as presently studied, the time origin is immaterial, but the time interval t between two successive states is important. Thus, data recorded at various time origins along the trajectory are suitably combined to evaluate $C(\zeta'\eta',t\,|\zeta\eta,0)$, provided that $t \ll t^*$, where t^* is the total duration of simulation.

2.2.2. Cooperative Kinematics Model

In a recent series of papers[38,39,41], the correlated motions of chain atoms in dense media are investigated using CK. In these studies, the term dense media is used in reference to polymers in the bulk state, above glass transition temperature, where the femtosecond librations and fluctuations due to acceleration are neglected. The most probable trajectory of chain atoms accompanying the rotameric transitions of a given bond from one rotational isomeric minimum to another is obtained, by considering the torsional potentials and the frictional resistance exerted by the environment[41]. The basics of the CK method are outlined below.

The Lagrange equation of motion for a chain is expressed as

$$\frac{\mathrm{d}}{\mathrm{d}t}\left[\frac{\partial L}{\partial \dot{\boldsymbol{q}}_j}\right]-\frac{\partial L}{\partial \boldsymbol{q}_j}+\frac{\partial \mathscr{F}}{\partial \dot{\boldsymbol{q}}_j}=0 \qquad (2.21)$$

where $\boldsymbol{q}$ represents the set of generalized coordinates, the dot denotes the time derivative, L is the Lagrangian and $\mathscr{F}$ is the Rayleigh's dissipation function whose gradient with respect to the velocity of any atom gives the frictional force experienced by that atom. Backbone atoms are numbered from 0 to n+1. The set $\boldsymbol{q}$ includes the following variables: (i) the position vector $\mathbf{R}_o$ = col[X_o, Y_o, Z_o] of the zeroth atom relative to a laboratory-fixed coordinate system, (ii) the Euler angles, Φ, Ψ, χ, defining the absolute orientation of the chain in space, (iii) the internal torsional angles, φ_i. In a highly viscous medium, such as that

experienced by a polymer chain in the bulk state, the kinetic energy term in L and the acceleration contribution may be neglected, and the equation of motion simplifies to

$$\frac{\partial V}{\partial q_j}+\frac{\partial \mathcal{F}}{\partial \dot{q}_j}=0 \tag{2.22}$$

where V is the potential. Following this approximation, the problem of finding the optimal changes in the generalized coordinates in response to a torsional rotation reduces to the solution of

$$\left.\begin{aligned} &\frac{\partial V}{\partial \varphi_i}+\frac{1}{2}\frac{\partial \delta W_\xi}{\partial \delta \varphi_i}=0 \quad ; \qquad 2\le i\le (n-1)\\ &\frac{\partial \delta W_\xi}{\partial \delta \Phi}=\frac{\partial \delta W_\xi}{\partial \delta \Psi}=\frac{\partial \delta W_\xi}{\partial \delta \chi}=\frac{\partial \delta W_\xi}{\partial \delta \mathbf{R}_0}=0 \end{aligned}\right\} \tag{2.23}$$

Here δW_ξ denotes the differential work done by the chain against friction during small incremental displacements δR_i in chain units occurring within short time intervals δt. It is expressed in terms of the Rayleigh dissipation function and the effective friction coefficient ξ as,

$$\delta W_\xi = 2\mathcal{F}\partial t = (\xi/\partial t)\sum_i \partial \mathbf{R}_i \cdot \partial \mathbf{R}_i \tag{2.24}$$

A complete derivation of the above equations and a detailed presentation of the mathematical formalism of the CK approach is given in Appendix C.

According to the CK approach, a bond in the middle of the chain is rotated by small increments, and the new values of the remaining degrees of freedom are determined at each step from the simultaneous solution of the n+4 equations implicit in Equation 2.23. The incremental variation procedure is repeated until the rotating bond completes a full isomeric transition. This operation leads to the cooperative response of the all the chain elements in the particular original configuration to the rotational isomerization of the given bond. For assessing the general response of chain irrespective of the original configuration, it is essential to take average over an ensemble of minimum 500 chains. In MC generations, dihedral bond angles are assigned to each bond in conformity with the equilibrium distribution of rotational states of the polymer being investigated.

Results are conveniently expressed in terms of a dimensionless ratio relating the strength of the two factors affecting the mechanism of motion, *i.e.*, the frictional resistance and the internal rotational barriers, as

$$k_0 = \frac{2k_\varphi}{l^2 \xi / \Delta t} \tag{2.25}$$

where k_φ is the barrier height for the single bond rotation, l is the bond length, ξ is the friction coefficient. Δt is the mean time it takes for the isomerization to take place and is assigned a fixed value irrespective of the environmental conditions of the chain.

3. LOCAL MOTIONS IN POLYMERS

3.1. Contribution of Short-Range Intramolecular Interactions to Local Chain Dynamics

Short-range intramolecular interactions in polymers have been broadly classified as first and second order interactions (Appendix A). The former involves interactions between atoms separated by three bonds. The latter refers to those between atoms separated by four bonds. Chains composed of conformationally independent bonds are devoid of second order interactions.

The effect of second order interactions on equilibrium chain conformations in polymers has been addressed in numerous studies. In particular, the strong repulsive interactions between backbone atoms separated by four bonds when the middle two bonds assume *gauche* rotational states of opposite sign, have been recognized to significantly effect the equilibrium statistics of polyethylenelike chains, and commonly referred to as the "pentane effect" (Figure A.1). In what follows, the effect of such second order interactions on the *dynamics* of polymer chains are investigated. BD and DRIS are undertaken to assess the influence of bond interdependence on the mechanism of local motions. Comparison of DRIS predictions with simulations allows to establish the validity and/or limitations of the DRIS formalism, as far as the local conformational transitions of real chains are concerned.

In previous BD studies[5,9,22,62,63], backbone bonds were assumed to be subject to independent rotational potentials, i.e. no intrachain interactions other than chain connectivity and first order interactions along the chain were included. Cooperativity between torsional transitions of bonds i and $i+2$ emerged in these studies as a requirement for the localization of the motion along the chain, thus stipulating the intrinsic effect of chain connectivity and geometry. The role of intrachain cooperativity in conformational transitions has been addressed by Adolf and Ediger in the BD study of polyisoprene[24,51,63]. A recent review by Adolf and Ediger gives a comprehensive summary of the work done using BD method[47]. In the present work, the specific changes in the conformational dynamics of

PE chains arising from the inclusion of second order interactions are analyzed. The calculations are carried out so as (i) to compare simulations including second order interactions to those that do not, and (ii) to provide a possible assessment of the validity of the DRIS formalism as a first approximation for treating local chain dynamics. Furthermore, the contribution of neighboring bond interdependence to the type and frequency of correlated transitions of longer range along the chain is analyzed.

In carrying out the comparison mentioned in item (i) above, results from two classes of calculations are utilized: The chain model with independent bonds using *only* V_l, V_θ and V_φ (Equations A.2-A.4) will be referred to as Model I. In Model II, on the other hand, interactions between chain atoms separated by four bonds leading to pentane effect, are included. In this chain model such interdependent bonds which are characterized by the LJ potential (Equation A.5) in addition to the potentials given by Equations A.2 - A.4 are operative. In the present work, $V_{LJ}(r_{ij})$ will be taken as zero for $|j - i| \geq 5$. Thus, interactions between atoms that are close in their location in space but far from each other along the contour of the polymer are not considered in the calculations. These are called long-range interactions and a representative case is presented in Figure A.2. The simulations are carried out for polyethylene chains of $n + 1 = 50$ units at 300 K.

A first configuration of the chain is generated by Monte Carlo method using equilibrium values of bond lengths and bond angles. For the calculations with Model II, the occurrence of $g^{\pm} g^{\mp}$ states in the original conformer is excluded, to avoid a highly unfavorable energy state. The integration time step is chosen as 5×10^{-6} ns which gives satisfactory convergence to equilibrium values. Equilibration runs of 10^5 time steps (0.5 ns total duration) are made in order to achieve more realistic orientations in space to use at zero time. Results are recorded every 1000 steps until a 25 ns trajectory is performed. Calculations in Sections 3.1.3 and 3.1.4, require investigating very short time dynamics for which simulations with 5×10^{-7} ns time steps are performed for a total duration of 50 ns in the form of six independent trajectories, with results recorded every 200 steps.

3.1.1. Probability Distributions of Bond Torsional Angles

First the distribution of bond rotational angles resulting from simulations is considered. The *trans* probabilities are obtained as 0.669 and 0.738, using Models I and II

respectively (Table 3.1). These are evaluated from the average over all bonds *i*, excluding the five terminal bonds at both ends, *i.e.* $6 \leq i \leq n\text{-}5$. Likewise, all equilibrium and transition probabilities reported below are determined from the average behavior of the same subset of internal bonds. Although the stretching, bending and torsion parameters are the same in both models, the *trans* population is enhanced in Model II. This is a direct consequence of the inclusion of second order interactions. The probability of *trans* conformers obtained for Model II agrees with the molecular dynamics (MD) value of 0.718 calculated by Rigby and Roe[64] for 20-segment chains at 301K.

TABLE 3.1. Probabilities of various states[a]

state	probability (Model I)	probability (Model II)
t	0.669	0.738
tt	0.445	0.512
$tg^{\pm}$ or $g^{\pm}t$	0.113	0.111
$g^{\pm}g^{\pm}$ or $g^{\mp}g^{\mp}$	0.026	0.018
$g^{\pm}g^{\mp}$ or $g^{\mp}g^{\pm}$	0.026	0.0014

a) $g^{\pm}$ means g^{+} and g^{-} states may be used interchangeably.

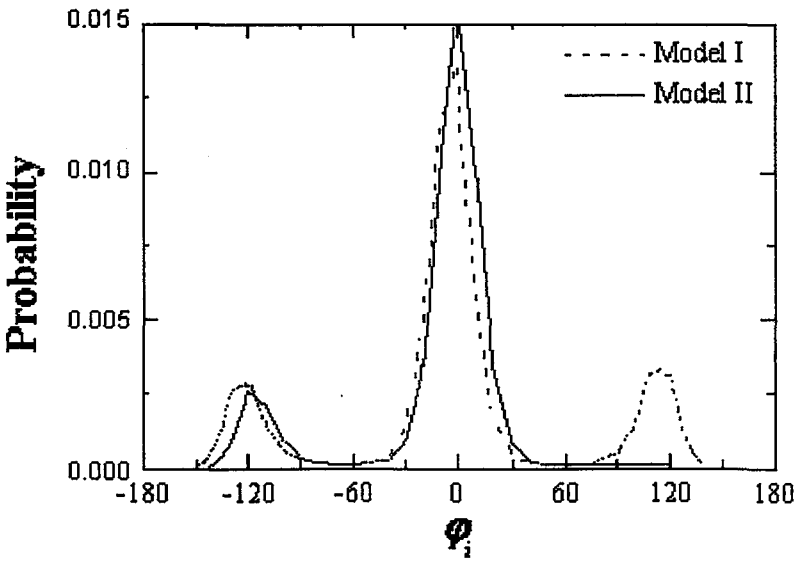

FIGURE 3.1. Probability distribution of bond dihedral angles given that state $\varphi_{i+1} = -120°$.

The equilibrium probability distributions $p(\varphi_i, \varphi_{i+1})$ for the joint state of two consecutive dihedral angles, φ_i and φ_{i+1} exhibit the difference between Models I and II clearly. The cross-section at -120° of the two-dimensional probability distribution surface resulting from Models I and II is displayed in Figure 3.1.

The peaks belonging to g^+g^- and g^-g^- are identical therein for Model I. In the curve for Model II, however, the peak belonging to g^+g^- is absent altogether. The energy difference between these two distinct states, E_ω, may be estimated from

$$E_\omega = -RT \ln\left[\frac{p_{g+g-}}{p_{g+g+}}\right] \tag{3.1}$$

where (p_{g+g-}/p_{g+g+}) is the ratio of the equilibrium probabilities p_{g+g-} and p_{g+g+} of the respective rotameric states $g^\pm g^\mp$ and $g^\pm g^\pm$ for consecutive bonds. The probability of a state is evaluated from the volume element enclosed under the corresponding peak in the normalized probability distribution surface[16,61,66]. For example, p_{g+g-}, is evaluated from

$$p_{g+g-} = \frac{\int_{-\pi}^{-\pi/3}\int_{\pi/3}^{\pi} p(\varphi_i, \varphi_{i+1}) d\varphi_i d\varphi_{i+1}}{\int_{-\pi}^{\pi}\int_{-\pi}^{\pi} p(\varphi_i, \varphi_{i+1}) d\varphi_i d\varphi_{i+1}} \tag{3.2}$$

the integration therein being approximated by summation over grids of size 10°. The probabilities of various states calculated accordingly by adding up discrete probabilities at the center of surface elements of 10°x10° intervals, are also presented in Table 3.1. In Model I, there is no difference between the probabilities of $g^\pm g^\mp$ and $g^\pm g^\pm$ states, and hence $E_\omega = 0$. In Model II, on the other hand, an E_ω value of 1.54 kcal/mol is obtained by using equations 3.1 and 3.2. A more rigorous relationship which makes use of interdependent probability distribution surfaces of the MD trajectories for the formulation of statistical weight matrices

is given by Mattice et al[65]. Using that scheme, E_ω turns out to be 1.47 kcal/mol. Note that in the original work of Abe, Jernigan and Flory[66] a value of $E_\omega = 2.0$ kcal/mol is adopted. The use of a lower E_ω has the effect of reducing the characteristic ratio of PE, although this effect may be more than counterbalanced by varying the equilibrium dihedral angle $\varphi_{g\pm}$ of the $g^\pm$ state. Ranges of parameter E_ω affording good agreement with experiments on characteristic ratio and its temperature coefficient are pointed out[42] to be $1.7 \leq E_\omega \leq 2.0$ kcal/mol for $\varphi_{g\pm} = \pm 120°$ and $1.3 \leq E_\omega \leq 1.6$ kcal/mol for $\varphi_{g\pm} = \pm 112.5°$, which are in satisfactory agreement with the value $E_\omega = 1.51 \pm 0.04$ kcal/mol presently obtained.

3.1.2. Conditional Probabilities of Rotational Transitions

3.1.2.1. Comparison of BD Results from Models I and II. Time-dependent conditional probabilities of bond rotations give information both on the dynamics of transitions between isomeric states and on their equilibrium probabilities. The conditional probabilities, $C(\zeta'\eta',t|\zeta\eta,0)$, are obtained by tabulating the total number of initial and final states assumed by two consecutive bonds at various time differences t and then dividing these by the sum of the 81 different transitions recorded.

TABLE 3.2. Most probable pairs of initial and final states[a]

type of states	$\zeta\eta \rightarrow \zeta'\eta'$
1	$tt \rightarrow tt$
2	$tg^\pm \rightarrow tg^\pm$
3	$g^\pm g^\pm \rightarrow g^\pm g^\pm$
4	$g^\pm g^\mp \rightarrow g^\pm g^\mp$
5	$tg^\pm \rightarrow tt$
6	$tt \rightarrow tg^\pm$
7	$g^\pm g^\pm \rightarrow tg^\pm$
8	$g^\pm g^\mp \rightarrow tg^\mp$
9	$g^\pm g^\mp \rightarrow tt$
10	$tg^\pm \rightarrow g^\mp t$

a) In cases 1-4 the states of the bonds remain unchanged; cases 5-10 refer to rotational transitions of one or both bonds of the pair.

Table 3.2 gives a list of the most probable transitions of pairs of adjacent bonds, $\zeta\eta \rightarrow \zeta'\eta'$. Here ζ and η stand for the rotational isomeric states t, g^+, g^-. In the transitions 1 - 4, the original pair of rotameric states $\zeta\eta$ is identical to the final state $\zeta'\eta'$. Thus, in a strict sense, those are not passages between rotameric states but refer to the cases in which the state of a given bond pair remains unchanged.

First, the time evolution of $C(\zeta'\eta',t \mid \zeta\eta,0)$ in the absence of bond interdependence is studied. The results for those cases with $\zeta'\eta' = \zeta\eta$ and $\zeta'\eta' \neq \zeta\eta$ are presented in Figures 3.2(a) and 3.2(b), respectively.

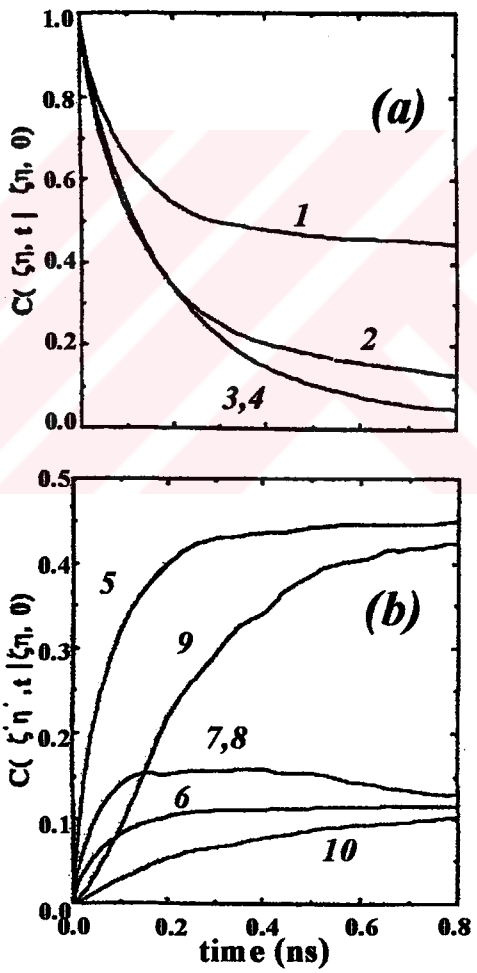

FIGURE 3.2. Time-dependent conditional probabilities of bond pairs subject to independent rotational potentials. (a) Initial state of bond is maintained; (b) initial and final states are different. See Table 3.2 for the definition of the curve labels.

In these figures, the values asymptotically approached represent the equilibrium probabilities of the state $\zeta'\eta'$ and are consistent with the values in Table 3.1. It is also worth noting that in all the curves, equilibrium probabilities have been reached within 1 ns. The transitions $g^{\pm}g^{\pm} \rightarrow g^{\pm}g^{\pm}$ and $g^{\pm}g^{\mp} \rightarrow g^{\pm}g^{\mp}$obey identical kinetics in the absence of secondary interactions; these are represented by the curve labeled 3,4 in Figure 3.2(a). This follows from the equivalence of $g^{\pm}g^{\pm}$ and $g^{\pm}g^{\mp}$states when bond interdependence is neglected. The same is true for transitions $g^{\pm}g^{\pm} \rightarrow g^{\pm}t$ and $g^{\pm}g^{\mp} \rightarrow g^{\pm}t$ (in Figure 3.2(b), curves 7,8).

The counterpart of Figure 2(a) in the presence of second order interactions is Figure 3.3(a). That of Figure 3.2(b) is presented in two distinct figures, 3.3(b) and 3.3(c), for clarity. The major difference between results from Models I and II is observed in the time evolution of the pair of *gauche* bonds. In Model II, the passage $g^{\pm}g^{\mp} \rightarrow g^{\pm}g^{\mp}$ (Figure 3.3(a), curve 4) is distinct from $g^{\pm}g^{\pm} \rightarrow g^{\pm}g^{\pm}$ (Figure 3.3(a), curve 3), there is an immediate escape from the state $g^{\pm}g^{\mp}$and the corresponding low equilibrium value is quickly reached. One can also observe that the transition probabilities for the passages $g^{\pm}g^{\pm} \rightarrow g^{\pm}t$ and $g^{\pm}g^{\mp} \rightarrow g^{\pm}t$ (*i.e.* Figure 3.3(b), curve 7, and Figure 3.3(c), curve 8) reach a maximum at short times, before converging to the equilibrium probability of the $g^{\pm}t$ state. In particular, that of $g^{\pm}g^{\mp} \rightarrow g^{\pm}t$ is very pronounced, in contrast to the time dependence of the same transition displayed in Figure 3.2(b) in the absence of second order interactions along the chain.

In the transition curves for the Model II, the fluctuations in the time evolution of the passage $g^{\pm}g^{\mp} \rightarrow tt$ and $g^{\pm}g^{\mp} \rightarrow tg^{\pm}$ (Figure 3.3(c), curves 9 and 8) are due to the very small sample space of the $g^{\pm}g^{\mp}$ population. The $g^{\pm}g^{\mp} \rightarrow tg^{\pm}$ transition is affected by the strong tendency to escape from the $g^{\pm}g^{\mp}$ state, indicated by the short time peak in the 30 ps range in Figure 3.3(c). It has a time dependence separate from that of the $g^{\pm}g^{\pm} \rightarrow tg^{\pm}$ transition, whereas the two transitions are represented by the same curve for Model I, Figure 3.2(b).

The two transitions $g^{\pm}t \rightarrow tt$ (Figure 3.3(b), curve 5) and $g^{\pm}g^{\mp} \rightarrow tt$ (Figure 3.3(c), curve 9) exhibit similar time dependence in Model II provided that the oscillations induced by $g^{\pm}g^{\mp}$ state are overlooked. This phenomena is explained by the two-step character of transition 9, which occurs through the mechanism $g^{\pm}g^{\mp} \rightarrow tg^{\pm} \rightarrow tt$. Here, the first transition, (Figure 3.3(c), curve 8) is fast, and the second, which corresponds to transition 5 itself, is the rate controlling one. The same argument cannot be made for Model I, since the two steps of transition 9 evolve in comparable times. As a result, there are two distinct curves corresponding to transitions 5 and 9, as shown in Figure 3.2(b).

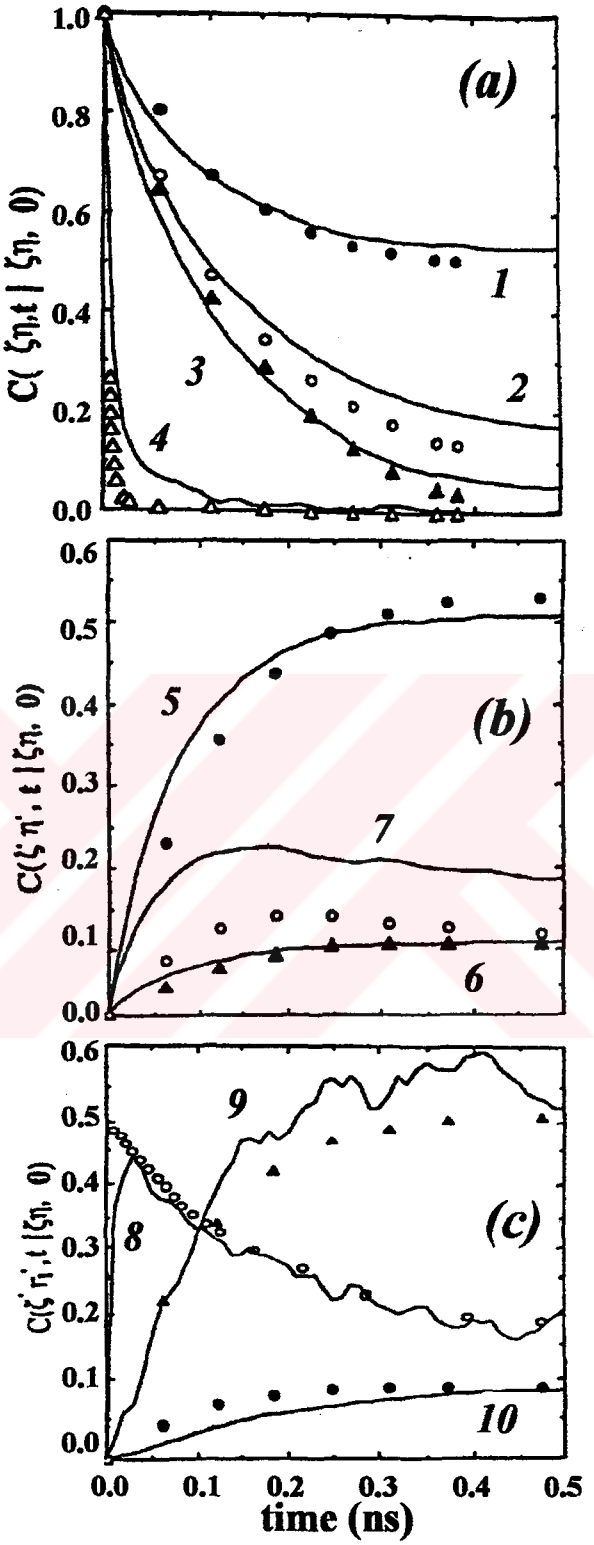

FIGURE 3.3. Time-dependent conditional probabilities of bond pairs subject to independent rotational potentials. (a) Initial state of bond is maintained; (b-c) initial and final states are different. Symbols represent DRIS results. The curve labels are defined in Table 3.2.

From the above comparison, it is deduced that the types and rates of rotational transitions taking place during the Brownian motion of real chains are rather sensitive to second order interactions along the chain. The second order interactions result in the coupling of the torsional states and transitions of neighboring bonds, and give rise to a mechanism of relaxation different from that observed in the absence of bond interdependence, as described above in terms of the time evolution of transition probabilities. Simulations with energy functions and parameters disregarding second order interactions along the chain, as has been performed in a number of BD studies, may lead to serious departure from real chain behavior and should be interpreted with caution.

3.1.2.2. Comparison of DRIS Results to BD Simulations. Results of DRIS calculations at 300 K are presented by the circles and triangles in Figures 3.3(a-c). The calculations are performed with the kinetic scheme and activation energy data given in reference 29. The basic assumption therein is the pairwise interdependence of bonds. In order to compare the results from DRIS approach with those of BD in the presence of bond interdependence, the front factor A_o (Section 2.2.1), which accounts for the frictional resistance to motion in the expressions for k_{ij}, is adjusted to match that of BD simulations ($\zeta = 10^5$ ns^{-1}). Hence, A_o is rescaled to fit the $tt \rightarrow tt$ decay curve (1) of the two approaches, which yields $A_o = 5.72 \times 10^{11}$ s^{-1}. Using this value in the rest of the calculations for all transitions, not only qualitative but also quantitative correspondence between DRIS model and BD simulations is accomplished.

In both techniques, equilibrium values are reached within 1 ns. DRIS predicts a slightly stronger tendency to escape from the $g^{\pm}g^{\mp}$ state compared to BD. This is attributed to the fact that part of the repulsive force produced in the $g^{\pm}g^{\mp}$ state is normally taken on by the distortions in the bond lengths and angles so that the escape from this configuration is weakened. However, these distortions are not included in the DRIS Method. The only transition where there is no quantitative agreement is $g^{\pm}g^{\pm} \rightarrow tg^{\pm}$ (Figure 3.3(b), transition 7). There, the passage through a peak is well predicted by DRIS but the equilibrium value of 0.11 is reached quicker than BD simulations. On the other hand, here BD simulations exhibit a faster rate of escape from the $g^{\pm}g^{\pm}$ state at short times. In all other curves there is good qualitative and quantitative agreement between the results from BD and those from DRIS. This proves DRIS to be a well suited method for the prediction of bond pair dynamics.

3.1.3. Near Neighbor Transitions

The importance of correlated transitions occurring among near neighbors along the chain have been pointed out in BD studies[15,24,62], and later discussed in MD simulations of Zuniga et al.[16]. Successive transitions occurring within 5 ps approximately, are identified as correlated transitions, in general. In the present study, first passage times between successive transitions have been accordingly analyzed in BD trajectories resulting from both Models I and II. Simulations of six different starting configurations, using ten times shorter time steps, *i.e.* 5×10^{-7} ns, have been followed up to a total duration of 50 ns. The regions determining the isomeric states have been identified as in reference 16 as $|\varphi_i| < 30°$ for t, and $90° < |\varphi_i| < 135°$ for $g^{\pm}$; the rest of the dihedral angles are assigned their last definite states. This procedure avoids the redundant counting of passages over saddle points, during the evaluation of first passage times between rotational isomeric states. A total of 12310 transitions have been recorded using Model I, whereas 13981 transitions occur during the same time interval, with the same initial configurations when Model II is used. Thus, the presence of a high energy state ($g^{\pm}g^{\mp}$) renders the chains of Model II more susceptible (by 14 per cent) to rotational transitions.

The time evolution of coupled transitions between near neighbors from six different trajectories of total duration 50 ns is shown in Figure 3.4.

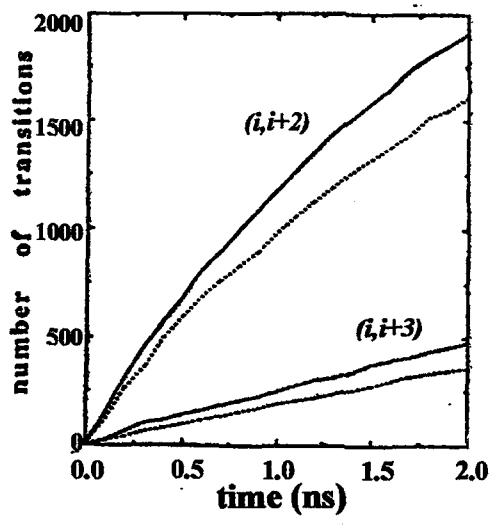

FIGURE 3.4. Time evolution of coupled transitions among second neighbors along the chain. The solid and dashed curves are obtained from BD simulations with Models I and II, respectively.

The solid curves in the figure are calculated using Model I, for the pair of second and third neighbors, as indicated by the labels; their counterparts obtained with Model II are shown by the dashed curves.

The curves in these figures are calculated according to the following procedure: First, the time at which a given bond k undergoes an isomeric jump is recorded; then, one observes the ith topological neighbor, and the time interval Δt elapsed until bond $k+i$ changes its rotational state is recorded. This procedure is repeated up to Δt = 2 ps, for all internal bonds in the chain, throughout the whole trajectory, except for the terminal five bonds, which are not considered because of end effects. The number of coupled transitions between second and third neighbors are found to increase by the interdependence of backbone torsional states, as may be observed from the deviations between the solid and dashed curves in Figure 3.4. In particular, the number of coupled transitions between third neighbors (i = ±3) increase by 42 per cent. Those between second neighbors (i = ±2) increase by 35 per cent. The results for i = 1 and 4, whose frequencies of occurrence were lower compared to i = 2 or 3, are not displayed in the figure, for clarity. Those of first neighbors (i = 1) are also augmented (by about 30 per cent) upon consideration of second order interaction, whereas the number of correlated transitions between fourth neighbors was almost insensitive to the model, suggesting that correlated transitions involving farther neighbors, if any, are less affected by second order interactions. Calculations performed for farther neighbors (i = 10, for instance) verified that the corresponding time evolution curves exhibit the same behavior as that of the overall ensemble of transitions (15 per cent deviation), and hence the rotational motion of such distant bonds are not affected by intramolecular correlations.

3.1.4. Mechanisms for Localization of Motion

When a transition occurs at one of the internal bonds of a chain, the near neighbors of the rotating bond rearrange so as to minimize the spatial displacements of the atoms and the total energy of the system. If a rotational jump of a reference bond is accompanied by small rotations (±30°) of the nearby bonds, this is called an *isolated* transition. Alternatively, the polymer may compensate for the energy difference created by a rotational transition by making a *cooperative* rotameric transition at one or more neighboring bonds. Well known mechanisms of the latter type are gauche migration ($g^{\pm}tt \leftrightarrow ttg^{\pm}$), gauche pair creation ($ttt \rightarrow$

$g^{\pm}tg^{\mp}$) and annihilation ($g^{\pm}tg^{\mp} \rightarrow ttt$) [4,62]. These are identified as motions where the remainder of the chain does not change shape but just translates.

Of the total number of transitions taking place within the 50 ns trajectories of Section 3.1.3, the percentage of isolated transitions is found to be 70.3 ± 0.05 per cent at 300 K, irrespective of second order interactions. Note that this proportion of isolated and cooperative transitions compares favorably with that obtained at 330 K by Weber and Helfand[61] in the absence of second order interactions (70.7 per cent).

Although the proportion of the cooperative transitions among all transitions is the same in both models, their distribution among different types of passages are different in the two approaches. For example, the numbers of the most frequently occurring types of second neighbor transitions are presented in Table 3.3. The last column indicates the percent change in the rates of those passages upon inclusion of second order interactions. There is a considerable increase in these transitions, which is substantially larger than the overall enhancement of transition rates (*i.e.* 14 per cent) in Model II. In particular, gauche pair annihilation, shown in the third row of the table, is found to increase by 27 per cent upon inclusion of second order interactions.

TABLE 3.3. Number of most probable cooperative transitions among second neighbors

transition	Model I	Model II	% increase
$g^{\pm}tt \rightarrow ttg^{\pm}$	957	1144	20
$ttt \rightarrow g^{\pm}tg^{\mp}$	395	479	21
$g^{\pm}tg^{\mp} \rightarrow ttt$	338	430	27

Note that in both models the frequency of gauche pair creation exceeds that of gauche pair annihilation. This might suggest at first sight some gradual increase and eventual saturation in the population of gauche states during simulations. However, it should be recalled that Table 3.3 is constructed for a subset of transitions only, mainly *cooperative* transitions among *second* neighbors. There is a much larger number of transitions, either isolated or cooperative between other neighbors, contributing to the equilibration of the population of different rotameric states, and maintaining the state of dynamic equilibrium (detailed balance) conforming with the specific chain statistics.

3.2. Kinematics of Polymer Chains in Dense Medium. Effect of Backbone Geometry and Application to Polybutadiene

The problem of cooperativity between the motions of chain units in polymers during the rotameric transition of a given bond is central to the study of local polymer dynamics. From spectroscopic measurements and numerical simulations, it is now known that the motions induced by rotameric jumps are highly localized in space for chains in the bulk state as well as for those in dilute solution[5,25,26,46,61,67]. The localization is established through correlations between the motion of the bond undergoing the rotameric transition and the neighboring atoms, either along the chain or in the surrounding medium.

Calculations show that the mechanism of localization involves three types of motions of neighboring bonds: (i) Correlated torsions. For PE, a rotational transition results in correlated torsions up to sixth neighboring bonds on each side of the rotating bond. The second neighbors show the strongest response in the form of a counterrotation. (ii) An overall reorientation, in space, of a few bonds including and adjoining the bond that undergoes the rotameric transition. In PE, the bond undergoing the rotameric transition is itself reoriented by about 25 - 35°. The first neighbors on each side exhibit the largest reorientations (~ 50 - 60°) and the extent of reorientations is vanishingly small beyond sixth neighbors. (iii) Displacement of atoms in space. For PE, mean translations of about 0.8 Å were observed in the atoms located at both ends of the rotating bond. These results, which are obtainable with a minimum computational effort by the CK approach, were shown to conform closely with those extracted from BD runs.

BD and MD simulations carried out for different polymers, and in particular the comparison of the results for PE and polyisoprene (PIP) [45], suggest that the local chain geometry is an important property determining the type and strength of intramolecular correlations. Here, the kinematics of PBD chains in dense environment is investigated in order to assess the possible importance of chain geometry. Due to the presence of double bonds and non-tetrahedral bond angles along the backbone, as well as the possibility of *cis* and *trans* isomers, the backbone geometry of these chains depart significantly from that of PE studied in references 38,39,41. In the following the results for PBD are compared with recent MD simulations of PBD[68,69] and of polyisoprene[25] in the bulk state. The predominant role of the backbone geometry in prescribing the mechanism of local conformational motions is emphasized.

3.2.1. Chain Model and General Calculation Procedure

A segment of a *cis*-PBD chain of n backbone bonds is presented in Figure 3.5. The backbone carbon atoms and their pendant hydrogens are taken as united groups. All bond lengths, l, and bond angles, θ, are fixed to their equilibrium values. Only the dihedral angles, φ_i, about the single bonds are assumed to rotate. The bonds labeled as α_1 and α_2 in the figure, are structurally equivalent and will be referred to as α bonds throughout the text. The rotatable CH_2 - CH_2 bond confined between two α bonds is termed as β type. The structure shown in Figure 3.5 corresponds to the *cis*-isomer. The *trans*-isomer is obtained by a 180° rotation about the double bonds. Thus, a repeat unit comprises of one double bond, one bond of type β and two bonds of type α.

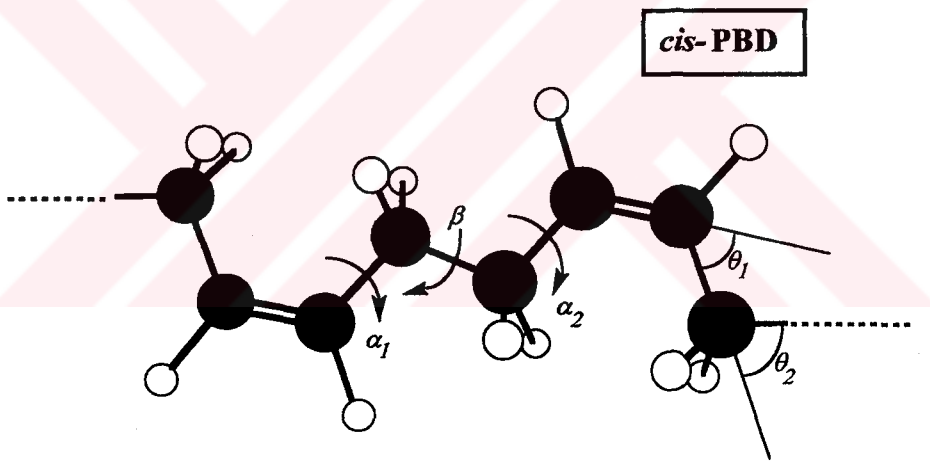

FIGURE 3.5. A segment of *cis*-PBD chain.

The rotational potential of each backbone bond is expressed as a polynomial in the form given in Equation A.4. The values of k_φ, and the coefficients a_m, are taken from reference 45. These are given in Table IV according to the type of bond considered. An average value of 1.5 Å is adopted for all bond lengths for computational simplicity, although in reality the double bond is shorter (~1.32 Å), the α bond is 1.53 Å and β is 1.51 Å. The supplements of the bond angles defined by CH-CH_2-CH_2 and CH-CH-CH_2 units are fixed at the respective values of $\theta_1 = 65.4°$ and $\theta_2 = 60.0°$.

In the calculations, the response of the chain to the rotation of either an α or a β bond is seeked. For this purpose, the procedure outlined in Section 2.2.2 is applied. 500 Monte Carlo (MC) chains are generated for the cases of all *cis*- or all *trans*-PBD, although averaging over 50 chains is verified to yield approximately the same results. Calculations are performed for $n = 25$ while no major differences are observed between the results for $n = 25$ and 39 bonds. This confirms that the motion is localized to only a few neighboring units.

The states accessible to different types of bonds and their probabilities are presented in Table 3.4[70-72]. In *trans*-PBD, there is a third order interdependence between the α_1 and α_2 bonds located within a repeat unit[70]. The conditional probabilities calculated from the statistical weight matrices provided in reference 70 are presented in Table 3.5. It is shown in the table that the conditional probabilities are rather close to those of the independent bonds presented in Table 3.5. In fact, the calculations show that results obtained using conditional probabilities differ insignificantly from those obtained by the use of independent probabilities.

TABLE 3.4. Rotational isomeric states of each type of bond in PBD and their equilibrium probabilities

Bond Type	Isomeric States[a] and Their Probabilities[b]		
α bond (*cis*-PBD)	A^+ (0.48)	A^- (0.48)	t (0.04)
α bond (*trans*-PBD)	A^+ (0.44)	A^- (0.44)	c (0.12)
β bond	t (0.38)	g^+ (0.31)	g^- (0.31)
double bond[c]	t / c (1.00)		

a) t: *trans* (0°); c: *cis* (180°); $A^{\pm}$: *anticlinal* (±60°); $A^{\pm}$: *gauche* (± 120°)
b) in parentheses
c) depends on *cis*- and *trans*- forms

In this study, the k_o value (Equation 2.25) must be carefully selected because there are three different types of bonds on the backbone and the rotational potential coefficient k_φ takes on distinct values depending on the bond considered (Table B.3). In order to compare the results obtained for PE and PBD at the same frictional environment, it proves convenient to fix k_φ of the β bond (8.09 kJ/mol) for all classes of bonds and rescale the a_m values.

In the following, *cis*- and *trans*-PBD are separately considered and their mechanisms of localization of motion in various environmental conditions are compared. The response to

120° rotation of each type of bond, α and β, in the middle of the chain are considered for both stereoisomers. In each case, the kinematics is analyzed from three perspectives: (i) changes in dihedral angles, (ii) angular displacement of backbone bonds, (iii) translation of chain atoms.

TABLE 3.5. Conditional probabilities for *trans*-PBD bonds in a repeat unit

State of $\alpha_1\beta$	State of α_2		
	c	A^+	A^-
ct	0.12	0.44	0.44
A^+t	0.12	0.44	0.44
A^-t	0.12	0.44	0.44
cg^+	0.12	0.44	0.44
A^+g^+	0.02	0.49	0.49
A^-g^+	0.02	0.49	0.49
cg^-	0.12	0.44	0.44
A^+g^-	0.02	0.49	0.49
A^-g^-	0.02	0.49	0.49

3.2.2. β Bond Isomerization

The β bond is composed of two tetrahedrally bonded CH_2 groups; this type of bond is common to PE and PBD, and therefore allows for the comparison of the behavior of PE, *cis*-PBD and *trans*-PBD chain segments, in response to the isomerization of the given type of bond. The localization mechanism for each of the three polymers is investigated for $k_o l^2$ = 0.01 Å^2 or $\xi/\Delta t$ = 1.62 x 10^8 kg/(mol·ns^2) which is approximately representative of the frictional resistance experienced by flexible chains in dense environment. The torsional motions of the neighboring bonds accompanying the isomerization of the β bond are presented in Figures 3.6(a - b).

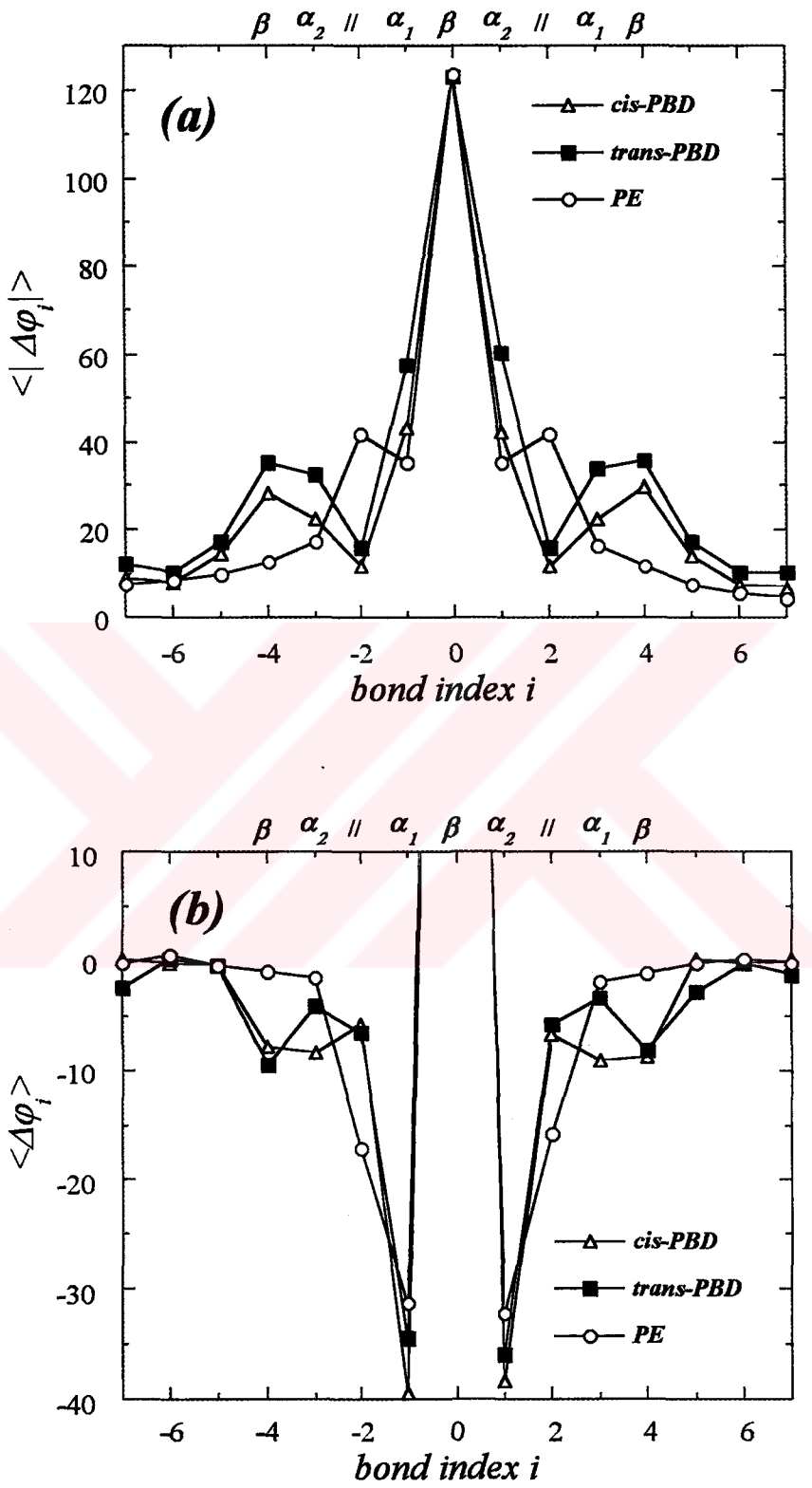

FIGURE 3.6. Average changes in the dihedral angles in response to β bond rotation. The absolute values are provided in (a).

In Figure 3.6(a), the change in absolute dihedral angles $<|\Delta\varphi|>$, averaged over 500 different configurations, is plotted as a function of serial bond index. The bond undergoing the torsional rotation is shown as the zeroth bond. For both *cis*- and *trans*-PBD, the response of the first neighbors, α bonds, is observed to be stronger than that of farther neighbors. This is different from the behavior of PE where the tendency of second neighbors to rotate is stronger. Also, in PE, the response of bonds beyond second neighbors is quickly lost while in PBD the torsional motion of the third and fourth neighbors are quite significant. That of the second neighbor, which is a double bond, is severely restricted.

In Figure 3.6(b), the actual values of torsional rearrangements resulting from the rotational transition of the zeroth bond are presented as a function of bond index. The full 120° rotation of the zeroth bond is not shown along the ordinate in order to see the rotations of the neighbors on a larger scale. The term *corotation* will be used in the following in reference to torsional motions of bonds in the same sense as the zeroth bond and *counterrotation* for those in the opposite sense. In PBD, the four nearest neighbors on both sides of the rotating β bond exhibit counterrotations of various amplitudes, whereas in PE the counterrotations are confined to the first and second neighbors only. The first neighbor exhibits the largest counterrotation (~35°) in all cases. The fourth neighbor, i.e. the β bond of the adjacent repeat unit, is the bond which exhibits the next strongest response in *trans*-PBD, whereas in *cis*-PBD, the counterrotations of the third and fourth neighbors are of comparable strength. Figures 3.6(a - b) already reveal that the coupling between bond rotational motions is not confined to nearest neighbors in PBD, but extends to third or fourth neighbors, departing from the behavior of PE bonds.

The spatial reorientations of backbone bonds accompanying the isomerization of the zeroth bond are presented in Figure 3.7. These angular displacements, including that of the bond undergoing the torsional transition, are postulated to play an important role in localizing the transition[41]. The zeroth bond is observed to reorient by 40-45° in PBD, which is slightly larger than that of PE. The spatial reorientation of the first neighbors for the *trans*- and *cis*-PBD are observed to be 50°, approximately, indicating that the angular change of 109.5° induced by the rotameric jump of the β bond is equally distributed among the first neighboring bonds on both sides. Interestingly, the α bond of the adjoining repeat unit, *i.e.* the third neighboring bond along the chain, exhibits a large amplitude spatial reorientation in PBD, and in *cis*-PBD in particular, which strongly departs from the behavior of PE.

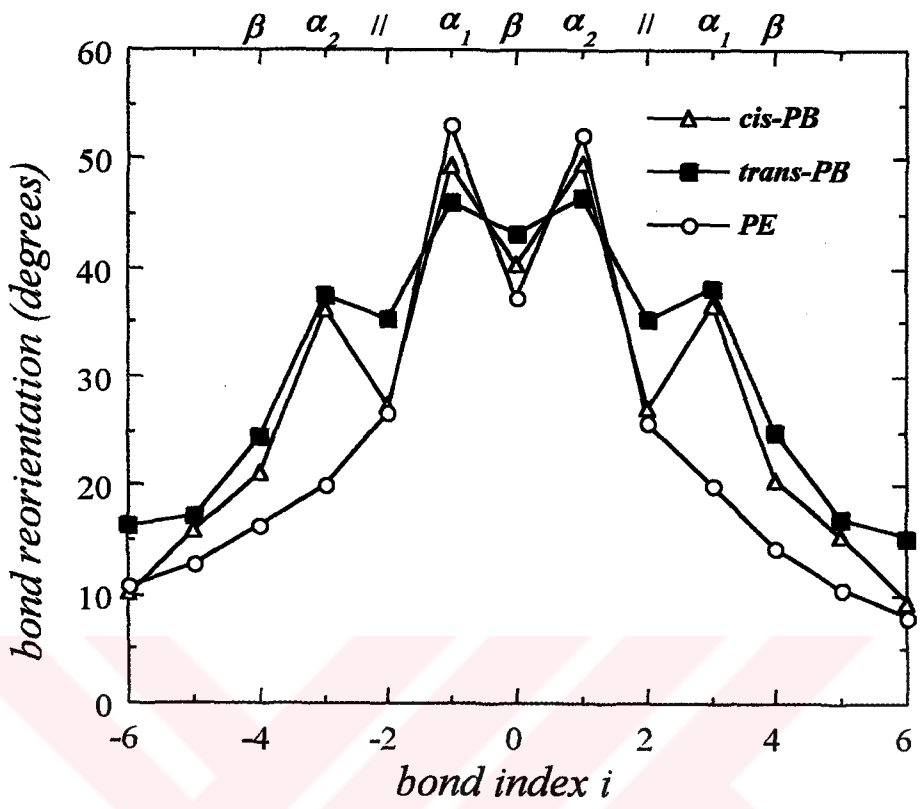

FIGURE 3.7. Average spatial reorientations of bond vectors in response to the rotation of β bonds.

The average translations of backbone atoms during the rotational isomerization of a central bond are presented in Figure 3.8. The ordinate represents the mean displacements of the backbone atoms while the β bond between the 13th and the 14th atoms undergoes a rotameric transition as indicated in the figure. The atoms directly attached to the rotating β bond go through the largest displacement, as expected: 1.2 Å for *trans*-PBD, 1.0 Å for *cis*-PBD. In *cis*-PBD, the next highest displacement (~ 0.8 Å) is observed in the 11th and 12th atoms, and their symmetric counterparts, 15th and 16th atoms. These are the atoms flanking the two closest neighboring double bonds of the rotating β bond. In *trans*-PBD, on the other hand, the largest displacement (~ 0.8 Å) among neighbors is observed in the 10th atom and its symmetric counterpart, *i.e.* the 17th. These are the atoms at the inner termini of the nearest β bonds along the chain.

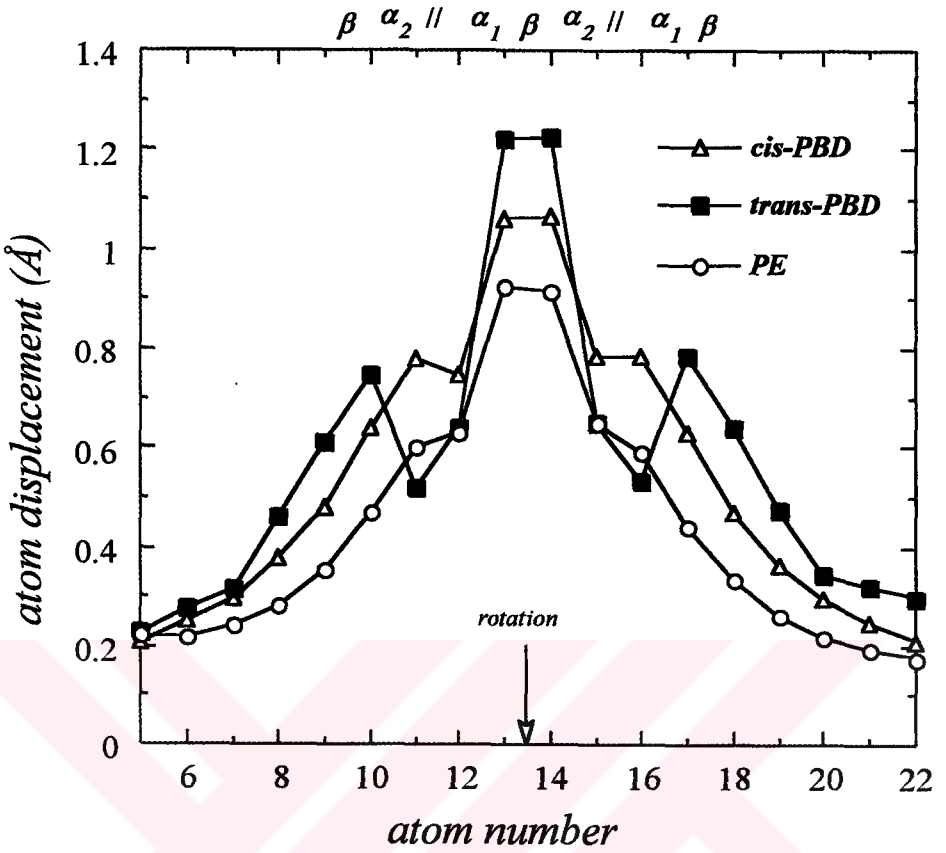

FIGURE 3.8. Average spatial displacements of chain atoms in response to the rotation of β bonds.

3.2.3. α Bond Isomerization

The torsional energy barrier associated with α bonds is significantly lower than that of β bonds (Table B.3), which implies that the rotational isomerization of α bonds is more frequent than that of β bonds. This property is also verified by the bulk simulations of Gee and Boyd[69]. The chain response is now asymmetric with respect to the rotating bond. The results are displayed for the rotation of α_1. The results for α_2 are symmetrically related and are not shown separately.

For comparative purposes, it is more convenient to examine the results obtained under the same frictional environmental resistance as in the previous section. This necessitates the readjustment of k_ϕ such that the ratio $\xi/\Delta t$ is held constant in analyzing either α or β bonds. Thus, we introduce the variable $k_\phi^* \equiv k_\phi\,(k_{\phi,\beta}/k_{\phi,\alpha})$ is introduced where $k_{\phi,\alpha}$ and $k_{\phi,\beta}$represent the torsional potential barrier heights for α and β bonds, respectively.

The absolute changes in the dihedral angles of *cis*- and *trans*-PBD bonds following the rotation of an α_1 bond, $\langle|\Delta\phi|\rangle$, are presented as solid curves in Figure 3.9(a) for $k_\phi^* l^2$ = 0.01 Å^2 or $\xi/\Delta t$ = 1.62x10^8 kg/(mol·ns^2). The dashed line is obtained for *cis*-PBD on the basis of a subset of conformations in which the excluded volume effect is taken into consideration; precisely, configurations involving non-bonded atom pairs ($|j - i| \geq 5$) closer than 3.8 Å are not included in the original set of MC chains. In intermediate or final steps, on the other hand, states violating excluded volume are verified to be rare, and are neglected. The excluded volume effect is negligibly small in *trans*-PBD chains of n = 25 presently explored.

In both *cis*- and *trans*-PBD, the response of the second neighbors (bond α_2) are found to be quite strong. In *cis*-PBD, the α_2 bond across the β bond exhibits the strongest response, whereas in *trans*-PBD, the nearest α_2 bond across the double bond is rotated by $|\Delta\phi| > 80°$, on the average. The response of the adjacent β bond (i = 1) and α_2 bond across the β bond (i = 2) in *cis*-PBD are significantly affected by volume exclusion.

A qualitative comparison of these results with those from the MD simulations of bulk PBD performed by Gee and Boyd[69] and Kim and Mattice[68] is possible. In the former study, the largest correlation when rotating an α bond is shown to occur between second neighbors, for both *cis*- and *trans*-PBD. A detailed analysis of the types of correlated (i, $i \pm 2$) transitions, where i is the rotating bond, is provided therein: These make up 30.1 per cent of all the α bond transitions in *cis*-PBD and 35.3 per cent in *trans*-PBD. Furthermore, among the coupled transitions between bonds i and $i \pm 2$, 2.6 times as many is reported[69] to occur across the β bond than across the double bond in *cis*-PBD, in qualitative accordance with the present results. This ratio is 0.5 in *trans*-PBD, *i.e.* correlated transitions occur most probably between α bonds separated by a double bond (i = 0 and -2), and not between those separated by a β bond as in the *cis*- form. These results are in agreement with the picture provided by CK theory in Figure 3.9(a).

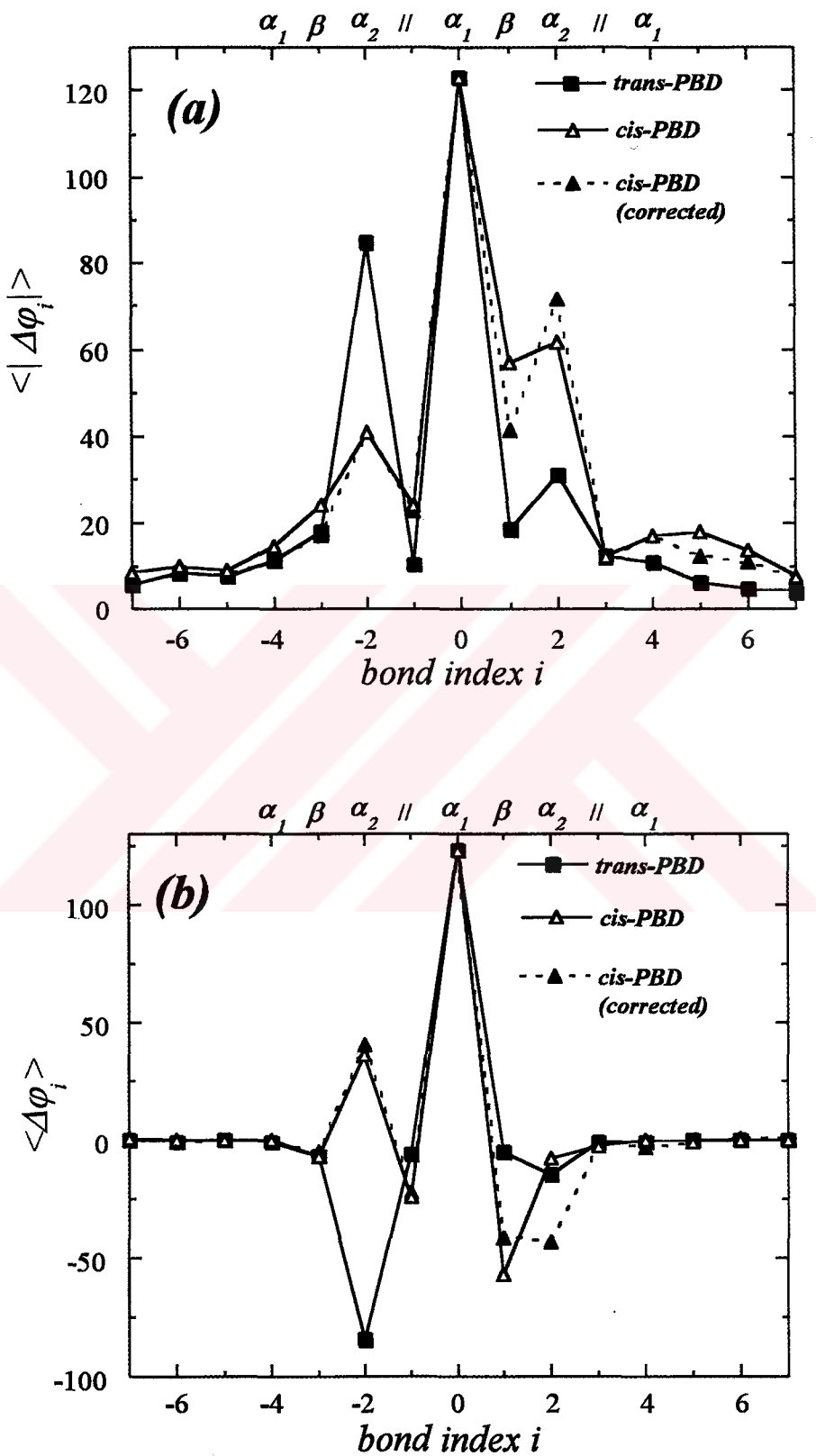

FIGURE 3.9. Average changes in the dihedral angles in response to α bond rotation. The absolute values are provided in (a).

Apart from the absolute changes in dihedral angles, the mechanism of coupling between local torsional motions may be assessed from the $<\Delta\varphi_i>$ curves displayed in Figure 3.9(b). Again, the dashed line is obtained by explicitly considering non-bonded interactions. In *trans*-PBD, the rotation of the α bond is accompanied predominantly by a strong (-80°) counterrotation of the second neighbor across the double bond. The other neighbors, which are demonstrated in Figure 3.9(a) to undergo some torsional motions in response to the isomerization of the zeroth bond, do not exhibit a distinct preference for counterrotation or corotation. The situation is different in the *cis*- form where corotations of the α bond across the double bond (i = -2) are observed. The first neighboring β bond (i = 1) exhibits a counterrotation, whose strength is diminished when excluded volume effects are considered. Likewise, the response of the other second neighbor, i.e. the α bond (i = 2) next to the β bond on the right, depends strongly on the original set of MC chains considered: a counterrotation is observed only if atoms in the generated chains do not violate their respective van der Waals radii (dashed curve). Neglect of the excluded volume effect leads to an underestimation of the response of that particular bond.

In *trans*-PBD, 67.2 per cent of correlated transitions between second neighbors are reported to occur between the pairs of α bonds flanking the double bond, and 95.8 per cent of them are manifested in the form of counterrotations[69]. That the strongest coupling between bond torsions in *trans*-PBD occurs between the pair of bonds flanking the double bond is unambiguously indicated by the CK results obtained for i = 0 and -2 in Figure 3.9(a); and that this coupling is in the form of counterrotations is clear from Figure 3.9(b). Also, the cooperative motion of bonds 0 and 2, *i.e.* the pair of α bonds flanking a β bond, is reported to involve counterrotations 62.3 per cent of the time, which is also consistent with the present results, where a weak tendency to counterrotate is observed in bond i = 2. The results concerning the behavior of second neighbors are in agreement with the findings of Kim and Mattice from MD simulations in a similar environment[68]. In the latter study, information on the nearest 10 neighbors on either side of the isomerizing bond within 400 ps of rotation in both *cis*- and *trans*- forms is given. The distribution provided by Figure 4 in Kim and Mattice, and that of the rotations of the dihedral angles for *trans*-PBD presented in Figure 3.9(b) show close agreement. In comparing the two pictures, note that the bond subject to full rotation in their study is α_2 in contrast to the α_1 bond rotated here. For this reason, the two figures are mirror images of each other with respect to the i = 0 axis.

In *cis*-PBD, on the other hand, only 17.9 per cent of all the correlated jumps across the double bond are in the form of counterrotations[69], *i.e.* the coupling between these α bonds (i = 0 and -2) is expressed by corotations, which is in conformity with present predictions. The type of correlations between the pair of α bonds separated by a β bond, on

the other hand, is shown in Figure 3.9(a - b) of the present work to depend on non-bonded interactions beyond nearest neighbors. Likewise, the coupling between adjacent α and β bonds exhibits some dependence on long-range interactions. MD simulations indicate that 90.9 per cent of the correlated motions between bonds α_1 and α_2 occur in the form of counterrotations. This is mainly due to the excessive occurrence of anticlinal pair inversion across the *trans* conformation of the β bond, $A^+ t A^- \leftrightarrow A^- t A^+$ transitions. A preference for counterrotation of the two α bonds is also indicated by the distribution of correlations obtained by Kim and Mattice. Such a preference for counterrotation is obtained in CK method only if long-range effects are approximately taken into account, as the comparison of the dashed and solid curves at $i = 2$ reveals. At the same time, the preferential response of the first neighbor (β bond, $i = 1$) is weakened. This trend is further enhanced if a subset of MC configurations is considered where the middle repeat unit is constrained to assume the state $A^+ t A^-$ in 90 per cent of the MC chains. Also, it will be demonstrated below that a slight reduction in the strength of intermolecular resistance to motion relative to intramolecular torsional barriers, *i.e.* decreasing $\xi/\Delta t$, improves the accord between CK predictions and MD simulations.

The above comparison of MD simulations and CK predictions lay evidence for the strong effect of long-range intramolecular interactions in *cis*-PBD which should be explicitly considered for a rigorous assessment of the conformational kinematics. The results for *cis*-PBD in the following are obtained accordingly. It should be noted that the results obtained from CK and MD are in good qualitative agreement in general, although the computational time requirement of CK approach is 2 - 3 orders of magnitude lower than that of bulk state MD simulations: The CPU time required by a CK calculation applied to 500 PBD chains with 25 bonds is only 470 seconds on a Silicon Graphics Challenge L series computer with 150 MHz R4400 CPU.

It is worth emphasizing that the localization mechanisms considered so far occur as a direct consequence of the backbone geometry rather than frictional factors or side group contributions. In fact, Moe and Ediger[25] have recently performed MD calculations for *cis*-PIP in the bulk. According to their calculations, the major response to the isomerization of an α bond is observed at the α bond across the β bond in the form of counterrotations, irrespective of the type of the α bond undergoing rotational isomerization. This is in exact agreement with our results. The response of an α bond with a CH_3 group in PIP was observed to be more sluggish, resulting from the enhanced frictional resistance due to the size of this group.

In Figure 3.10, the average reorientations of bonds in space following the isomerization of an α bond are presented for $\xi/\Delta t$ = 1.62x10^8 kg/(mol·ns^2). The central bond, which undergoes the torsional rotation, sweeps at the same time an average angular displacement of ~25° in space in both *cis*- and *trans*- forms. A striking difference in the behavior of *cis* and *trans* chains is observed upon examination of the reorientation of the bonds in the close neighborhood of the zeroth bond: In *trans*-PBD, average reorientations of ~65° and ~35° are undergone by the adjacent double bond (i = -1) and β bond (i = 1), respectively. The response of the first neighbors is totally reversed in *cis*-PBD. In addition, a considerable amount of reorientation (~30°) takes place in the second neighbor across the β bond as may be observed for the case of i = 2. This neighbor is an α_2 bond, like the rotating bond itself which suggests an enhanced cooperativity between the motion of α bonds across the β bond in *cis*-PBD, compared to *trans*-PBD.

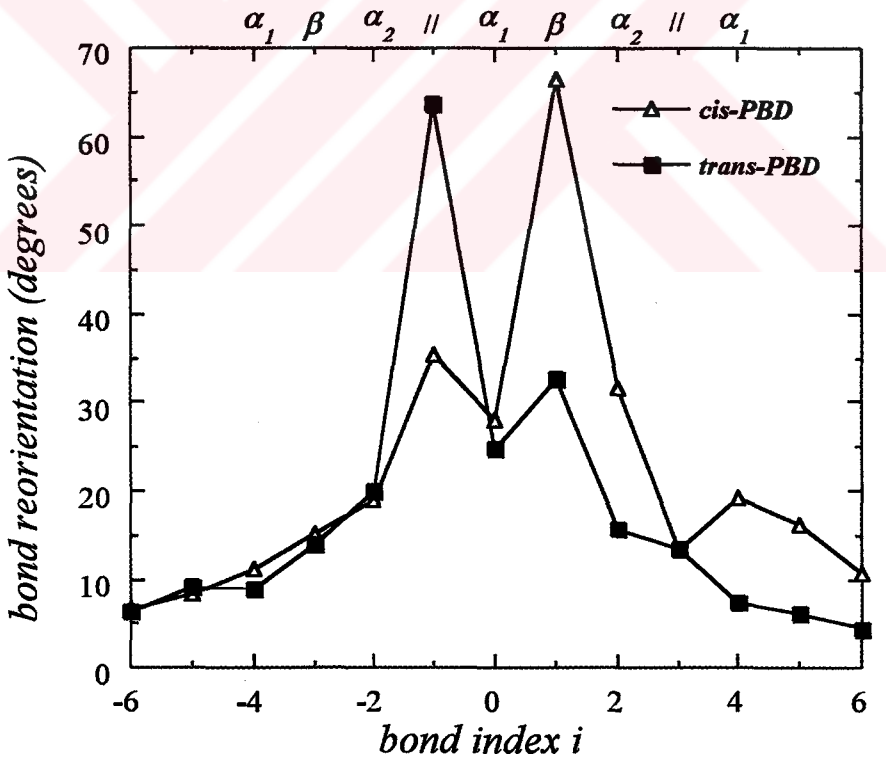

FIGURE 3.10. Average spatial reorientations of bond vectors in response to the rotation of α bonds.

In Figure 3.11, the displacements of backbone atoms are compared for *cis*- and *trans*-PBD. Calculations are again obtained from the average of 500 chains in the same frictional environment as before, *i.e.* $\xi/\Delta t = 1.62\text{x}10^8$ kg/(mol·ns^2). The atom displacements are in general higher in *cis*-PBD, although the frictional resistance is taken to be the same in both cases. Thus, on the basis of the response of the chain to the isomerization of an α bond, *cis*-PBD exhibits a larger amplitude motion compared to *trans*, which is inherently induced by the conformational state of the double bond.

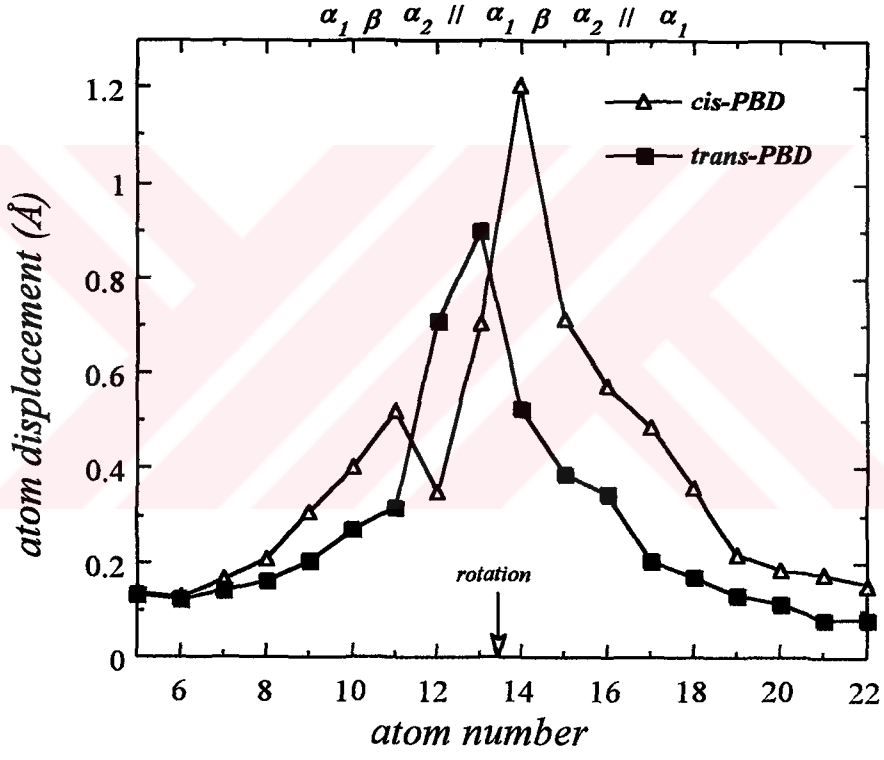

FIGURE 3.11. Average spatial displacements of chain atoms in response to the rotation of α bonds.

The area under the curves in Figure 3.11 may be viewed as a measure of the amplitude of local motion undergone by the associated polymer. The areas under the curves for *cis*- and *trans*-PBD are found to be 7.83 Å and 5.70 Å, respectively. Note that in Figure

3.8, which is the counterpart of Figure 3.11 for the case of a β bond undergoing isomerization, the areas under the curves are 9.19 Å for PE, 11.07 Å for *cis-PBD*, and 11.99 Å for *trans*-PBD. Thus, the rotational transition of an α bond induces a larger scale translation in *cis*-PBD segments, compared to *trans*-PBD, whereas that of the β bond results in a slightly more restricted motion in *cis*-PBD. In order to understand which of the rotations, α or β, plays a predominant role in prescribing the overall conformational kinematics of PBD, we turn to the MD simulations of Gee and Boyd[69]: Only 23.6 per cent of all transitions occur at the β bond of *cis*-PBD at 300 K in the bulk state and the remainder at α bonds. The situation is much more severe for *trans*-PBD where the percentage of rotating β bonds reduces to 1.8 per cent. These observed percentages is accepted to be proportional to the *a priori* probabilities of occurrences of the respective transitions. Within the limits of this approximation, the amplitude of local motions in *cis*-PBD appears to exceed that of *trans*- chains by a ratio of 1.48 : 1.00.

Another interesting feature, which emerges from both Figures 3.10 and 3.11 is that, in *cis*-PBD the most extensive cooperativity during the collective motion of chain segments takes place between units located in the same repeat unit (between two successive double bonds), and that the double bond somehow suppresses the propagation of the motion along the chain. This effect is not distinguishable in *trans*-PBD; on the contrary, the position and orientation of the double bond is observed to be significantly affected by the rotation of the adjoining bond, and apart from the strong reorientation of the double bond, the translational and orientational motions diffuse almost evenly on both sides of the rotating bond.

3.2.4. Effect of Environment

In a previous CK study[41], special attention was given to the effect of environment on chain behavior. It was demonstrated that the type of coupling between bond torsions depend on the interplay between intramolecular effects and environmental friction, accounted for through the ratio given by Equation 2.25. The precise values of the ratio corresponding to the bulk state simulations mentioned above are not known. It is of interest to find out if changes in the frictional resistance of the surrounding medium would induce modifications in the mechanism of various relaxation phenomena.

An examination of Equation 2.25 reveals that changing k_o is equivalent to a proportional change in the strength of internal barriers to rotation relative to frictional effects. In this section, the α bonds whose transition probabilities are higher due to the low barrier heights between rotameric states are considered. The analysis is further restricted to *cis*-PBD which is experimentally and commercially more important. In fact, negligible differences are observed in the localizing motions of *trans*-PBD; the governing mechanisms remain unaltered to changes in the environmental conditions in response to the isomerization of α bonds.

In the following, the $\xi/\Delta t$ value is varied by a factor of 20 between 1.62×10^7 - 3.24×10^8 kg/(mol·ns^2). Excluded volume effects are considered in generating the original chains in all cases. In Figure 3.12(a), the absolute changes in the dihedral angles, $<|\Delta\varphi|>$, of *cis*-PBD upon the manipulation of $\xi/\Delta t$ values are presented for the rotational isomerization of α_1 bonds. The corresponding $<\Delta\varphi>$ curves are given in Figure 3.12(b). An increase in $\xi/\Delta t$ is equivalent to increasing the strength of the frictional resistance relative to intramolecular torsional potentials. Alternatively, this may be viewed as diminishing the intramolecular barriers to rotation in a given environment and gradually approaching the behavior of a freely rotating chain of equilibrium statistics where internal rotational barriers have little importance and the dynamics is controlled by the surrounding medium. An examination of Figures 3.12 (a - b) shows that the mechanism of conformational relaxation is not affected by the frictional effects, in general. By adopting $\xi/\Delta t = 2 \times 10^7$ kg/(mol·ns^2), the behavior predicted by the MD simulations in bulk state is obtained, *i.e.* second neighboring α bond across the β bond undergoes the largest torsion in response to the rotation of an α bond.

The effect of changing environment on the reorientation of bond vectors is displayed in Figure 3.13. The $\xi/\Delta t$ values considered are in the same range as those of Figures 3.12(a - b). Excluded volume effects are taken into consideration in each case. The rotameric transition occurs at bond 0. Increasing the friction coefficient tends to decrease the reorientation of the neighboring β bond (i=1) while the reorientation of the first neighboring double bond (i = -1) and that of the nearest α bonds on both sides (i = ±2) increase.

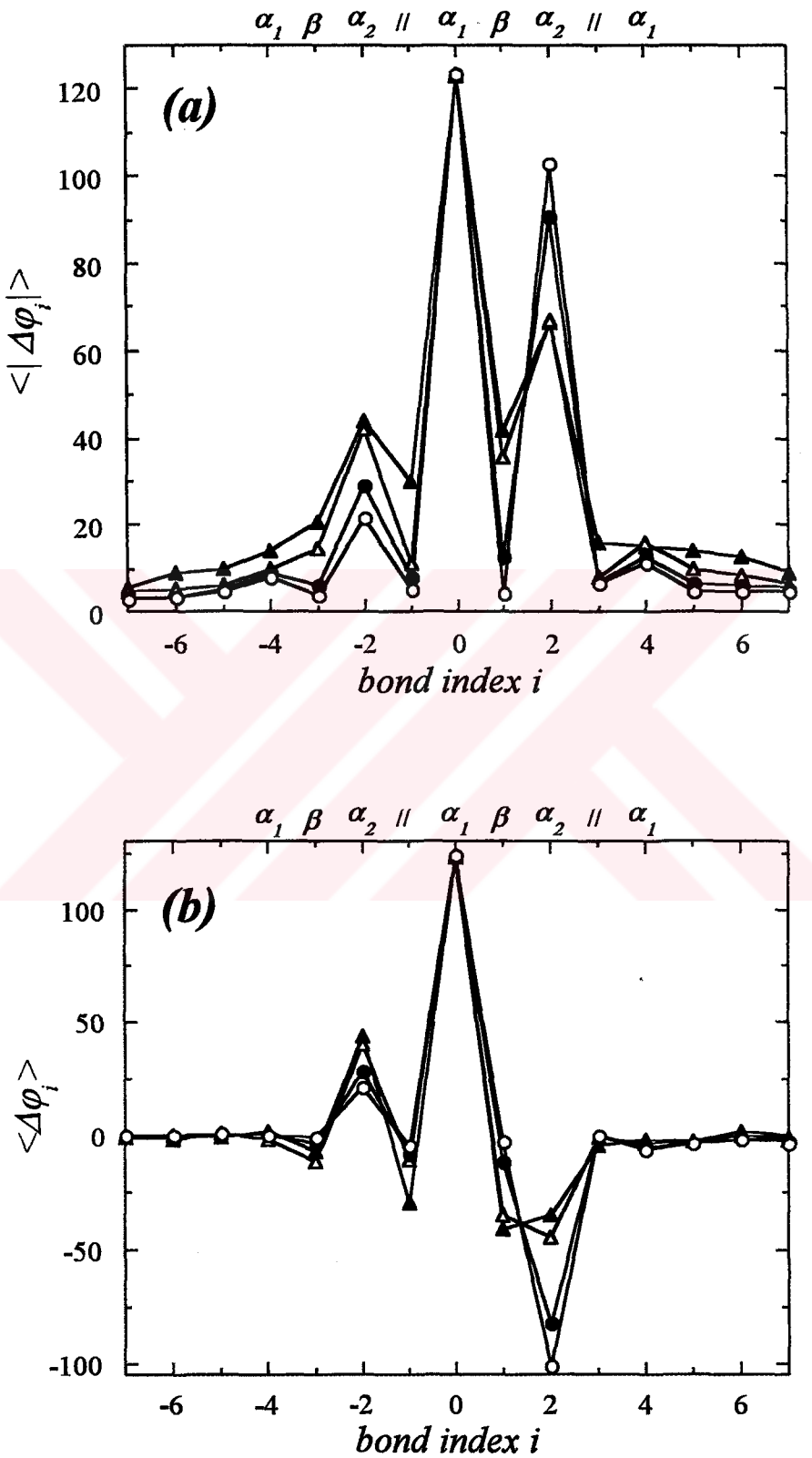

FIGURE 3.12. Effect of increasing friction coefficient on average changes in the dihedral angles of bonds of *cis*-PBD in response to α bond rotation.

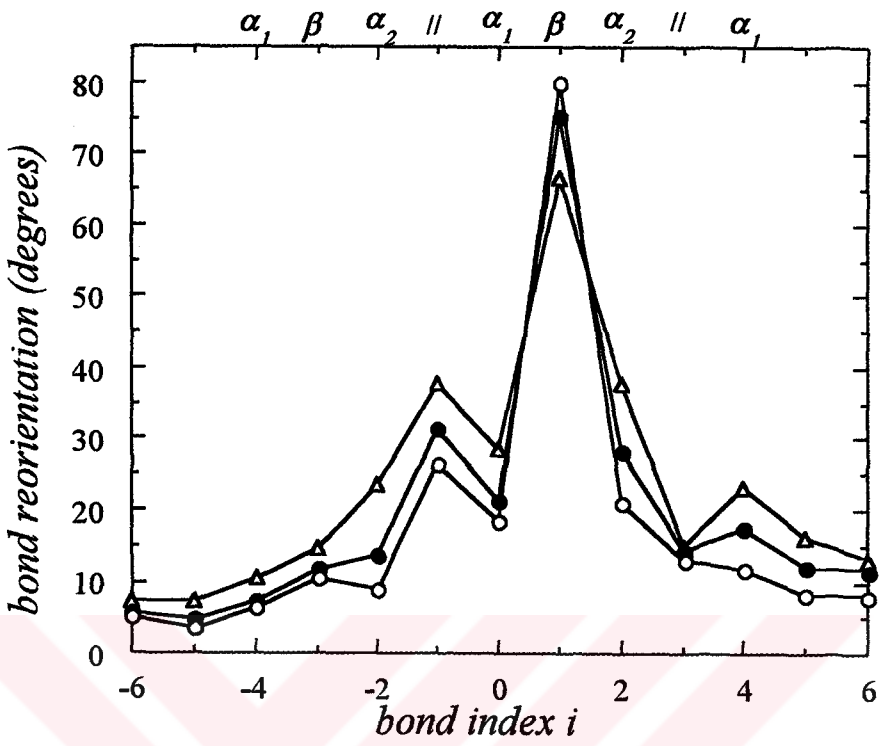

FIGURE 3.13. Reorientation of bond angles in response to α bond isomerization in various frictional environments for cis-PBD.

Another interesting feature which emerges in PBD chains irrespective of the type of conformer (*cis*/*trans*) or the type of bond going through rotameric transition (α/β) is that the reorientations and atomic displacements of the farther neighbors ($|i| \geq 6$) do not depend on the environmental friction. In a previous CK study[41] where the corresponding displacements of PE chains were investigated, some dependence of these localization mechanisms on friction coefficient was observed. This invariance in PBD chains is attributed to the constraints induced by the existence of rigid double bonds.

3.2.5. Energetic Calculations and Relative Isomerization Rates

Another key item that needs to be clarified is the isomerization rate of various bonds. Even though time is not explicitly involved in CK simulations, it is possible to resolve the

problem of relative isomerization rates by making use of the energy required to overcome barriers to internal rotation, $V-V_o$. In Figure 3.14 the cumulative evolution of this energy in response to the rotation of the two distinct types of bonds, α and β, is presented for the all-*cis* and all-*trans* stereoisomers.

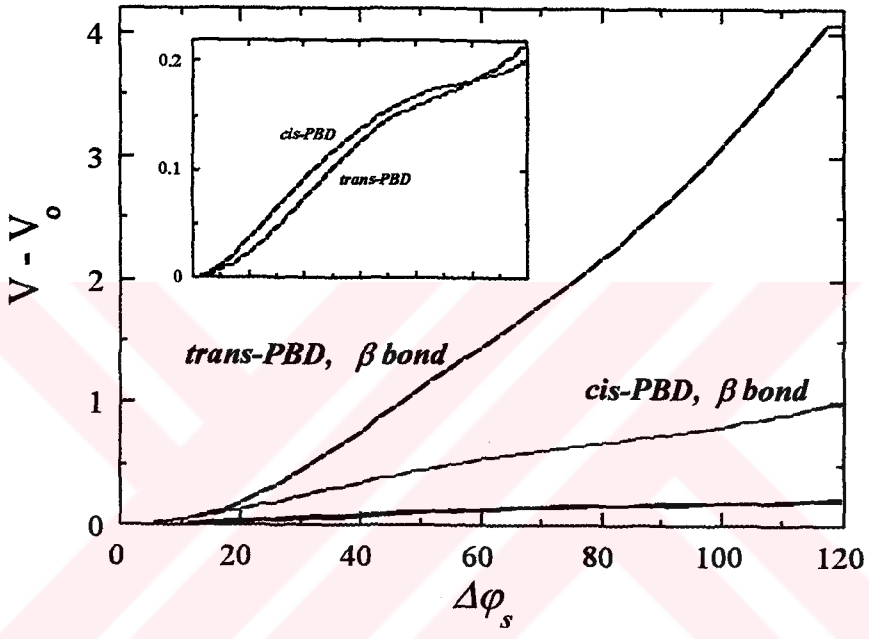

FIGURE 3.14. The cumulative evolution of the energy required to overcome barriers to internal rotation.

At the same temperature, the energy needed by the α bonds of both *cis*- and *trans*-PBD, enlarged in the inset, is about the same: they require almost equal amounts of energy to surmount the internal rotation barriers. Since these bonds have the same k_φ value, it seems plausible that this should be the case. However, the β bond in *trans*-PBD requires four times as much energy to accomplish the same type of isomerization as that in cis-PBD even though these two bonds also have the same k_φ. Thus, the barrier to rotation is not due to the rotating bond only but requires the collective contribution of its immediate environment. These results are in agreement with the MD findings of Kim and Mattice[68] in the bulk state which indicates that the difference in torsional relaxation between two rotatable bonds, α and β, is less pronounced in *cis*-PBD. Likewise, in the similar study of Gee and Boyd[69]

β bond transitions make up 1 - 5 per cent of all transitions in *trans*-PBD in the temperature range of 200 - 450 K whereas they occur 10 - 30 per cent of the time in *cis*-PBD over the same temperature range.

Examination of the energy spent against the environment, W, for the various transitions complements the information from V values that the β bond transitions in *trans*-PBD are very improbable both energetically and entropically ($W_{\alpha,cis}$ = 1.02 kcal/mol, $W_{\alpha,trans}$ = 3.08 kcal/mol, $W_{\beta,cis}$ = 3.77 kcal/mol, $W_{\beta,trans}$ = 23.7 kcal/mol). The subscripts denote the rotated bond and the isomer, respectively. The W values also indicate that the rate of conformational transitions of α bonds in *cis*-PBD should be faster. This is contrary to the findings of previous bulk MD simulations.[68,69] However, it must be born in mind that the potential functions used in all these studies are diverse. The fact that the overall quality of the results is the same contrary to the variety of the torsional potentials applied confirms the viewpoint that the local behavior of the polymers is controlled by chain geometry.

3.2.6. Copolymers of *cis*- and *trans*-PBD

Finally, CK is applied to copolymers of *cis*- and *trans*-PBD. Thus, the ξ value of the copolymers are necessary. Chen and Ferry have provided the diffusion coefficients, D, at room temperature for various microstructures[73]. Using the relation $\xi = k_BT/D$, and plotting per cent cis content versus log ξ, one obtains the linear relation

$$\text{per cent cis content} = -106 \log \xi - 650 \qquad (3.3)$$

through which ξ (in dyn s^{-1} cm^{-1}) for any microstructure is calculable.

In Figure 3.15(a), $\langle \Delta\varphi_i \rangle$ for the isomerization of the α_1 bond for polymers at various microstructures are shown, each under room temperature conditions. The responses of the neighbors occur as a distribution between the two extreme cases: pure *cis*- and pure *trans*-PBD.

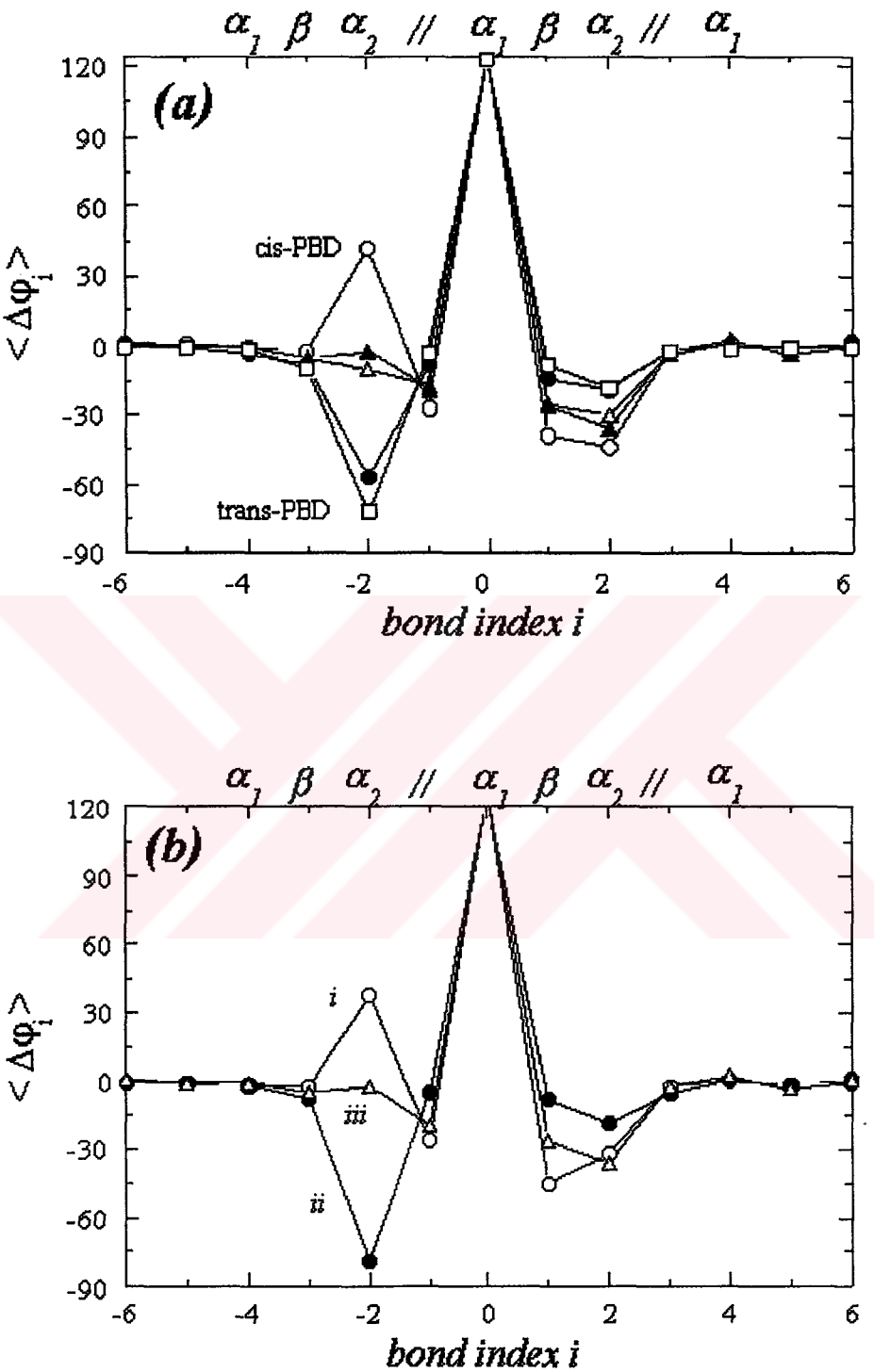

FIGURE 3.15. Average changes in the dihedral angles of bonds upon α bond isomerization (a) for polymers at various microstructures; (b) for 75 per cent cis content polymer and the rotating bond constrained to be in cis (i), trans (ii) states and with no constraints (iii).

The location of the *cis* and *trans* units within the polymer are random, *i.e.* the identity of the unit containing the rotating bond may be either *cis* or *trans*, occurring at the probability dictated by the microstructure. Next the case where the rotating bond is constrained to be within a particular type of monomeric unit is taken up. An example case for 75 per cent *cis* content copolymer is given in Figure 3.15(b) where the rotating bond in the sample chains are constrained to be either in *cis* or *trans* monomeric units (curves i and ii, respectively), or no such constraint is imposed (curve iii). In each constrained case, the behavior is similar to that of their pure polymer. This demonstrates that the rotation is localized and that only the near neighbors are influenced. An exception is observed in the constrained *cis* case where the relative strength of the 1st neighboring β bond and the α bond across the β bond (i = 1 and 2) are interchanged, *i.e.* the motion is even more localized. The curve (iii) corresponding to totally random sequences shows a behavior that is the weighted mean of the constrained cases. This implies that the behavior of the whole polymer is governed by the independent motions of each monomeric unit. Yet it is not possible to make such a strong statement by just examining the $<\Delta\varphi>$ curves. Another route is adopted to question this point further: Instead of performing the CK calculations using the friction coefficient ξ from Equation 3.3 which is characteristic of the given composition, each monomeric unit is subjected to the ξ value of its pure polymer depending on its identity. Surprisingly, the quantities calculated in the CK method are identical no matter which approach is adopted in the calculations. In fact, using the CK method it is possible to determine the ξ of copolymers of any composition from the knowledge of the ξ of their pure forms alone.

3.3. Modal Correlation Analysis of Coupling between Different Modes in Local Chain Dynamics

Local chain dynamics may be divided into two groups[25]: (1) High-frequency motions such as bond-angle bending, bond stretching, and small-amplitude oscillations about rotational energy minima of backbone bonds; and (2) bond rotameric transitions in the form of discrete jumps from one rotational isomeric state to another.

There is a growing interest in analyzing the first group of motions via normal mode (NM) analysis especially for biological macromolecules[74-76]. The overall motion is described therein as a superposition of a set of independent harmonic oscillators conforming

with a linearized analysis. The general nonlinear dynamics of the chain manifests itself in the combination of the first and the second groups of motions. Recently, Dauber-Osguthorpe and Osguthorpe[77] found a way to characterize the motion in MD simulations by using digital signal processing techniques. They first used Fourier transform (FT) to obtain the frequency distribution of the operating modes. Then, using filtering techniques, they focused on the frequency ranges of interest and eliminated the rest[78-80]. In addition, Levitt suggested an alternative filtering method that employs a smoothing function in time domain known as finite impulse response and takes considerably less computational time in programs[81].

The analysis of the trajectories in the frequency domain leads to the identification of *characteristic modes* of motion operating at different frequency ranges (windows). In analogy with eigenvectors describing the normal modes of linear systems in NM analysis, Dauber-Osguthorpe and Osguthorpe[77] have extracted vectors defining the characteristic motion for each frequency in MD simulations. Thus, the nonlinear motion is partitioned into its characteristic modes. The authors have observed for acetamide that in the absence of rotameric transitions, the eigenfrequencies obtained from NM analysis and the characteristic frequencies from MD almost coincide. These two approximations disagree if rotameric transitions are observed, which indicates the existence of correlations between the characteristic modes in the general nonlinear dynamics of the chains[82].

A generally accepted view of local chain dynamics of polymers is that the degrees of freedom with higher frequencies, such as bond stretching and bending, form a bath for those associated with lower frequencies, *i.e.*, for the rotameric transitions of backbone bonds. The extent of cooperativity between these motions is of utmost interest. Several pioneering studies by Moro[27,28] show that the librational motions operating after a transition contribute to the attainment of the new equilibrium state. This means that after a rotational jump, librational motions operating consecutively bring the chain to a new equilibrium configuration. Therefore, there must be a continuous kinetic energy transfer between the bath (librational motions at high frequencies) and the anharmonic oscillators of interest (rotameric transitions at low frequencies).

Cooperativity that is perceived as energy flow between pertinent modes of a given system is a well-studied problem introduced first by Fermi, Pasta, Ulam, and Tsingou[83]. The more recent reviews of the problem are given by Benettin[84] and Ford[85]. The proposed model of Fermi *et. al.*[83] holds for an isolated chain, and the energy is therefore preserved. It is now known that though the whole energy is initially given to a few modes of the chain, a significant amount of energy flow occurs from these initially excited modes to

other characteristic modes. The interest in analyzing the kinetic energy transfer from one chain atom along the backbone to another, using constant temperature MD simulations, originates essentially from the work of Fermi *et al.* It will be further important to identify the pertinent modes through which the chain backbone atoms communicate.

In the present study, the analysis of the coupling between various modes of frequencies will be performed on the basis of a *modal correlation function* the structure of which is inspired by the work of Noda and collaborators[86-88]. In their interpretation of two-dimensional infrared spectroscopy, Noda *et al.* define the absorptive-intensity cross-correlation function[86]

$$\chi(\nu_i, \nu_j, \tau) = \left\langle A'(\nu_i, t) A'(\nu_j, t+\tau) \right\rangle \tag{3.4}$$

in terms of a pair of time-dependent variations of IR signals or dynamic absorbance, $A'(\nu, t)$, measured at two different frequencies, ν_i and ν_j. Here $\chi(\nu_i, \nu_j, \tau)$ may be expressed as an n x n matrix for discrete frequencies with i = 1, 2, ..., n, and j = 1, 2, ..., n, for each τ. This correlation function is used to define two independent correlation spectra, $\Phi(\nu_i, \nu_j)$ and $\Psi(\nu_i, \nu_j)$, referred to as the synchronous and the asynchronous parts of the dynamic spectrum, respectively. The former characterizes the degree of coupling between the spectral intensities measured at two different frequencies, while the latter represents the sequential, or unsynchronized, changes in spectral intensities, and increases with the degree of incoherence. In the absence of a time delay τ, the asynchronous part vanishes. A method for decomposing Equation 3.4 into its synchronous and asynchronous parts and a discussion of the potential application areas are recently given by Noda[88]. A similar 2D spectral plane is used in the present analysis in order to understand the coupling between various modes of motion. The use of the FT of MD trajectories provides the frequency spectrum of the characteristic modes. The FT of the time series related to several properties such as kinetic energy fluctuations, atom displacements, bond length or angle oscillations, shows that the characteristic modes are not pure but are spread to overlapping frequency ranges, indicating the inherent nonlinearity of chain dynamics.

In the following, the modal correlation analysis is described and modes of interest lying in the lowest part of the frequency spectrum are examined. In Section 3.3.1, the basic

formalism and the computational methods used in the modal analysis are outlined. Then, the application of the present methodology to local chain motions is presented in Section 3.3.2. It will be shown that the strongest mode-mode coupling occurs between the lowest frequency modes of the spectrum associated with rotameric transitions; whereas the correlations between the characteristic modes belonging to distinct frequencies are weaker in general but are significantly enhanced during bond rotameric jumps.

3.3.1. Theoretical

3.3.1.1. Details of the Molecular Dynamics Method. The time evolution of chain properties, such as internal bond torsions or the kinetic energies of backbone atoms is generated by MD simulations. In order to exclude any effects but those coming from the chain itself, the simulations are carried out *in vacuo*. A PE chain of 100 CH_2 units with the hydrogen atoms collapsed onto the backbone carbon atoms is used. The effective potential consists of the bond stretching, bond bending, and bond torsion potentials as well as the interactions between non-bonded atom pairs that are within 1.2 nm cutoff distance of each other. The exact forms of the potentials are presented in Appendix A, and their parameters are given in Appendix B. The time evolved coordinates and velocities of the atoms are recorded at 4 fs intervals. 25 ps equilibration time is allowed in each run. Two independent runs are performed for each set of variables to ensure the reproducibility of the results. The temperature of the system is constant at 400 K.

Since the major part of the work consists of employing FT techniques, the total duration of the simulation and the time interval, δt, between each recorded set of data, *i.e.* the frequency of sampling in the time domain must be carefully selected. The resolution of the frequency domain is inversely proportional to the total duration of the simulation. Also, truncation of the periodic time domain function due to finite simulation duration gives rise to band broadening and artificially introduces additional frequency components, which are particularly pronounced in short simulations. On the other hand, the value of δt determines the highest frequency to be explored. When the whole frequency range is not covered, the high frequency components appear in a position below the maximum frequency. The details of these two phenomena referred to as *leakage* and *aliasing*, respectively, are provided by Dauber-Osguthorpe and Osguthorpe[79]. In order to avoid aliasing, δt is chosen as 4 fs, which corresponds to a maximum frequency of ~4170 cm^{-1}. The total duration of each

simulation is chosen as 131.072 ps yielding 2^{15} data points for each atom group. This duration satisfies the condition required by the Fast Fourier Transform (FFT) technique[89] that the number of data to be transformed should be a power of two.

3.3.1.2. Filtering Technique. The trajectories obtained from the MD simulations are stochastic. Yet, much valuable information is hidden therein. A portion of the time evolution of a torsional angle is displayed by the lowest curve (a) in Figure 3.16. It is evident from this curve that the torsional motion is made up of (i) librations about rotational minima of potential wells and (ii) occasional jumps between the minima. However, the exact nature of the motion is not well understood from this figure alone.

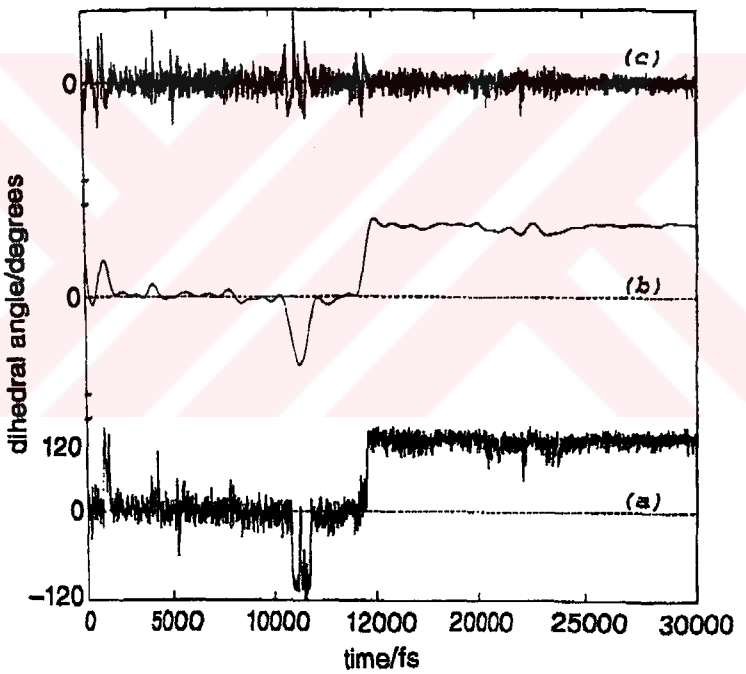

FIGURE 3.16. Effect of filtering on a given dihedral angle trajectory.

In order to determine the effect of various modes on the observed trajectory $A(t)$, a filtering method is applied, which consists of;

a) Fourier transforming the trajectory, $A(t)$, into the frequency domain,

$$\hat{A}(\nu) = \int_{-\infty}^{\infty} A(t)\exp(-j\nu t)\,dt \tag{3.5}$$

b) applying a filter function $F(\nu)$ which removes all the frequency components outside the range of interest by equating their values to zero,

$$\left.\begin{aligned} \hat{A}(\nu) &= \hat{A}'(\nu)F(\nu) \\ F(\nu) &= \begin{cases} 1; & \nu_{\min} < \nu < \nu_{\max} \\ 0; & \nu < \nu_{\min}, \nu > \nu_{\max} \end{cases} \end{aligned}\right\} \tag{3.6}$$

c) inverse Fourier transforming $\hat{A}'(\nu)$ back to the time domain so as to obtain the frequency filtered trajectory $A'(\nu_{\min} < \nu < \nu_{\max}, t)$ as

$$A'(\nu_{\min} < \nu < \nu_{\max}, t) = \int_{-\infty}^{\infty} \hat{A}'(\nu)\exp(j\nu t)\,dt \tag{3.7}$$

In the following, $A'(\nu_{\min} < \nu < \nu_{\max}, t)$ will be replaced by $A'(\nu_i, t)$ where ν_i symbolically represents the region between $\nu_{\min}$ and $\nu_{\max}$. Thus, a characteristic mode of frequency ν_i, which will be conveniently referred to as the *i*th mode, will be representative of all operating modes whose frequencies lie in the interval $\nu_{\min} < \nu < \nu_{\max}$.

In the curve (b) of Figure 3.16, the trajectory obtained with a low-pass filter of 20 cm^{-1}, *i.e.* by preserving only frequencies below 20 cm^{-1} is displayed. Here most of the librations are eliminated and the major component of motion is the isomeric transition. The curve (c), on the contrary, shows the trajectory with the frequency components below 20

cm^{-1} removed. This trajectory consists of mainly the librational motions of the original trajectory. From this simple analysis, it may be deduced that modes related to isomeric transitions are confined to the region below 20 cm^{-1}. This is only a rather small portion of the whole spectrum, which covers modes with frequencies as high as 4000 cm^{-1}. Low-pass frequency of 20 cm^{-1} is selected with the purpose of emphasizing the coupling between the rotational isomeric jumps and higher frequency motions. It should be noted that the amplitude of coupled fluctuations in curve (c) diminishes by the choice of threshold values ν > 20 cm^{-1}. The configurational space spanned by a subset of effective modes is called the *essential space* by Amadei *et al.*[90]. An interesting observation in curve (c) is the occurrence of relatively large amplitude oscillatory motions each time a rotational transition from one isomeric state to another takes place. This indicates the enhanced coupling between low and high frequency modes during the passages over the rotational energy barriers.

3.3.1.3. Filtered Kinetic Energy Trajectory of Backbone Atoms. The fluctuation $\Delta E_k(t)$ in the kinetic energy trajectory $E_k(t)$ of the kth atom is given by

$$\Delta E_k(t) = E_k(t) - \langle E_k(t) \rangle \tag{3.8}$$

where the angular brackets refer to the time average over the total sampling period. $\Delta E_k(t)$ is filtered using Equations 3.6 and 3.7 to obtain the frequency filtered trajectory of the kinetic energy fluctuations, $\Delta E'_k(\nu_i, t)$. The latter is averaged over all atoms as

$$\overline{\Delta E'(\nu_i, t)} = n^{-1} \sum_{k=1}^{n} \Delta E'_k(\nu_i, t) \tag{3.9}$$

The overbar here and in the following indicates averaging over all atoms.

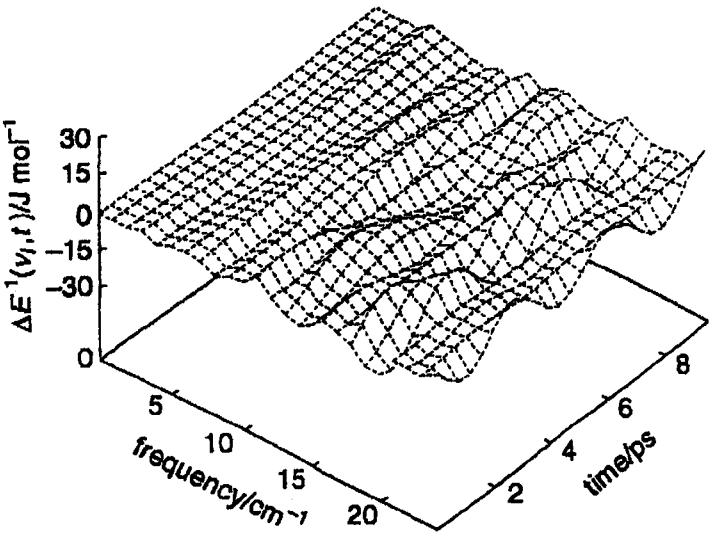

FIGURE 3.17. Time-resolved spectra of fluctuations in kinetic energy.

Results of calculations based on Equation 3.9 are presented in Figure 3.17. 25 non-overlapping frequency intervals of width ν_{max} - ν_{max} = 1 cm^{-1}, in the range 0-25 cm^{-1} are considered for filtering the trajectories. The two-dimensional plot displays the time evolution of the kinetic energy fluctuations induced by each of the characteristic frequency range. The average kinetic energy fluctuations of the chain atoms, $\overline{\Delta E'(\nu_i,t)}$, exhibit periodic fluctuations as time proceeds, the wavelength of which decreases as higher frequency domains are approached. This feature may be verified by examining the time evolution of various constant frequency slices.

3.3.1.4. Modal Correlation Function. The correlations between the fluctuations in the kinetic energies of pairs of atoms will be expressed by the *modal correlation function* defined as

$$\chi(\nu_i,\nu_j,l,\tau)=\left\langle \overline{\Delta E'_k(\nu_i,t)\Delta E'_{k+l}(\nu_j,t+\tau)} \right\rangle \qquad (3.10)$$

where the subscript $k+l$ refers to the lth neighbor of atom k. $\chi(\nu_i, \nu_j, l, \tau)$ gives the correlation between the kinetic energy fluctuations of an atom k induced by modes of a given frequency ν_i and that of the lth neighbor driven by another frequency ν_j after a time delay, τ. Note that the correlation involves averaging over both original time (t) and space (k) indicated by the angular brackets and the overbar, respectively. A positive correlation means that an increase (or decrease) in the kinetic energy of the kth backbone atom associated with modes of frequency ν_i is accompanied, after a time delay of τ by an increase (or decrease) in the kinetic energy of its lth neighbor, which is contributed by mode of frequency ν_j. A negative correlation means a negative (or positive) contribution from the ith mode to the kinetic energy of the kth atom is accompanied by a positive (or negative) change in kinetic energy of its lth neighbor, induced by mode j. A zero value for $\chi(\nu_i, \nu_j, l, \tau)$ means no correlation between the ith and jth modes operating on the kinetic energy fluctuations of the two atoms.

3.3.1.5. Modal Correlation Matrix. When the time interval τ and the neighbor number l are fixed, the correlation function of Equation 3.10 defines a matrix of modal correlations with two independent axes of spectral variables, ν_i and ν_j. Such a correlation matrix may be readily decomposed into its symmetric and antisymmetric parts as

$$\Phi(\nu_i, \nu_j) = \left[\frac{\chi(\nu_i, \nu_j) + \chi(\nu_i, \nu_j)^{\mathrm{T}}}{2} \right] \tag{3.11}$$

$$\Psi(\nu_i, \nu_j) = \left[\frac{\chi(\nu_i, \nu_j) - \chi(\nu_i, \nu_j)^{\mathrm{T}}}{2} \right] \tag{3.12}$$

For simplicity, the arguments l and τ are not explicitly shown in Equations 3.11 and 3.12, although it should be recalled that both the modal correlation matrix and its symmetric and antisymmetric parts do depend on the space and time variables l and τ, respectively. Omission of the latter from the arguments implies that the related results hold for fixed, predefined values of l and τ.

The physical meanings of the symmetric and the antisymmetric parts of the modal correlation matrix may be envisaged as follows: The function $\chi(\nu_i, \nu_j)$ describes the correlation between the *i*th mode of the *k*th atom at a given time, and the *j*th mode of the atom *k+l*, at a later time $t+\tau$. $\chi(\nu_i, \nu_j)$ will depart from zero, in the positive or negative direction if a given energy fluctuation of atom *k*, induces a well defined energy fluctuation (of same or opposite sense) in atom *k+l*. Likewise, the transpose of $\chi(\nu_i, \nu_j)$ indicates the coupling between atoms *k* and *k+l*, initiated this time by *j*th mode operating on atom *k+l*. On the basis of this explanation, $\Phi(\nu_i, \nu_j)$ may be viewed as a measure of the communication or energy exchange between the *i*th and *j*th modes operating on the respective atoms *k* and (*k+l*), averaged over both directions of energy flow.

A large absolute value for $\Phi(\nu_i, \nu_j)$ means that the modes ν_i and ν_j are strongly coupled, positive and negative values referring to *correlated* and *anticorrelated* motions. Although a large absolute value for $\Phi(\nu_i, \nu_j)$ invariably indicates strong coupling between the respective modes *i* and *j* operating on atoms *k* and *k+l* with a time lag τ, a small value does not necessarily imply the absence of coupling. In fact, a small $\Phi(\nu_i, \nu_j)$ may result from the average of a highly correlated motion (large, positive $\chi(\nu_i, \nu_j)$) generated by the mode *i* of the *k*th atom and a highly anticorrelated one (large, negative $\chi(\nu_i, \nu_j)$) induced by the mode *j* of the *l*th neighbor. This situation in which a strong coupling leads to an overall small $\Phi(\nu_i, \nu_j)$ value will be referred to as a coupled but *incoherent* relaxation process. The term incoherent is used here to indicate that the effect induced by bond *k* on bond *k+l* is in the opposite sense to that induced by bond *k+l* on bond *k*. The antisymmetric component small $\Psi(\nu_i, \nu_j)$ is large in all incoherent motions. In fact, the degree of incoherence is reflected by the magnitude of $\Psi(\nu_i, \nu_j)$. The latter approaches zero if the two modes induce energy fluctuations in the same direction. In this case, the time-delayed effect of the *i*th mode on the *j*th conforms with that of the *j*th mode on the *i*th. In this case, the coupled motion of atoms *k* and *k+l* is said to be coherent.

In summary, three types of mode-mode coupling may occur, which are expressed by the symmetric and antisymmetric parts of the modal correlation function as: (i) a large absolute value, $|\Phi(\nu_i, \nu_j)|$for the symmetric component, and a low value for the antisymmetric one, $|\Psi(\nu_i, \nu_j)|$. This typifies *correlated* (or *anticorrelated* if $\Phi(\nu_i, \nu_j)$ is negative) and *coherent* motions generated by the *i*th mode operating on atom *k*, and *j*th mode on atom *k+l*; (ii) a small $|\Phi(\nu_i, \nu_j)|$ and a large $|\Psi(\nu_i, \nu_j)|$ characterizes correlated (or anticorrelated) but *incoherent* motions; and (iii) both $|\Phi(\nu_i, \nu_j)|$ and $|\Phi(\nu_i, \nu_j)|$ are small, which corresponds to *uncorrelated* motions. The coupling between different modes will be analyzed on the basis of this classification in the following section.

Inasmuch as the antisymmetric part $\Psi(\nu_i, \nu_j)$ of the modal correlation function represents the deviations from the coherent motion due to the time and space differences, τ and l, it is possible to view it as an extension of the asynchronous correlations of the dynamic spectrum defined by Noda[86,87]. On the other hand, by definition, the diagonal elements of $\chi(\nu_i, \nu_j)$ are equal to those of the symmetric part of the modal correlation matrix, whereas the antisymmetric part $\Psi(\nu_i, \nu_j)$ has zero diagonal elements. Owing to these definitions, the symmetric and antisymmetric parts of the correlation function may be respectively associated with the synchronous and asynchronous component of the absorptive-intensity cross-correlation function defined by Noda.

3.3.2. Results

3.3.2.1. Modal Autocorrelation Function. In order to understand the time evolution of the coupling between modes operating on a given atom with a time delay, the modal autocorrelations ($\nu_i = \nu_j$) are examined as a function of τ for $l = 0$. A comparison of the function for the cases (i) $0 \leq \nu_i \leq 4167$ cm^{-1}; (ii) $0 \leq \nu_i < 20$ cm^{-1}, and (iii) $20 \leq \nu_i \leq 4167$ cm^{-1} is presented in Figure 3.18. Results for case (i) are shown by the solid curve. The latter comprises all operating modes. A rapid drop in correlation within 1 ps followed by slow oscillations around the zero line is the general trend. Case (ii), which reflects the contribution of the slowest modes only, is shown by the dashed curve superposed on the solid curve. The close coincidence of the two curves suggests that this small subset ($\nu < 20$ cm^{-1}) of the total frequency spectrum successfully describes the overall behavior, particularly after ~2 ps. On the other hand, the correlations in the relatively broad frequency range $\nu \geq 20$ cm^{-1} are short-lived as shown by the lower dashed curve, and rapidly decay to zero.

For a better understanding of the effect of slower modes on the overall dynamics of the chain, a comparative plot of the correlation functions obtained by further filtering the low frequency modes is presented in the inset of Figure 3.18 with the abscissa and the ordinate confined to the ranges 0 - 10 ps and 0 - 2.0x10^5 (J/mol)^2, respectively. The curves are drawn for the cases where the low-pass filtering has been restricted to frequencies below 20 cm^{-1}, 5 cm^{-1} and 2 cm^{-1} along with the curve comprising all frequencies (solid curve). It is interesting to observe that, for times larger than ~3 ps, even the modes in the frequency range $\nu_i < 2$ cm^{-1} lead approximately to the same time decay of the correlation function as that obtained from the unfiltered trajectory.

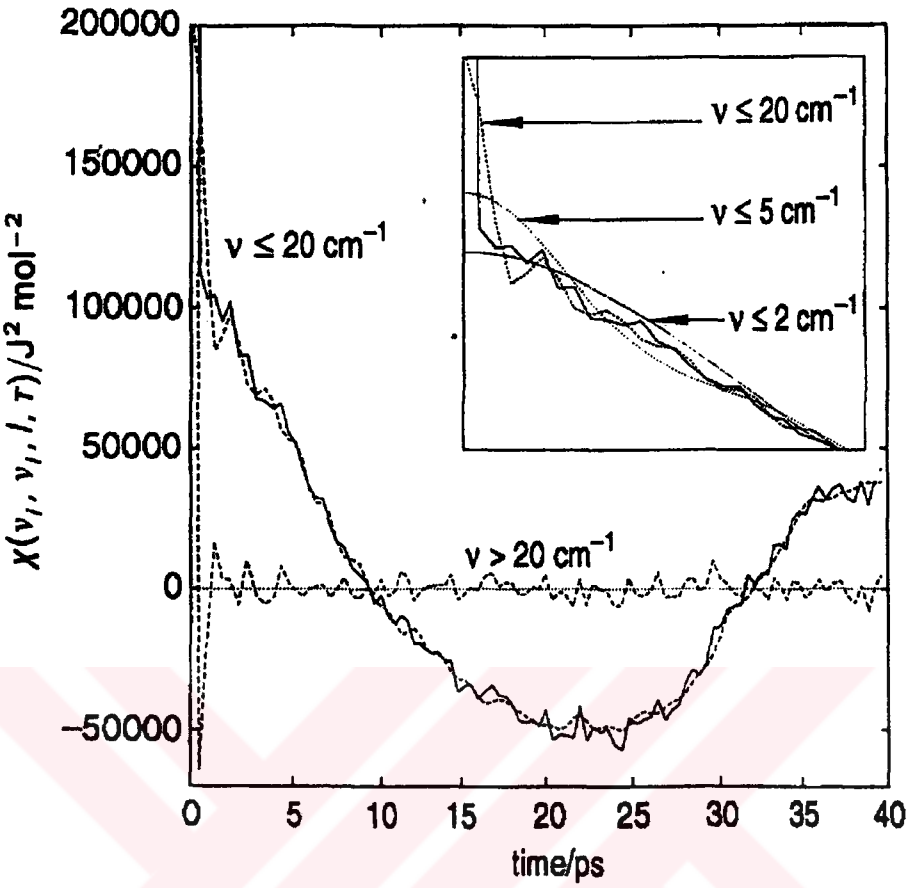

FIGURE 3.18. Autocorrelation function for fluctuations in kinetic energies filtered in various ranges.

The short time region where the effect of different frequency modes on the correlation of kinetic energy is distinguishable ($\sim\tau < 3$ ps) corresponds to the time scale at which coupled transitions occur. Coupled transitions refer to successive transitions undergone by the pair of bonds k and $k\pm l$ within time intervals much shorter than the mean isomerization time of the bonds. The mean isomerization time is found as 68 ps in the present MD simulations. This value is deduced from the hazard analysis of the dihedral angle trajectories, a method introduced by Helfand[8] for studying conformational transition rates in polymers.

3.3.2.2. Diagonal Elements of the Modal Correlation Matrix . Here the dispersion of the diagonal elements $\chi(\nu_i, \nu_j)$ of the modal correlation function will be examined for various l. τ is set equal to 1 ps in order to capture the dynamics of the coupled transitions between

bonds. This value corresponds to a frequency of ~16.7 cm^{-1}, which is in the slower end of the spectrum within the scale of torsional motions.

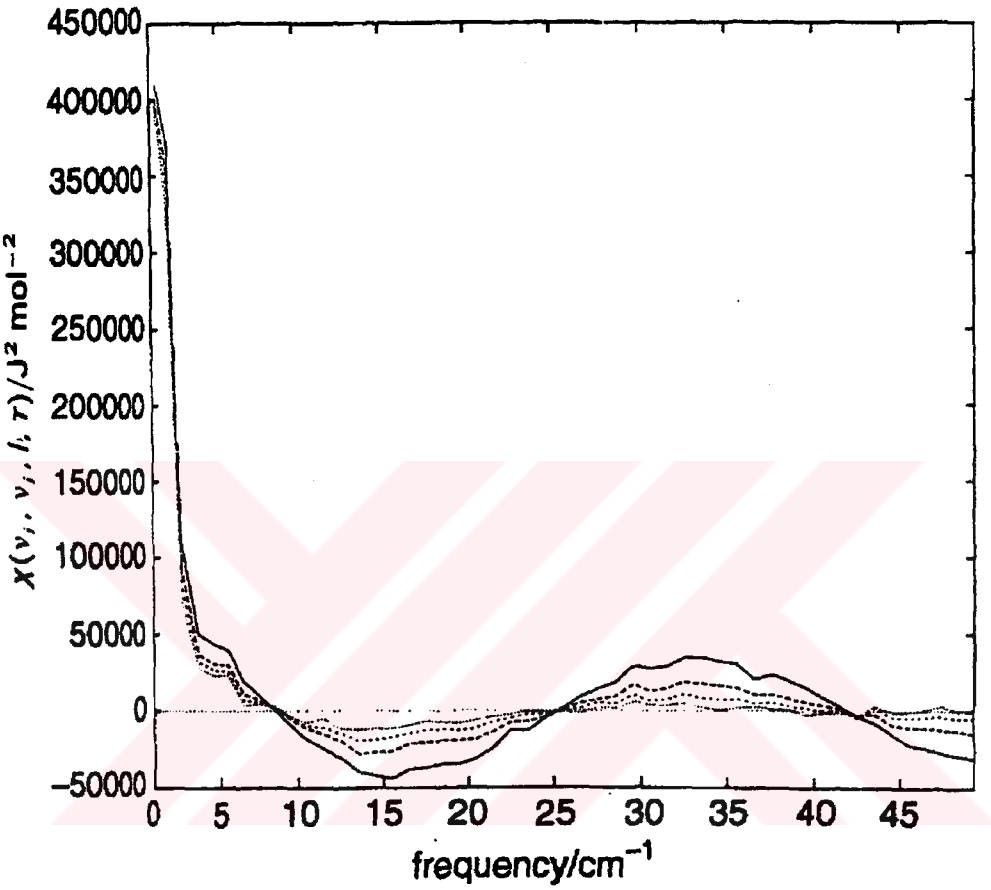

FIGURE 3.19. Diagonal terms of the modal correlation function for $\tau = 1$ ps.

The results are presented in Figure 3.19 for l = 0-3. For neighbors that are farther apart ($l \geq 4$), the contribution from frequencies $\nu \geq 5$ cm^{-1} is vanishingly small as may be verified from the figure. From these curves it may be deduced that the kinetic energy transfer between near neighbors ($l \geq 3$) along the chain proceeds mostly through lowest frequency modes, and exhibits a periodic dependence on the operating frequency above $\nu_i \geq 5$ cm^{-1}. In fact such a picture suggests that in some regions of the spectrum, the communication between chain atoms takes place through a simultaneous increase or decrease in energy, *i.e.* the kinetic energy fluctuations are correlated, whereas in some others, a time delay of 1 ps causes anticorrelated energy fluctuations.

At the lowest frequencies ($1 \leq \nu_i \leq 3$ cm^{-1}), the correlations of the atom with itself and with its near neighbors are almost indistinguishable in Figure 3.19, in contrast to the deviations between the curves observed in the rest of the spectrum. The modes at low frequencies are associated with the overall motion of the chain, the torsions accompanying bond isomerizations, and the large amplitude rotational fluctuations involved in the localization of the motions. Thus, various mechanisms may be responsible for the close similarity of the curves for l = 0 - 3 in this range. In order to clarify the effect of various modes, filtered dihedral angle trajectories are examined next.

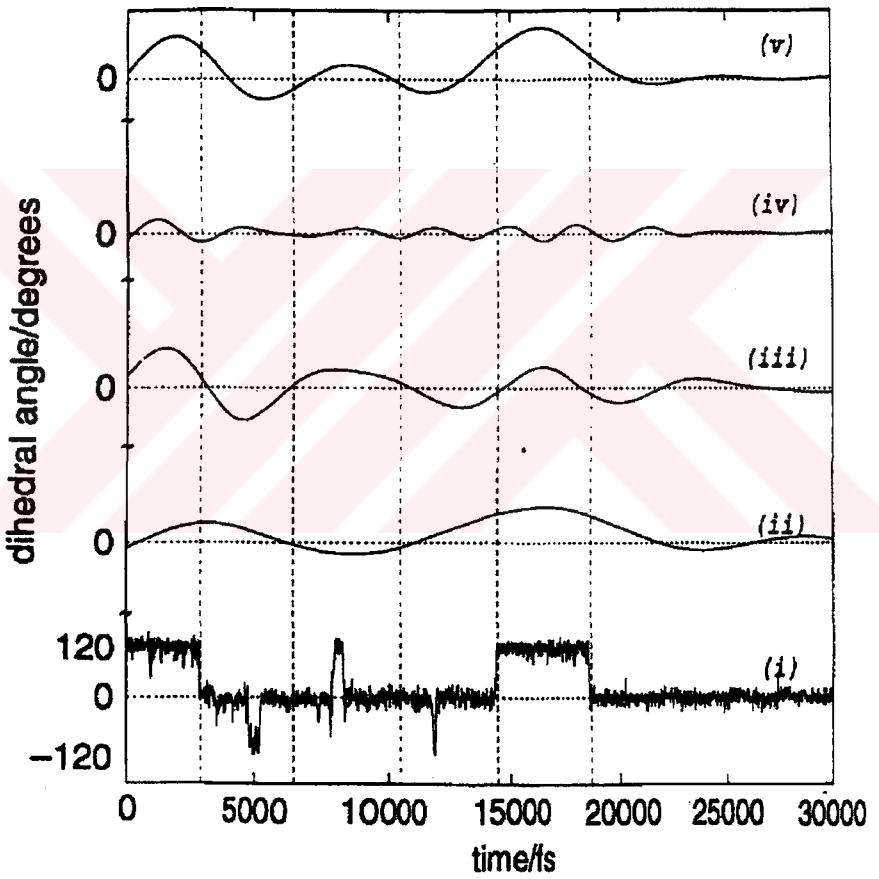

FIGURE 3.20. Time evolution of the dihedral angle trajectory of an internal bond obtained from the complete MD run without filtering (i), and from filtered trajectories. The trajectories are subdivided by vertical lines to guide the eye.

In Figure 3.20, a portion of the trajectory of an internal bond dihedral angle is presented in curve (i), along with the same trajectory filtered to keep frequencies in the ranges: $0 \leq \nu_i \leq 1$ cm^{-1}, $1 \leq \nu_i \leq 2$ cm^{-1}, and $2 \leq \nu_i \leq 3$ cm^{-1} in curves (ii) - (iv), respectively. Finally, a superposition of the frequency ranges of curves (ii) - (iv) is compiled in curve (v) as a low-pass filtered trajectory below 3 cm^{-1}. The time coordinate is subdivided by vertical lines so as to visualize the role of these characteristic modes.

It is possible to classify the rotameric transitions observed in curve (i) into two major categories: These are either stable transitions that take the bond from one of its isomeric minima to another, or else occasional jumps that occur due to the strains arising within the chain and are restored back to the original state in a very short time (< 0.5 ps) period. In the sample trajectory of Figure 3.20, there are three transitions which may be considered to be of the former, and three jumps of the latter type. In fact, after the first transition from g^+ to t state, the first unstable jump occurs at about 5 ps. Yet, at this point the preference to stay at the t state dominates and the bond returns to its stable isomeric state. The bond attempts two more such jumps, one to the g^+ state and the other to g^- state, before it makes its second isomerization to the state g^+ at $\tau \approx 14.5$ ps. The state of the bond remains stable for about 5 ps before it undergoes its last isomeric transition to the t state.

Curve (v), which conveys only those motions with characteristic frequencies less than 3 cm^{-1}, embodies the general tendencies of the marked regions. The following may be deduced from a careful examination of these curves: (1) The transitions between isomeric minima are predominantly determined by the modes operating at frequencies between 1 and 2 cm^{-1} as presented in curve (iii), (2) The modes belonging to the range $2 \leq \nu_i \leq 3$ cm^{-1}, are responsible for torsional fluctuations around the average value of 0°, as exemplified by curve (iv); although these fluctuations are large in magnitude (±30°), they do not indicate any isomerization phenomena; 3) Finally, the slowest modes ($\nu_i \leq 1$ cm^{-1}), shown in curve (ii), seem to be correlated with the stable isomeric transitions but do not sense the three occasional jumps in the original trajectory (curve (i)) which are quickly restored back.

The low frequency range of Figure 3.19 now gains more meaning. In the $0 \leq \nu_i \leq 1$ cm^{-1}, the energy coupling between atoms is diminished as one considers interactions between farther neighbors. This hierarchy is broken in the range $1 \leq \nu_i \leq 2$ cm^{-1} where the modal autocorrelation between near neighbors is the same for all cases. The latter suggests that the torsional fluctuations of near neighbors ($l \leq 3$), which are driven by the modes in the frequency range $1 \leq \nu_i \leq 2$ cm^{-1}, are strongly cooperative. In fact, the modes in this frequency range effectively prescribe the conformational dynamics of the chain, as

evidenced by the curve (iii) of Figure 3.20. This cooperativity between near neighbors along the chain gradually diminishes beyond $\nu_i \geq 2$ cm^{-1}.

3.3.2.3. Symmetric Part of the Modal Correlation Matrix. The calculations for the symmetric part $\Phi(\nu_i, \nu_j)$ of the correlation matrix $\chi(\nu_i, \nu_j)$ indicate that the diagonal elements ($\nu_i = \nu_j$) are predominantly large. The diagonal terms of $\Phi(\nu_i, \nu_j)$ have already been presented in Figure 3.19. This dominance is explained by the fact that the major contribution to the flow of kinetic energy between motions occurring at some frequency is through the same frequency. Yet, some leakage of energy between modes must be present for the coupling to occur. In fact, off-diagonal terms *do* exist, although this is on a scale about two orders of magnitude lower than that of diagonal elements. $\Phi(\nu_i, \nu_j)$ provides a measure of coupling and coherence between modes located at different frequencies when interpreted together with $\Psi(\nu_i, \nu_j)$.

For visual clarity, only the off-diagonal elements of the $\Phi(\nu_i, \nu_j)$ surface are presented in Figure 3.21(a). The space and time variables are set to $l = 0$ and $\tau = 1$ ps. ν_i and ν_j are varied in the range 0-40 cm^{-1} using 1 cm^{-1} bins as in the curves of Figure 3.15. It is observed that for low frequency range ($0 < \nu < \sim 5$ cm^{-1}) the magnitude of $\Phi(\nu_i, \nu_j)$ is notable, indicating that the energy fluctuations of the modes within this frequency range are significantly coupled. It is further detected from Figure 3.19a that $\Phi(\nu_i, \nu_j)$ is low in regions which are far away from the diagonal, and vanishes periodically even near diagonal elements.

3.3.2.4. Antisymmetric Part of the Modal Correlation Matrix. The antisymmetric part of $\chi(\nu_i, \nu_j)$ shows the degree of incoherence between the energy fluctuations observed at different wavenumbers. By definition (see Equation 3.12) the diagonal terms are equal to zero; cross-peaks appear if there is an incoherent correlation between different modes.

$\Psi(\nu_i, \nu_j)$ matrix for $l = 0$ and $\tau = 1$ ps is shown in Figure 3.21(b), which demonstrates that the energy fluctuations successively imparted by different characteristic modes on a given atom are not necessarily coherent but do exhibit some incoherence, even in the low frequency regions of the spectral plane where a strong modal coupling has been shown to occur. A periodic change in the degree of incoherence is observed in the 2D spectral plane, in analogy with the symmetric part of the modal correlation function. The antisymmetric parts are not zero for all regions where the symmetric part is vanishingly small. For instance, the degree of incoherence is large in the region $20 < \nu_i, \nu_j < 30$ cm^{-1}, while the corresponding $\Phi(\nu_i, \nu_j)$ are low, as seen in Figure 3.21(a). This indicates that the modes characterized by such frequencies are still coupled, but this coupling is expressed via

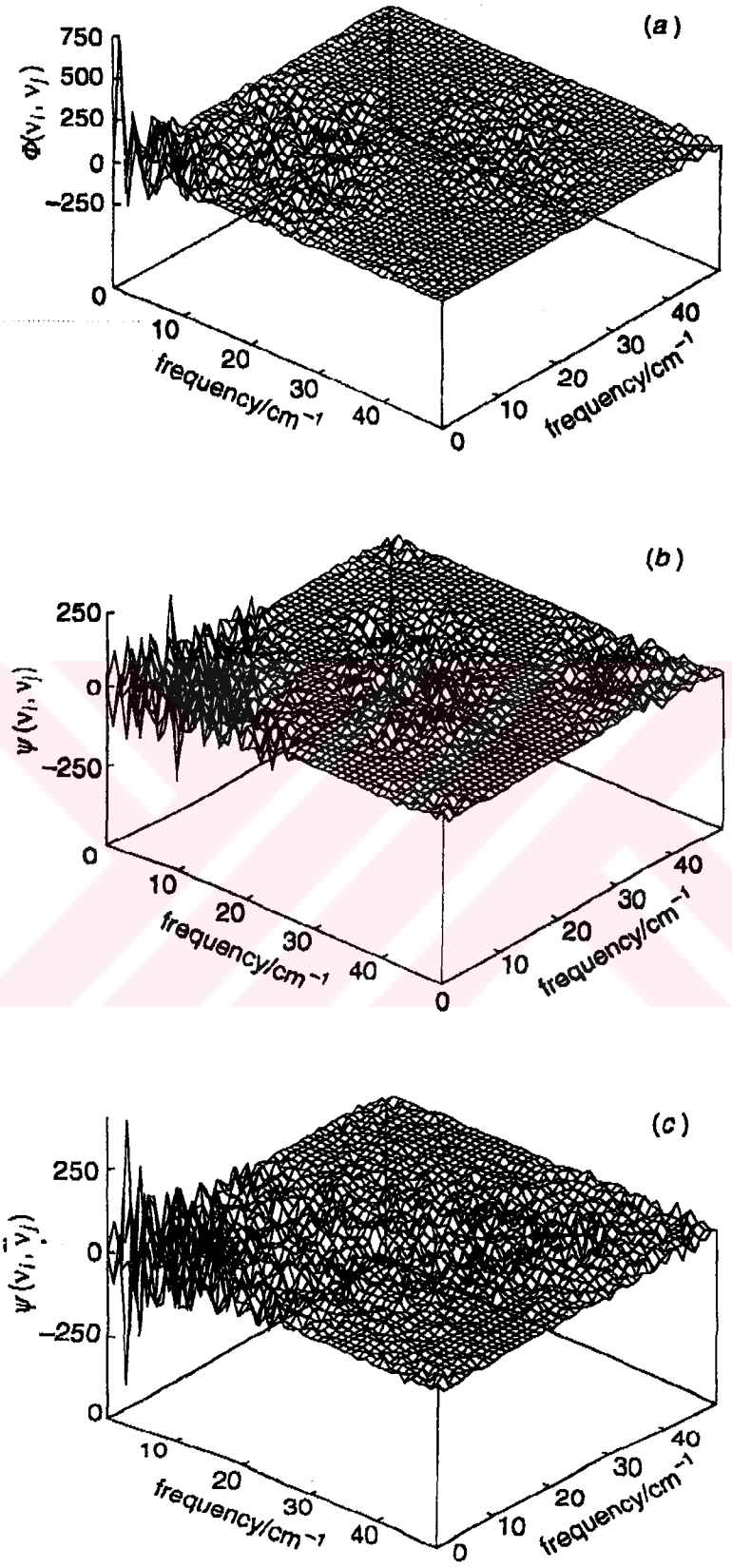

FIGURE 3.21. Symmetric and antisymmetric parts of the modal correlation matrix: (a) $\Phi(\nu_i, \nu_j)$, $l = 0$ and $\tau = 1$ ps; (b) $\Psi(\nu_i, \nu_j)$, $l = 0$ and $\tau = 1$ ps; (a) $\Psi(\nu_i, \nu_j)$, $l = 2$ and $\tau = 1$ ps;

incoherent energy fluctuations, as discussed above. On the other hand, the fact that $\Psi(\nu_i, \nu_j)$ is very low in the neighborhood of $\nu_i = \nu_j = 15$ cm^{-1} in spite of the corresponding large $|\Psi(\nu_i, \nu_j)|$ reveals the strong coherence of the modes operating at these frequencies.

The magnitude of the incoherent correlations is notable for the range $0 < \nu_i, \nu_j < 10$ cm^{-1}. Modal correlations always exist between frequencies which are close to each other. On the other hand, as one proceeds away from the diagonal, both components of the modal correlation function in Figure 3.21(a) and 3.21(b) are attenuated, indicating that the modes of distinct frequencies are weakly correlated or almost uncorrelated.

For understanding the spatial effects on the degree of incoherence among various modes, calculations are repeated for $l = 2$. The resulting $\Psi(\nu_i, \nu_j)$ are shown in Figure 3.21(c). The $\Phi(\nu_i, \nu_j)$ surface for $l = 2$ exhibits the same characteristics as Figure 3.21(c), and hence is not separately shown. Thus, the off-diagonal regions of the spectral plane are depressed in both cases, indicating the absence of correlations between modes whose frequencies differs by more than 15 cm^{-1}, approximately.

Comparison of Figures 3.21(b) and 3.19(c) shows that the correlations between modes operating on a given atom with a given time delay, and those between the modes operating on second neighbors along the chain, exhibit quite distinct characteristics. The periodic dependence of $\Psi(\nu_i, \nu_j)$ on the frequency is no longer discernible. Instead, a more or less uniform degree of incoherence is observed between modes of comparable frequencies, $|\nu_i - \nu_j| \leq 15$ cm^{-1}, except for the lowest frequency region of the spectral plane where the fluctuations in $\Psi(\nu_i, \nu_j)$ are relatively enhanced.

The above correlation analysis was also performed for $\tau = 68$ ps, the mean isomerization time of the chains. The diagonal terms located at the lowest end of the spectrum ($\nu \leq 4$ cm^{-1}) were the major elements of the corresponding $\chi(\nu_i, \nu_j)$ matrices. Furthermore, these were approximately one order of magnitude weaker compared to the corresponding peaks for $\tau = 1$ ps. Thus, at these long time scales, the effect of high frequency modes is vanishingly small, and the kinetic energy flow occurs only through a few slowest characteristic modes of motions.

3.4. Molecular Dynamics Analysis of Coupling between Librational Motions and Isomeric Jumps in Chain Molecules

One way of quantifying the cooperativity between librational motions and isomeric jumps is to monitor the conformational and orientational motions of chain segments. Conformational motions are those that may be described without reference to an external coordinate system, such as the transitions between t, g^+ and g^- states and the fluctuations in bond dihedral angles. Orientational motions, on the other hand, require a coordinate system for their specification. The angle between a bond at a given time and another bond at a later time is an example. Both conformational and orientational motions are characterized by time-delayed correlation functions (CF) and the associated correlation times. These are not only predictable by computational methods, but also measurable by experiments, such as time-resolved fluorescence or nuclear magnetic resonance. However, the assumptions made in interpreting the experimental results can only be rationalized by computer simulations.

Although there have been several attempts to express the experimental relaxation curves by analytical functions[26], most approaches have either neglected the torsional librations[91] or confined the motion to a few bonds only[92]. Some studies do not consider three-dimensional motions[93] and others associate high frequency effects with additional fast anisotropic processes[49] incorporating Howarth's reflections on librations[94-96]. Meanwhile, derivation of correlation functions by using analytical models become rather complex in three-dimensions. Therefore, Cook and Helfand[97] developed a one-dimensional analytical model and showed a single exponential decay for the conformational state merging single and cooperative transition processes. A similar model was used by Moro where the coupling between librations and conformational jumps was analyzed on the basis of a linear chain of rotors. Therein it is demonstrated that librational motions operating after a transition are responsible for attaining the new equilibrium state[98]. Recently Kim and Mattice[68] have taken another path in that they investigated the effect of libration on the time evolution of the conformational autocorrelation functions (CACF) for dihedral angles. Interestingly, they found that the adoption of discrete conformational states excluding librations, as in the basic approach of DRIS theory, results in an overestimation of conformational correlation times.

In all of the above treatments some questions remain to be answered: How is the time decay of CFs affected by the contribution of librational motions? Do the librations have a random character so that the overall chain dynamics can be adequately predicted by

removing them and adopting a DRIS-like treatment? Is the superposition of an additional single exponential type fast relaxation mechanism on the relaxation spectrum sufficient to account for the effect of librations, as performed in several studies? Or do librations act in some cooperative manner and exert different effects on different types of correlations? If some cooperativity exists, *i.e.* if librations are actively involved in the initiation or localization of rotameric jumps for example, is it possible to retain the effect imposed by librations on large amplitude movements by simply eliminating the high frequency components of the overall motion?

In the present study, an MD trajectory is analyzed with the objective of testing the validity of various assumptions made in interpreting experiments and clarifying the above raised issues. Time series obtained from MD simulations are filtered as outlined in Section 3.3.1.2 to obtain smoother trajectories where only low frequency modes remain. The fluctuations in bond lengths and angles and/or dihedral angles are also turned off, and the consequences of eliminating these degrees of freedom on the relaxation mechanism are explored. Alternatively, these degrees of freedom are assigned Gaussianly distributed random variables about their equilibrium values. CFs calculated by using these modified trajectories are compared to those determined from actual MD, in order to assess the effects of different levels of approximation.

3.4.1. Method and Calculations

3.4.1.1. Correlation Functions. The effect of librations on the local relaxation phenomenon is explored on the basis of two types of autocorrelation functions: (i) The OACF associated with the reorientation of backbone bonds. This is expressed in terms of the instantaneous unit vector $\mathbf{l}_i(\tau)$ along the ith bond as

$$M[l(\tau)] = \frac{1}{2}\left\{3\overline{\left\langle\left[\mathbf{l}_i(t)\cdot\mathbf{l}_i(t+\tau)\right]^2\right\rangle} - 1\right\} \qquad (3.13)$$

Equation 3.13 is similar to Equation 2.6; the unit vector is affixed to the C-C backbone bond in the former and to the C-H vector in the latter. (ii) The second conformational autocorrelation function CACF describing the time evolution of the rotational isomeric states of backbone bonds. This is given by

$$M[\varphi(\tau)] = \frac{1}{2}\left\{3\overline{\left\langle \cos^2\left[\varphi_i(t+\tau) - \varphi_i(t)\right]\right\rangle} - 1\right\} \tag{3.14}$$

where $\varphi_i(\tau)$ is the dihedral angle of the ith bond. The angular brackets in Equations 3.13 and 3.14 refer to the ensemble average over internal bonds, and the overbar denotes the time average over all conformational transitions starting at various t and occurring within the time interval τ.

3.4.1.2. Details of the Molecular Dynamics Method. MD simulations are carried out for a united atom model polyethylene (PE) chain of n = 100 CH_2 units. The time evolved coordinates of atoms are obtained as an array of position vectors $\mathbf{r}_i(t) = [x_i(t)\ y_i(t)\ z_i(t)]^T$, $0 \le i \le n$. These are transformed into a set of generalized coordinates, consisting of (i) bond dihedral angles φ_i, $2 \le i \le n$-1, (ii) bond angles, θ_i, $1 \le i \le n$-1, (iii) bond lengths, l_i, $1 \le i \le n$, of the particles at any instant in time, following the formulation presented in Appendix A. Here the time arguments are omitted for brevity. For convenience, the transformation matrix or operator that permits the passage from the set of position vectors to that of the generalized coordinates is denoted as $\mathbf{Q}_1$:

$$\mathbf{Q}_1 : \begin{bmatrix} x_i \\ y_i \\ z_i \end{bmatrix} \rightarrow \begin{bmatrix} l_i \\ \theta_i \\ \varphi_i \end{bmatrix} \tag{3.15}$$

The inverse operator $\mathbf{Q}_1^{-1}$, transforms from the generalized coordinates $[l_i, \theta_i, \varphi_i]^T$ to the set of position vectors, $[x_i, y_i, z_i]^T$. The set of generalized coordinates, obtained for all units in a sequence of 40 bonds located in the middle of the chain, and recorded at 4 fs intervals, will

be referred to as the *original* trajectory. The latter will be subjected to various operations as will be presented below.

The chain is chosen to be *in vacuo* so that only those interactions generated by the polymer itself are operative. The overall potential is the sum of (i) a harmonic bond stretching (Equation A.1) and (ii) a harmonic bond bending function (Equation A.2); (iii) a quintic function which accounts for the intrinsic torsional potential of dihedral angles and first order interactions between chain atoms separated by 3 bonds (Equation A.3), and (iv) an LJ potential (Equation A.4) which operates on atom pairs that are separated by 4 or more bonds and are within 12 Å distance of each other. Initially, a 25 ps equilibration time is allowed. The total simulation duration after equilibration is ~260 ps. The temperature is kept constant at 300 K.

3.4.1.3. Reconstruction of Trajectories Subject to Various Operations. The *original* MD trajectories are subjected to the following operations to obtain the so-called *modified* trajectories:

(a) The fluctuations in bond lengths and bond angles are removed from the trajectories by replacing these variables with their mean values. This may be expressed by the operation

$$\mathbf{Q}_2:\begin{bmatrix} \bar{l}_i + \Delta l_i \\ \bar{\theta}_i + \Delta\theta_i \\ \varphi_i \end{bmatrix} \rightarrow \begin{bmatrix} \bar{l}_i \\ \bar{\theta}_i \\ \varphi_i \end{bmatrix} \tag{3.16}$$

where the instantaneous bond lengths and bond angles are expressed as a sum of their mean values and their fluctuations, as

$$\left.\begin{aligned} l_i &= \bar{l}_i + \Delta l_i \\ \theta_i &= \bar{\theta}_i + \Delta\theta_i \end{aligned}\right\} \tag{3.17}$$

The mean bond lengths and bond angles are 1.53 Å and 109.5°, for all bonds. Comparison of the modified trajectory with the original trajectories will provide information on the contribution of the librations in bond lengths and bond angles on the local chain relaxation mechanism. Clearly the modified set of position vectors may be generated by the application of the inverse operator $\mathbf{Q}_1^{-1}$ on the modified generalized coordinates obtained in Equation 3.15. In summary, a modified set of position vectors is obtained by premultiplication of the original array by $\mathbf{Q}_1^{-1}\,\mathbf{Q}_2\,\mathbf{Q}_1$.

(b) In addition to bond length and bond angles, torsional librations about rotational isomeric minima may be eliminated by replacing the original trajectories by a new one modified according to the operation

$$\mathbf{Q}_3:\begin{bmatrix} \bar{l}_i + \Delta l_i \\ \bar{\theta}_i + \Delta\theta_i \\ \bar{\varphi}_i + \Delta\varphi_i \end{bmatrix} \rightarrow \begin{bmatrix} \bar{l}_i \\ \bar{\theta}_i \\ \bar{\varphi}_i \end{bmatrix} \tag{3.18}$$

Here $\bar{\varphi}_i$ represents the rotational isomeric state values assumed by the ith dihedral angle. This is given by a step function of the form:

$$\bar{\varphi}_i(\tau) = \begin{cases} 0^\circ & -60^\circ \le \varphi_i(\tau) \le 60^\circ \\ 120^\circ & \varphi_i(\tau) > 60^\circ \\ -120^\circ & \varphi_i(\tau) < 60^\circ \end{cases} \tag{3.19}$$

(c) Alternatively, normal fluctuations may be superimposed on bond lengths and bond angles, which would provide insight into the differences between random librations and those occurring in the original MD trajectories. Accordingly, the instantaneous bond lengths and bond angles are expressed as Gaussianly distributed random variables with the mean values 1.53 Å and 109.5° and covariances 0.10 Å and 10°, respectively. This transformation may be written as

$$\mathbf{Q}_4:\begin{bmatrix} \bar{l}_i + \Delta l_i \\ \bar{\theta}_i + \Delta\theta_i \\ \varphi_i \end{bmatrix} \rightarrow \begin{bmatrix} \bar{l}_i + \Delta l_i^n \\ \bar{\theta}_i + \Delta\theta_i^n \\ \varphi_i \end{bmatrix} \tag{3.20}$$

Here the superscripts n refer to the normal distribution, and the dihedral angles are left unchanged.

(d) A final transformation to be considered in the calculations is $\mathbf{Q}_5$, represented as

$$\mathbf{Q}_5:\begin{bmatrix} \bar{l}_i + \Delta l_i \\ \bar{\theta}_i + \Delta\theta_i \\ \varphi_i \end{bmatrix} \rightarrow \begin{bmatrix} \bar{l}_i + \Delta l_i^n \\ \bar{\theta}_i + \Delta\theta_i^n \\ \bar{\varphi}_i \end{bmatrix} \tag{3.21}$$

which is identical to $\mathbf{Q}_4$, except for the replacement of the original torsional angles by their isomeric isomeric state values following Equation 3.18. Clearly, in all cases (a) - (d) the modified set of position vectors is constructed by application of the operation $\mathbf{Q}_1^{-1}\,\mathbf{Q}_m\,\mathbf{Q}_1$, with m = 2 - 5, on the original position vectors.

Table 3.6 provides a summary of the operations adopted in obtaining modified trajectories subject to various approximations, starting from the original MD trajectory. It should be noted that the perturbations applied to the various degrees of freedom do not result from a change in the potential field used in MD simulations. On the contrary, all trajectories originate from the same MD run with a given potential field. In the earlier work of Helfand *et al.*[99] the force constants in the potentials were changed so as to constrain l_i and θ_i. This is a different approach which can provide an estimation of the effect of constraining the librational motions on the relaxation mechanism. In contrast, the present approach provides a direct measure of the perturbation of the MD trajectories by several factors, including the elimination of a class of operating modes via filtering technique, the removal of the librational motions, which may be directed and/or random, the imposition of a white noise for approximating the additional mobility imparted by the high frequency librational motions.

TABLE 3.6. Characteristics of the trajectories utilized for extracting OACFs and their orientational correlation times[a]

OACF	operation	τ_c (ps)	τ_c/τ_{co}
(i)	none	7.81	1.00
(ii)	filtered[b]	9.39	1.20
(iii)	$Q_1^{-1} Q_2 Q_1$	5.62	0.72
(iv)	$Q_1^{-1} Q_3 Q_1$	4.09	0.52
(v)	$Q_1^{-1} Q_4 Q_1$	5.51	0.71
(vi)	$Q_1^{-1} Q_5 Q_1$	3.59	0.46

a) τ_c: orientational correlation times; τ_{co} : τ_c of original MD run
b) Using a low-pass filter of 20 cm^{-1}.

3.4.2. Results

3.4.2.1. Conformational Autocorrelations. The CACFs, $M[\varphi(\tau)]$, evaluated using different approaches are presented in Figure 3.22, up to $\tau = 100$ ps.

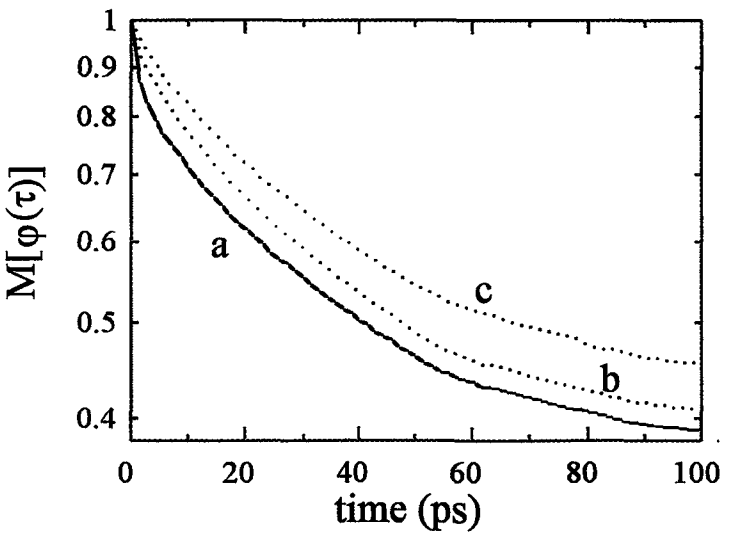

FIGURE 3.22. Conformational autocorrelation functions extracted from trajectories with various degrees of assumptions.

Curve (a) represents the result from the *original* MD trajectory. Curve (b) is obtained by applying a low-pass filtering below 20 cm^{-1}. Curve (c), on the other hand, is obtained by subjecting the original generalized coordinates to the transformation operator $\mathbf{Q}_3$. This eliminates all bond angle, bond length and torsional librations. However, eliminating the bond lengths and bond angles are inconsequential since the CACF is a quantity which depends purely on dihedral angles. In this approximation, the conformational dynamics corresponds to that adopted in the DRIS model. This curve also compares to that given by Kim and Mattice[68]. It is evident from the figure that both approximations (b) and (c) predict a slower decay compared to the original trajectory (a). The CACF from the filtered trajectory, curve (b), indicates that the departure between the approximated and original behavior arises primarily from a fast decay to about 0.86 of the ordinate value in curve (a) within tenths of picoseconds, which is absent in curve (b). This initial decay in curve (a) is clearly induced by the high frequency motions which have been eliminated in the filtered trajectory (b). The departure from the original CACF is even stronger in curve (c), where all torsional librations are extinguished following Equation 3.14.

A comparison along the same lines was made by Kim and Mattice for polybutadiene chains in the bulk state and a similar result was obtained[68]. Therein, it was argued that the dynamics is governed by two relaxation phenomena at separate time scales: one is responsible for librations and the other for conformational transitions. Thus, neglect of librational motions leads to slower relaxation insofar as the CACF is concerned. However, this approximation can be partly overcome by rescaling of the decay curves at short times. This explains the good agreement between the CACFs extracted from Brownian dynamics simulations and those predicted by the DRIS formalism in which librational motions are not accounted for (Section 3.1.2.2).

A mere analysis of the decays of CACF provides an incomplete picture of the relaxation mechanism. A more thorough understanding of the role of high frequency motions in local dynamics is gained by examining the time-dependent orientation of chain segments in space, in the presence and absence of librations.

3.4.2.2. Orientational Autocorrelations. The OACFs of bond vectors, $M[l(\tau)]$, obtained by subjecting a given MD trajectory to different operations, are presented in Figure 3.23, up to $\tau = 15$ ps.

Note that only the short time range is given to emphasize the differences between the initial decay of the curves. They all decay to zero eventually. Curve (i) represents the correlation function given by the original MD trajectory. The curves labeled (ii)-(vi) result from the

trajectories modified following the procedures summarized in Table 3.7. Mainly, curve (ii) refers to the low-pass (20 cm^{-1}) filtered trajectory. Curve (iii) and (iv), result from the application of the operators $\mathbf{Q}_1^{-1}\ \mathbf{Q}_2\ \mathbf{Q}_1$ and $\mathbf{Q}_1^{-1}\ \mathbf{Q}_3\ \mathbf{Q}_1$, respectively. This allows the extraction of the contribution of librational motions to the observed OACFs. Cases (v)-(vi), follow from the operations $\mathbf{Q}_1^{-1}\ \mathbf{Q}_4\ \mathbf{Q}_1$ and $\mathbf{Q}_1^{-1}\ \mathbf{Q}_5\ \mathbf{Q}_1$ applied to the set of position vectors recorded in the original MD trajectories. Here bond lengths and bond angles are assigned Gaussianly distributed random fluctuations, which permit the visualization of the difference between random librations and those cooperatively operating in the original MD run. The orientational correlation times τ_c and their ratios τ_c/τ_{co} with respect to that resulting from the original MD run, τ_{co}, are listed in the last two columns of Table 3.7 in order to provide a quantitative measure of the effect of the various operations on the apparent OACFs.

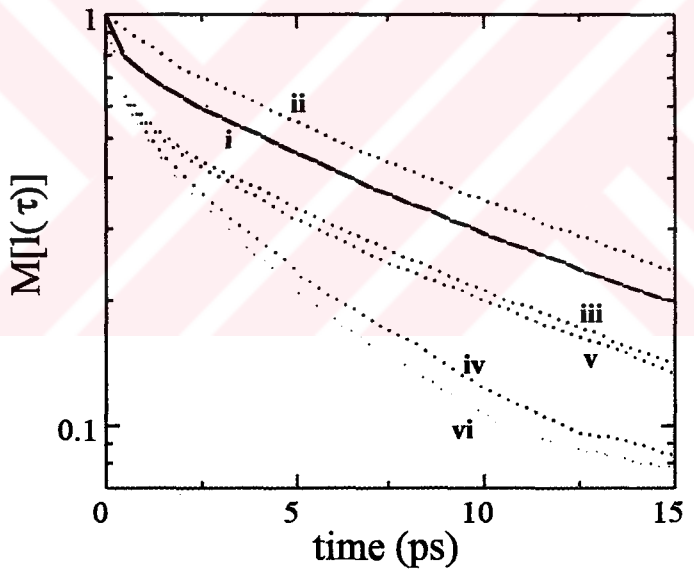

FIGURE 3.23. Orientational autocorrelation functions extracted from trajectories outlined in Table 3.6.

The low-pass filtered trajectory yields a slower decay of the OACF than that of the original trajectory, as the comparison of the curves (i) (solid) and (ii) reveals. The more interesting feature observed in Figure 3.23 is that all other curves, (iii)-(vi), exhibit faster decays compared to the original curve (i). Even the suppression of librations in bond lengths

and bond angles, which is represented by curve (iii), enhances the decay rate of $M[l(\tau)]$ by a considerable amount. A decrease in orientational correlation time of 28 per cent is induced by eliminating the vibrations in bond lengths and bond angles.

In many experimental and computational studies it is assumed that librations, especially those associated with stretching and bending, have a random character[48,94]. Curves (v) and (vi) in Figure 3.23 result from the imposition of Gaussianly distributed random fluctuations on the equilibrium values of bond lengths and angles. Examination of these curves demonstrates that the replacement of the original directed librational motions by random fluctuations leads to a significantly faster loss of orientation. The relaxation time is decreased by a factor of 0.71 and 0.46, respectively in curves (v) and (vi), compared to the original behavior. These results invite attention to the inadequacy of interpreting the stretching, bending and torsional librational motions as a random accelerating relaxation mechanism.

4. CONCLUSIONS AND RECOMMENDATIONS

4.1. Conclusions

Local motions in chain molecules are investigated using various computationally efficient methods. Localization is an important factor in that the isomerization at a bond induces various motions in the neighboring degrees of freedom so as to minimize the overall energy of the system. The mechanism of localization involves three types of motions of neighboring bonds. These are not independent processes but are closely interrelated. Namely they are (i) correlated torsions in the form of either coupled transitions or large amplitude motions (±30°) within the current isomeric minimum; (ii) an overall spatial reorientation of bonds; and (iii) translational motion of atoms in space. In all the above mechanisms, the motion is highly localized to the rotating bond and the three to four bonds on its either side. Torsional motions play a dominant role in local chain dynamics. However, its mechanism and relaxation rate are controlled by librations. Librations originate from bond stretching, bond angle distortion, and small amplitude fluctuations in bond dihedral angles. They are observed to be strongly correlated with the rotational jumps of bonds between isomeric states. In this study conformational transitions and librations are investigated in detail. The major conclusions are itemized in the following:

1. *Second order interactions help localization.* The mechanism of conformational relaxation is strongly affected by second neighbor interactions along the chain. Specifically, upon inclusion of second order interactions in the simulation model, the time evolution of the transitions $g^{\pm}g^{\pm} \rightarrow g^{\pm}t$, $g^{\pm}g^{\mp} \rightarrow g^{\pm}t$, $g^{\pm}t \rightarrow tt$ and $g^{\pm}g^{\mp} \rightarrow tt$ changes significantly, as illustrated in the respective curves 7, 8, 5 and 9 of Figures 3.2(b) and 3.3(b-c). The overall conformational mobility of the chain is enhanced upon inclusion of second order interactions as discussed in Sections 3.1.3 and 3.1.4. Thus, the number of rotameric jumps is increased by 14 per cent. This increase is equally distributed among cooperative and isolated transitions. However, certain types of the cooperative transitions, such as gauche migration, gauche pair creation and gauche pair annihilations exhibit an even stronger (by 20, 21 and 27 per cent, respectively) enhancement. On the other hand, coupled transitions occurring within 2 ps among third neighbors undergo an increase of 42 per cent, in the presence of second order interactions.

2. *DRIS is a suitable formalism as a first approximation in treating local chain dynamics.* The comparison of BD results obtained in the presence of second order interactions, with the predictions of the analytical DRIS theory in Figures 3.3(a-c) shows that the DRIS formalism gives a satisfactory account of the probability distributions and rates of particular rotameric transitions. A major shortcoming of the DRIS formalism is that the tails are free to translate following a rotameric transition over an internal bond. In this sense, long range chain connectivity is not rigorously taken into account in the DRIS formalism. BD method, on the other hand, intrinsically incorporates cooperative interactions of longer-range resulting from chain connectivity. Despite this basic difference between the two methods, it is shown in Figures 3.3(a-c) that the passages between rotameric states of bond pairs obey similar time evolution in the two approaches. This is an important observation which lends support to the use of DRIS approach for describing the dynamics of local conformational motions in polymers.

3. *Motions in PBD are less localized than PE.* In contrast to the highly localized response of PE to bond rotational jumps, in which the strongest coupling between rotational motions is observed between second neighboring bonds, the coupling in PBD is shown to involve longer chain segments. This feature is demonstrated by the response of chain units to β bond isomerization in PBD which is identical to torsional bonds of PE. Comparisons made in Figures 3.6 - 3.8 reveal that the isomerization of β bonds is distinguished by strong correlations extending up to third and fourth neighbors along the chain.

4. *Relaxation mechanisms differ for cis- and trans- conformers of PBD.* Even though the energetics of the two conformers are identical, their response to the same type of isomerization is different. This feature is discussed in detail in Section 3.2.3. The isomerization of an α bond in *trans*-PBD is systematically accommodated by the counterrotation of the α bond across the double bond. In *cis*-PBD, the same two α bonds exhibit corotations; also, major coupled torsions in the form of counterrotations take place at second neighboring α bonds across the β bond. Furthermore, upon rotating an α bond, the strongest orientational and translational coupling is observed in the first neighboring β bonds in *cis*-PBD and first neighboring double bonds in *trans*-PBD. Coordinated translational motions of atoms are observed in *cis*-PBD within the repeat unit where isomerization occurs. In *trans*-PBD, on the other hand, only the position and orientation of the neighboring double bond is significantly affected. As a result, under the same frictional environment, *cis*-PBD has higher mobility than the *trans* form by a factor of ~1.5. Finally, non-bonded intramolecular interactions have a strong influence on conformational relaxation in *cis*-PBD, whereas this influence is negligibly small in *trans*-PBD.

5. *Local dynamics is mainly controlled by backbone geometry.* It is demonstrated in Sections 3.2.2, 3.2.4, and 3.2.5 that the backbone geometry plays an important role in determining relative motions of near neighbors during rotational isomerization. Furthermore, in the case of copolymers of *cis*- and *trans*-PBD (Section 3.2.6), the behavior of the whole polymer is governed by the independent motions of each monomeric unit. Other factors such as the presence of large side groups and the resistance to motion of the environment are identified as additional contributions to the relaxation mechanism: these are not significant in the localization phenomena but they modulate the amplitudes of motion.

6. *CK is a suitable method for predicting local motions of polymers in the bulk state.* All of the predictions stated in items 3 - 5 above are in good agreement with the results from recent molecular dynamics (MD) simulations of PBD[68,69]. More interestingly, good agreement between the results obtained for *cis*-PBD and those from the bulk state MD simulations of *cis*-PIP[25] is found, confirming that backbone geometry has the major role in determining the mechanism of local conformational relaxations. The advantage of the present approach is that the computational time required is at least two orders of magnitude less than that of conventional MD simulations.

7. *Motions governing chain dynamics lie in the lower end of the frequency spectrum.* The relaxation behavior of the kinetic energy fluctuations, as well as the time evolution of bond rotameric states, are shown to be adequately described by a small subset of modes confined to the lowest end ($0 < \nu < 20$ cm^{-1}) of the total frequency spectrum ($0 < \nu < 4170$ cm^{-1}), as illustrated in Figure 3.16. An even more stringent analysis of the low-pass filtered ($\nu < 20$ cm^{-1}) trajectories reveals that, among the slow characteristic modes, those with frequencies in the interval $1 < \nu < 2$ cm^{-1} are predominantly responsible for the rotational isomerization of backbone bonds. In fact, the time evolution of the bond dihedral angles can be traced back in the trajectory prescribed by the modes lying in this interval alone, as the comparison of curves (i) and (iii) in Figure 3.20 demonstrates. This region of the spectrum is characterized by highly cooperative motions uniformly spread over nearest neighbors ($l = 0$ - 3), as evidenced by the superposition of the modal correlation functions.

8. *Coupling between low and high frequency nodes is enhanced during rotational isomerization.* This coupling between the low and high frequency modes is maximized during the transition of bond rotational states from one isomeric minimum to another. This is clearly demonstrated by the low-pass ($\nu < 20$ cm^{-1}) and high-pass ($\nu > 20$ cm^{-1}) filtered forms of the dihedral angle trajectory displayed in Figure 3.16. Relatively large amplitude oscillatory motions are observed in the high-pass trajectory, which occur precisely during the short time intervals (~2 ps) at which a rotameric jump takes place. This is in conformity with

the view that the rotameric transitions are coupled with large amplitude fluctuations which localize and/or compensate the motion[16,38], and with the work of Moro[27,28] which suggests that the librational motions operating after a transition contribute to the attainment of the new equilibrium distribution.

9. *A strong coupling persists between modes of comparable frequencies.* The modal correlation matrix $\chi(\nu_i, \nu_j)$ is split into its symmetric and antisymmetric components to further understand the mechanism of energy exchange underlying bond isomerization and anharmonic motions. The simultaneous examination of the surfaces drawn for the symmetric and antisymmetric components (Figure 3.21) permits the identification of the strength of coupling and degree of coherence between the various characteristic modes operating with a given time delay, on well defined atoms of the chain. Modes in the relatively low frequency region (ν_i, ν_j < 20 cm^{-1}) of the two-dimensional spectral plane, operating with a time delay of about 1 ps on a given atom, are highly correlated, as illustrated in Figure 3.21(a), and this coupling is shown in Figure 3.21(b) to be expressed by both coherent and incoherent exchange of kinetic energy. A relatively strong coupling persists between modes of comparable frequencies, in the neighborhood of the diagonals in Figures 3.21(a-c), around $|\nu_i - \nu_j|$ < 15 cm^{-1}, although this type of coupling exhibits a periodic dependence on the frequency.

10. *Librations cause a slower time decay of OACFs but a faster relaxation of CACFs.* Removal of frequencies higher than 20 cm^{-1} from the trajectory of Figure 3.16 results in the slowing down of the relaxation of conformational and configurational transitions shown by curve b in Figure 3.22 and curve ii in Figure 3.23. This is essentially due to the elimination of some pathways of relaxation from the trajectory which otherwise would lead to faster decay of correlations. Operating on the trajectory with $\mathbf{Q}_2$ (Table 3.6) eliminates all librations of bond lengths and angles and therefore excludes the possible localization effects that would result from the concerted motions of these degrees of freedom. Consequently, any change in a torsional angle of a given bond has to move the remaining parts of the chain as a rigid body which results in large displacements and leads to a rapid decay of the OACF shown in Figure 3.23, curve iii. Likewise, operating on the trajectory with $\mathbf{Q}_3$ (Table 3.6) eliminates all localization effects resulting from librations in torsional angles as well as those in bond angles and bond lengths. In the absence of such cooperative fluctuations, a jump in a torsional angle from one isomeric minimum to another induces large scale displacements of the tails flanking the torsional angle undergoing the jump. This results in large changes in the orientations of bonds with consequent rapid decay of the OACF as shown by curve iv of Figure 3.23. Although the rotameric jump induces large displacements of the tails in this manner, it does not affect the isomeric states of the remaining bonds along the chain. Thus,

removal of librations by the application of Q_3 does not result in faster decay of bond angle correlations, *i.e.*, the CACF's. On the contrary, a slow down in the decay of the CACF (Figure 3.22c) results because of the removal of the rapid pathways of relaxation.

11. *Librations are not random.* The replacement of the librations of the trajectory of Figure 3.16(a) with uncorrelated librations results in OACF curves (curves v and vi in Figure 3.23) which are significantly below the OACF curve of the actual trajectory. In fact the new OACF curves lie very close to the corresponding curves iii and iv obtained in the absence of librations. It may thus be concluded that random librations are far from representing the effects of the coordinated librations and may not be adopted as appropriate mechanisms of decay in the real motion of chains.

12. *CACF and OACF time decays obey different functional forms.* Functional forms of CACFs, and in particular that of Hall and Helfand[93], have been commonly used in literature for interpreting or fitting the time decay of OACFs, without a rational justification. In Section 3.4, it is demonstrated that the response of OACFs and CACFs to librations differ from each other. Consequently, the use of the same functional form to express both correlation functions may not be adequate.

4.2. Recommendations

The stringent analysis carried out in this thesis provides a comprehensive interpretation of the local phenomena. This information is to be utilized to define a subspace where only the essential dynamics operates. Thus, the uninteresting degrees of freedom will be eliminated while keeping their fundamental influence in the dynamic behavior. This will lead to defining the chain with a smaller number of degrees of freedom and/or achieving larger time steps in the simulations. The ultimate goal is to investigate the long-time dynamics since the phenomena of practical interest occurs on this time scale. For instance, the folding $\leftrightarrow$ unfolding dynamics in proteins occur on the order of milliseconds whereas only the nanosecond dynamics is observable with today's most efficient algorithms and fastest computers. Similarly, it is known that the glass transition phenomena is closely interrelated to local aspects but a detailed investigation necessitates observation of longer time dynamics. Finally, the quantities considered in Section 3.3 are closely interrelated to

those measured in 2D NMR experiments [100-103]. In principle, it is possible to correlate these results with experiments.

Another possible future application is to employ the CK method in the simulation of biopolymers. This method is ideal for investigating how various disturbances are accommodated in these stable molecules. Alternatively, CK may be developed into a dynamic simulation method: The rotations induced at a random bond will be followed by transitions at the other bonds of the chain. The usual incremental minimization procedure will be applied to each transition. The transitions will be accepted on the basis of the current state of the neighboring bonds and according to the probabilities of occurrence of coupled or isolated transitions. Short MD simulations must be utilized to deduce the kinetics of conformational transitions for the polymer being investigated. Such studies may give us more insight on the mechanism of local motions.

APPENDIX A. POTENTIAL FUNCTIONS AND INTERACTION TYPES OF CHAIN MOLECULES

The motion of a polymer chain is dictated by the potentials involved. In the most general case, the total potential operating on the system is written as the sum:

$$V = \sum_{1}^{n} V_l(l_i) + \sum_{1}^{n-1} V_\theta(\theta_i) + \sum_{2}^{n-1} V_\varphi(\varphi_i) + \sum_i \sum_j V_{LJ}(r_{ij}) \qquad \text{(A.1)}$$

Here, $V_l(l_i)$ is the potential energy due to the stretching of ith bond, given by the harmonic function

$$V_l(l_i) = \frac{1}{2} k_l (l_i - l_o)^2 \qquad \text{(A.2)}$$

where, k_l is the bond stretching force constant, l_i is the instantaneous length of the bond between atoms i-1 and i, and l_o is the equilibrium value about which the bond length fluctuates. The bond bending potential $V_\theta(\theta_i)$ is formulated by a similar expression,

$$V_\theta(\theta_i) = \frac{1}{2} k_\theta (\cos\theta_i - \cos\theta_o)^2 \qquad \text{(A.3)}$$

with k_θ being the bending force constant, θ_i the instantaneous supplementary bond angle of the ith atom, and θ_o is its equilibrium value. Several types of torsional potential functions have been used in literature, which are cubic or quintic functions of the dihedral angle. In the present simulations, the torsional potential, $V_\varphi(\varphi_i)$, proposed by Ryckaert et al.[104] and given by

$$V_\varphi(\varphi_i) = k_\varphi \sum_0^n a_n \cos^n \varphi_i \qquad \text{(A.4)}$$

is used. Here k_φ is the torsional constant, φ_i the torsional angle of the ith bond and the parameters a_n satisfying the proper distribution of the torsional potential. Equation A.4 contains the sum of two effects: the intrinsic torsional potential and first order interactions between chain atoms. The intrinsic torsional potential is due to the sp^3 hybrids of tetrahedrally bonded atom groups. It leads to three equally probable minima at φ = 0°, ± 120°. The first order interactions induce a preference for the *trans* state (φ = 0°) relative to the *gauche* (φ = ± 120°) states, which is expressed by Equation A.4. Non-bonded interactions may be readily accounted for via the Lennard-Jones (LJ) 6-12 potential, $V_{LJ}(r_{ij})$,

$$V_{LJ}(r_{ij}) = 4\varepsilon_{ij}\left[\left(\frac{\sigma_{ij}}{r_{ij}}\right)^{12} - \left(\frac{\sigma_{ij}}{r_{ij}}\right)^{6}\right] \qquad \text{(A.5)}$$

where $r_{ij} = |\mathbf{r}_j - r_i|$, ε_{ij} and σ_{ij} are the energy and length parameters characteristic of the specific pair of non-bonded atoms i and j, separated by 4 or more bonds, i.e. $|i\text{-}j| \geq 4$. The internal coordinates of the chain are described by the set of generalized coordinates $\{l_i, \theta_i, \varphi_i\}$. They are described in terms of the coordinates of atoms as:

$$\left.\begin{aligned} l_i &= \left|\mathbf{r}_i - \mathbf{r}_{i-1}\right| && 1 \le i \le n \\ \cos\theta_i &= \frac{\mathbf{l}_i \cdot \mathbf{l}_{i+1}}{l_i\, l_{i+1}} && 1 \le i \le n-1 \\ \cos\varphi_i &= \frac{\mathbf{l}_{i-1} \times \mathbf{l}_i}{\left|\mathbf{l}_{i-1} \times \mathbf{l}_i\right|} \cdot \frac{\mathbf{l}_i \times \mathbf{l}_{i+1}}{\left|\mathbf{l}_i \times \mathbf{l}_{i+1}\right|} && 2 \le i \le n-1 \end{aligned}\right\} \qquad \text{(A.6)}$$

Several types of interactions are present between the atoms of a polymer chain. These are mainly classified as local and non-local interactions. The former defines interactions among near neighbors in the chain sequence whereas the latter describes interactions among atoms that are distant along the contour of the polymer.

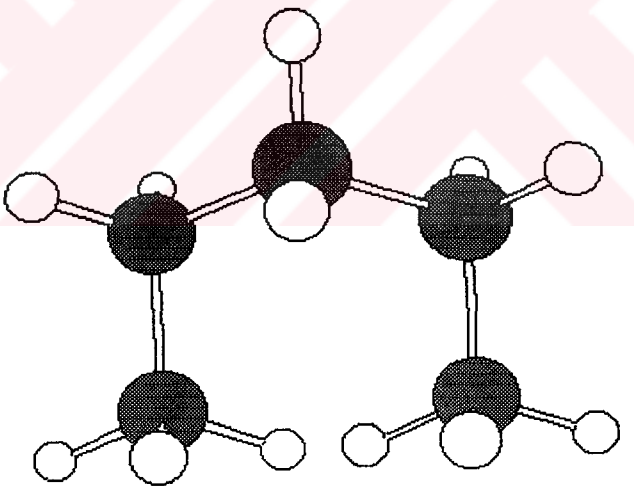

FIGURE A.1. An example of short-range intramolecular interactions: The pentane effect.

In that case, two consecutive bonds take on gauche states of opposite sign ($g^{\pm}g^{\mp}$) whereby severe steric overlap between the H atoms bonded to C atoms four bonds apart is

observed. In the most ideal case, all non-bonded interactions should also be taken into account so as to include the effect of long-range interactions between chain atoms; Figure A.2. Since such calculations are computationally expensive, cutoff values, r_{cut}, are set such that $V_{LJ} \rightarrow 0$ for $r_{ij} > r_{cut}$.

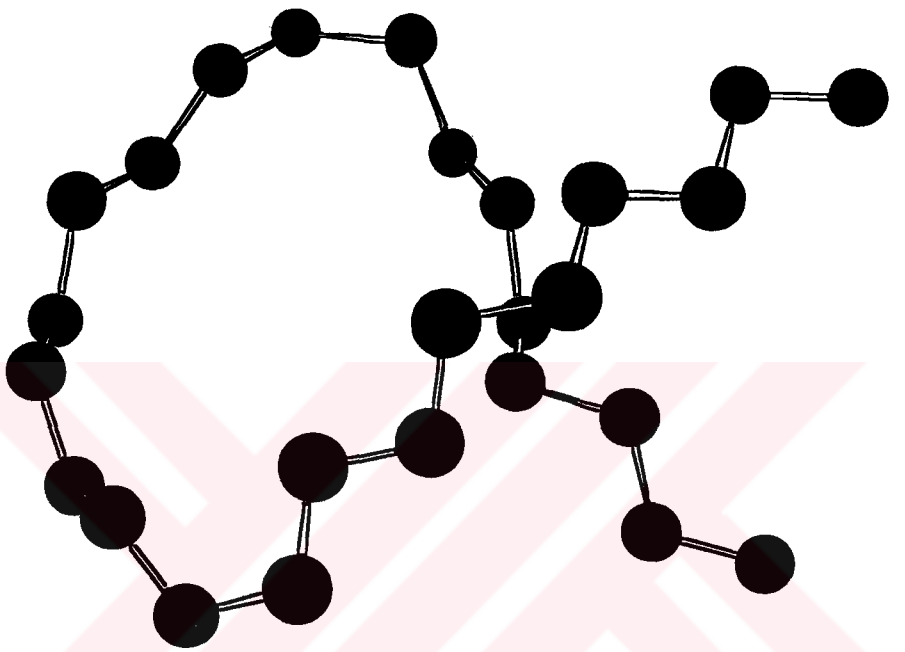

FIGURE A.2. Long-range intramolecular interactions.

The chain is best modeled when all such interactions are taken into account. However, depending on the problem being considered, simplifications are tolerable for the sake of computational efficiency. The simplest model chains must take into account bond stretching, bond bending, and torsional potentials; Equations A.2-4. If second-order interactions are also to be included, then non-bonded interactions between bonds separated by four bonds are added to the governing potential. A representative case where such interactions are important is the pentane effect in PE chains; Figure A.1.

APPENDIX B. POTENTIAL FUNCTION PARAMETERS

The parameters used in the potential functions of Appendix A are given explicitly for the three polymers studied in this work: PIP, PE, and PBD. The parameters in Tables B.1 and B.2 are applied to the polymer and in the Section specified in the last two columns.

TABLE B.1. Bond stretching potential parameters

	k_l (J/mol. Å^2)	l_o (Å)	Polymer	Section
CH_2 - CH	3.5×10^5	1.51	PIP	2.1.1
CH - CH	3.5×10^5	1.32	PIP	2.1.1
CH_2 - CH_2	3.5×10^5	1.54	PIP	2.1.1
C - C	3.5×10^5	1.53	PE	2.1.2
C - H	1.3×10^6	1.09	PE	2.1.2
CH_2 - CH_2	3.5×10^5	1.53	PE	3.1,3.3, 3.4
CH_2 - CH	none (fixed bond lengths)	1.5	PBD	3.2
CH - CH	none (fixed bond lengths)	1.5	PBD	3.2

TABLE B.2. Bond bending potential parameters

	k_θ (J/mol)	θ_o (degrees)	Polymer	Section
CH_2 - CH_2 - CH	5.2×10^5	114.6	PIP	2.1.1
CH_2 - CH - CH	10.4×10^5	120.0	PIP	2.1.1
CH - CH - CH_3	10.4×10^5	120.0	PIP	2.1.1
CH_2 - CH - CH_3	10.4×10^5	120.0	PIP	2.1.1
C - C - C	1.82×10^5	109.5	PE	2.1.2
C - C - H	1.67×10^5	109.5	PE	2.1.2
H - C - H	1.67×10^5	109.5	PE	2.1.2
CH_2 - CH_2 -CH_2	1.82×10^5	109.5	PE	3.1,3.3, 3.4
CH_2 - CH	none (fixed bond angles)	120.0	PBD	3.2
CH - CH	none (fixed bond angles)	114.6	PBD	3.2

TABLE B.3. Torsional potential parameters

	α bond [a]	β bond [b]	double bond [c]
k_φ (J/mol)	2594.3	8088.7	2.60×10^6
a_0	1.00	1.00	1.00
a_1	6.27	1.92	± 2.00 [d]
a_2	0.18	-0.55	1.00
a_3	7.45	-1.91	0.00
a_4	0.00	1.10	0.00
a_5	0.00	-1.56	0.00

a) CH_2 - CH_2 - CH - CH bond of PIP and PBD
b) CH - CH_2 - CH_2 - CH bond of PIP and PBD, and all bonds of PE
c) CH_2 - CH - CH - CH_2 bond of PIP and PBD
d) +2.00 for *cis*-PBD, -2.00 for *trans*-PBD

TABLE B.4. Non-bonded interaction parameters

	σ_{ij} (Å)	ε_{ij} (J/mol)
CH_x - CH_x ; x = 1-3	3.6	580.8
C - C	3.2	351.8
C - H	2.8	318.7
H - H	2.3	301.5

APPENDIX C. FORMULATION OF THE COOPERATIVE KINEMATICS METHOD

Consider the rotational potential V of the chain at a given instantaneous configuration **q**. This potential may be expressed as a Taylor series expansion in the close neighborhood of $\mathbf{q}^\circ = \{\varphi_1^\circ, \varphi_2^\circ, ..., \varphi_{n-1}^\circ, \Psi^\circ, X_o^\circ, Y_o^\circ, Z_o^\circ\}$ as

$$V = V_0 + \sum_i \left[\frac{\partial V}{\partial \varphi_i}\right]_{\mathbf{q}^\circ} \Delta\varphi_i + \frac{1}{2}\sum_i\sum_j \left[\frac{\partial^2 V}{\partial \varphi_i \partial \varphi_j}\right]_{\mathbf{q}^\circ} \Delta\varphi_i \Delta\varphi_j + \ldots \qquad \text{(C.1)}$$

For the particular form of V given by Equation A.4, the second derivative vanishes for $i \neq j$. Accordingly for small $\Delta\varphi_m$, the derivative of V with respect to the dihedral angle φ_m at configuration **q** reads

$$\partial V / \partial \varphi_m = \left(\partial V / \partial \varphi_m\right)_{\mathbf{q}^\circ} + \left(\partial^2 V / \partial \varphi_m^{\,2}\right)_{\mathbf{q}^\circ} \Delta\varphi_m \qquad \text{(C.2)}$$

In the following, the notation Δq_m and Δt, instead of δq_m and δt, will be adopted for small incremental changes in the generalized coordinates and for the corresponding time intervals, respectively. It is implicit in the notation that all incremental changes refer to differential variations consistent with the basic approach.

Inasmuch as $\partial V / \partial \varphi_m = \partial \Delta V / \partial \Delta \varphi_m$, the first line of Equation 2.23 may be written in the form

$$\frac{\partial[W_\xi/2+\Delta V]}{\partial\Delta\varphi_i}\equiv\frac{\partial[\Delta E]}{\partial\Delta\varphi_i}=0 \qquad \text{(C.3)}$$

in which the definition $\Delta E = W_\xi/2 + \Delta V$ is introduced.

On the other hand, the position vector $\mathbf{r}_i$ of the ith atom relative to the local frame $x_o y_o z_o$ affixed to the first atom of the chain is evaluated from

$$\mathbf{r}_i = [E \quad 0]\left[\prod_{k=1}^{i-1}\mathbf{G}_k\right]\begin{bmatrix}\mathbf{l}\\ \\ 1\end{bmatrix} \qquad \text{(C.4)}$$

where $\mathbf{l}$ is the local bond vector col(l 0 0) for bonds of length l, $\mathbf{E}$ is the identity matrix of order three, and $\mathbf{G}_i$ is the conventional generator matrix for determining $\mathbf{r}_i$[42]. The passage to absolute position vectors $\mathbf{R}_i$ is readily established by the identity

$$\mathbf{R}_i = \mathbf{T}(\Psi)\mathbf{T}(\Phi)\mathbf{r}_i + \mathbf{R}_0 \qquad \text{(C.5)}$$

where $\mathbf{T}(\Psi)$ and $\mathbf{T}(\Phi)$ are the transformation matrices accounting for the orientation of the first bond of the chain in space.

Adopting this framework, the first term in the first line of Equation 2.23 is obtained from

$$\frac{\delta t}{2\xi}\frac{\partial \delta W_{\xi}}{\partial \delta \varphi_m} = \sum_{j=1}^{n-1} u_{mj}\delta\varphi_j + p_m\delta\Psi + w_m\delta\Phi + \mathbf{v}_m \cdot \delta\mathbf{R}_0 \tag{C.6}$$

where the coefficients of the incremental generalized coordinates are defined as

$$p_m = \sum_{i=m+1}^{n}\left(\mathbf{a}_{im} \cdot \mathbf{Dr}_i\right) \tag{C.7}$$

$$w_m = \sum_{i=m+1}^{n}\left(\mathbf{a}_{im} \cdot \mathbf{Br}_i\right) \tag{C.8}$$

$$\mathbf{v}_m = \mathbf{T}(\Psi)\mathbf{T}(\Phi)\sum_{i=m+1}^{n}\mathbf{a}_{im} \tag{C.9}$$

$$u_{mj} = \sum_{i=k+1}^{n}\mathbf{a}_{im} \cdot \mathbf{a}_{ij} \tag{C.10}$$

with the summation index $k = \max(m, j)$, and

$$\mathbf{a}_{ij} = \left[\prod_{k=0}^{j-1}\mathbf{T}_k\right]\mathbf{A}\mathbf{T}_j\begin{bmatrix}\mathbf{E} & 0\end{bmatrix}\left[\prod_{k=j+1}^{i-1}\mathbf{G}_k\right]\begin{bmatrix}\mathbf{l}\\ \\ \mathbf{l}\end{bmatrix} \tag{C.11}$$

where **A**, **B**, and **C** are unitary matrices yielding the derivatives of the transformation matrices according to the relationships

$$\frac{\partial \mathbf{T}_j}{\partial \varphi_j} = \mathbf{A}\mathbf{T}_j; \quad \frac{\partial \mathbf{T}(\Phi)}{\partial \Phi} = \mathbf{T}(\Phi)\mathbf{B}; \quad \frac{\partial \mathbf{T}(\Psi)}{\partial \Psi} = \mathbf{T}(\Phi)\mathbf{C} \tag{C.12}$$

and finally **D** is defined as $\mathbf{D} = \mathbf{T}(\Phi)^{\mathrm{T}}\mathbf{C}\mathbf{T}(\Phi)$.

Equations C.2 and C.6 are inserted into Equation C.3 to obtain the equality

$$\sum_{j=1}^{n-1}\left(u_{mj} + V''_{mj}\right)\Delta\varphi_j + p_m\Delta\Psi + w_m\Delta\Phi + \mathbf{v}_m \cdot \Delta\mathbf{R}_0 + V'_m = 0 \tag{C.13}$$

V'_m and V''_{mj} are defined as

$$\left.\begin{aligned} V'_m &\equiv (\delta t / \xi)\left(\partial V / \partial \varphi_m\right)_{\mathbf{q}^0} \\ V''_{mj} &\equiv (\delta t / \xi)\left(\partial^2 V / \partial \varphi_m{}^2\right)_{\mathbf{q}^0}\delta_{mj} \end{aligned}\right\} \tag{C.14}$$

where δ_{mj} is the Kronecker delta.

If bond s is externally constrained to undergo a given rotational perturbation $\Delta\varphi_s$, Equation C.13 becomes

$$\sum_{\substack{j=1\\ j\neq s}}^{n-1}\left(u_{mj}+V''_{mj}\right)\Delta\varphi_j+p_m\Delta\Psi+w_m\Delta\Phi+\mathbf{v}_m\cdot\Delta\mathbf{R}_0=-V'_m-u_{ms}\Delta\varphi_s \qquad \text{(C.15)}$$

Likewise, the counterpart of the three equalities in the second line of Equation 2.23 in the presence of the constraint $\Delta\varphi_s$ are

$$\sum_{\substack{m=1\\ m\neq s}}^{n-1}p_m\Delta\varphi_m+\sum_{i=0}^{n}\left(\mathbf{Dr}_i\cdot\mathbf{Dr}_i\right)\Delta\Psi+\sum_{i=0}^{n}\left(\mathbf{Dr}_i\cdot\mathbf{Br}_i\right)\Delta\Phi+$$

$$\left[\mathbf{T}(\Psi)\mathbf{T}(\Phi)\sum_{i=0}^{n}\mathbf{Dr}_i\right]\cdot\Delta\mathbf{R}_0=-P_S\Delta\varphi_S \qquad \text{(C.16)}$$

$$\sum_{\substack{m=1\\ m\neq s}}^{n-1}w_m\Delta\varphi_m+\sum_{i=0}^{n}\left(\mathbf{Br}_i\cdot\mathbf{Br}_i\right)\Delta\Phi+\sum_{i=0}^{n}\left(\mathbf{Dr}_i\cdot\mathbf{Br}_i\right)\Delta\Psi+$$

$$\left[\mathbf{T}(\Psi)\mathbf{T}(\Phi)\sum_{i=0}^{n}\mathbf{Br}_i\right]\cdot\Delta\mathbf{R}_0=-w_S\Delta\varphi_S \qquad \text{(C.17)}$$

$$\sum_{\substack{m=1\\ m\neq s}}^{n-1}\mathbf{v}_m\Delta\varphi_m+\left[\mathbf{T}(\Psi)\mathbf{T}(\Phi)\sum_{i=0}^{n}\mathbf{Dr}_i\right]\Delta\Psi+\left[\mathbf{T}(\Psi)\mathbf{T}(\Phi)\sum_{i=0}^{n}\mathbf{Br}_i\right]\cdot\Delta\Phi+$$

$$(n+1)\Delta\mathbf{R}_0=-\mathbf{v}_S\Delta\varphi_S \qquad \text{(C.18)}$$

Equation C.15 - C.18 are the basic equations of motion to be solved simultaneously to determine the new set of generalized coordinates following the perturbation of the original configuration q°. This set of equations may be conveniently represented in matrix notation as

$$\begin{bmatrix} \mathbf{Q}_1 & \mathbf{Q}_2 \\ \mathbf{Q}_2^{\mathrm{T}} & \mathbf{Q}_4 \end{bmatrix} \begin{bmatrix} \Delta\varphi \\ \Delta\mathbf{X} \end{bmatrix} = \begin{bmatrix} \Delta\varphi^{\circ} \\ \Delta\mathbf{X}^{o} \end{bmatrix} \tag{C.19}$$

in which the solution is expressed in the form of an array of incremental changes in generalized coordinates, using the notation

$$\Delta\varphi = \begin{bmatrix} \Delta\varphi_1 & \Delta\varphi_2 & \cdots & \Delta\varphi_{s-1} & \Delta\varphi_{s+1} & \cdots & \Delta\varphi_{n-1} \end{bmatrix} \tag{C.20}$$

and

$$\Delta\mathbf{X} = \begin{bmatrix} \Delta\Psi & \Delta\Phi & \Delta X_0 & \Delta Y_0 & \Delta Z_0 \end{bmatrix}^{\mathrm{T}} \tag{C.21}$$

$\Delta\varphi^{\circ}$ and $\Delta\mathbf{X}^{\circ}$ depend on the rotational perturbation of the bond s and on the rotational potentials and are given by the expressions

$$\Delta\varphi^{\circ} = -\begin{bmatrix} u_{1,s} & u_{1,s} & \cdots & u_{s-1,s} & u_{s+1,s} & \cdots & u_{n-1,s} \end{bmatrix}^{\mathrm{T}} \Delta\varphi_s - \begin{bmatrix} V'_1 & V'_2 & \cdots & V'_{s-1} & V'_{s+1} & \cdots & V'_{n-1} \end{bmatrix}^{\mathrm{T}} \tag{C.22}$$

$$\Delta\mathbf{X}^{\circ} = -\begin{bmatrix} p_s & w_s & \mathbf{v}_s^{\mathrm{T}} \end{bmatrix}^{\mathrm{T}} \Delta\varphi_s \tag{C.23}$$

The matrices $\mathbf{Q}_1$, $\mathbf{Q}_2$ and $\mathbf{Q}_4$ in Equation C.19 is defined by

$$\mathbf{Q}_1 = \mathbf{U} + \mathbf{V}'' \tag{C.24}$$

$$\mathbf{Q}_2 \equiv \begin{bmatrix} p_1 & w_1 & \mathbf{v}_1^{\mathrm{T}} \\ p_2 & w_2 & \mathbf{v}_2^{\mathrm{T}} \\ \cdots & \cdots & \cdots \\ p_{s-1} & w_{s-1} & \mathbf{v}_{s-1}^{\mathrm{T}} \\ p_{s+1} & w_{s+1} & \mathbf{v}_{s+1}^{\mathrm{T}} \\ \cdots & \cdots & \cdots \\ \cdots & \cdots & \cdots \\ \cdots & \cdots & \cdots \\ p_{n-1} & w_{n-1} & \mathbf{v}_{n-1}^{\mathrm{T}} \end{bmatrix} \tag{C.25}$$

$$\mathbf{Q}_4 \equiv \begin{bmatrix} \sum_{i=0}^{n} \mathbf{Dr}_i \cdot \mathbf{Dr}_i & \cdots & \cdots \\ \sum_{i=0}^{n} \mathbf{Dr}_i \cdot \mathbf{Br}_i & \sum_{i=0}^{n} \mathbf{Br}_i \cdot \mathbf{Br}_i & \cdots \\ \mathbf{T}(\Psi)\mathbf{T}(\Phi)\sum_{i=0}^{n} \mathbf{Dr}_i & \mathbf{T}(\Psi)\mathbf{T}(\Phi)\sum_{i=0}^{n} \mathbf{Br}_i & (n+1)\mathbf{E} \end{bmatrix} \tag{C.26}$$

$\Delta\varphi$ and $\Delta\mathbf{X}$ are determined from

$$\begin{bmatrix}\Delta\varphi\\ \Delta\mathbf{X}\end{bmatrix}=\begin{bmatrix}\mathbf{Q}_1 & \mathbf{Q}_2\\ \mathbf{Q}_2^{\mathrm{T}} & \mathbf{Q}_4\end{bmatrix}^{-1}\begin{bmatrix}\Delta\varphi^{o}\\ \Delta\mathbf{X}^{o}\end{bmatrix} \tag{C.27}$$

which readily follows from Equation C.19.

REFERENCES

1. Rouse, P. E., "A Theory of Linear Viscoelastic Properties of Dilute Solutions of Coiling Polymers," Journal of Chemical Physics, Vol. 21, No. 7, pp. 1272-1280, 1953.

2. Zimm, B. H., "Dynamics of Polymer Molecules in Dilute Solution: Viscoelasticity, Flow Birefringence and Dielectric Loss," Journal of Chemical Physics, Vol. 24, No. 2, pp. 269-278, 1956.

3. Iwata, K., "Irreversible Statistical Mechanics of Polymer Chains. III. A Dynamic Model of Vinyl Polymers," *Journal of Chemical Physics*, Vol. 58, No. 10, pp. 4184-4202, 1973.

4. Helfand, E., "Theory of the Kinetics of Conformational Transitions in Polymers," *Journal of Chemical Physics*, Vol. 54, No. 11, pp. 4651-4661, 1971.

5. Helfand, E., "Dynamics of Conformational Transitions in Polymers," *Science*, Vol. 226, pp. 647, 1984.

6. Blomberg, C., "Kinetics of Small Segment Motion in Macromolecules with Applications to Hindered Motion in Polyethylene," *Chemical Physics*, Vol. 37, pp. 219-227, 1979.

7. Montgomery, J. A., S. L. Holmgren, and D. Chandler, "Stochastic Molecular Dynamics Study of *trans-gauche* Isomerization Processes in Simple Chain Molecules" *Journal of Chemical Physics*, Vol. 73, No. 8, pp. 3688-3694, 1980.

8. Helfand, E., "Brownian Dynamics Study of Transitions in a Polymer Chain of Bistable Oscillators," *Journal of Chemical Physics*, Vol. 69, No. 3, pp. 1010-1018, 1978.

9. Pear, M. R., and J. H. Weiner, "Brownian Dynamics Study of a Polymer Chain of

Linked Rigid Bodies," *Journal of Chemical Physics*, Vol. 71, No. 1, pp. 212-224, 1979.

10. Pear, M. R., and J. H. Weiner, "Brownian Dynamics Study of a Polymer Chain of Linked Rigid Bodies. II. Results for Longer Chains," *Journal of Chemical Physics*, Vol. 72, No. 7, pp. 3939-3947, 1980.

11. Fixman, M., "Simulation of Polymer Dynamics. I. General Theory," *Journal of Chemical Physics*, Vol. 69, No. 4, pp. 1527-1537, 1978.

12. Fixman, M., "Simulation of Polymer Dynamics. II. Relaxation Rates and Dynamic Viscosity," *Journal of Chemical Physics*, Vol. 69, No. 4, pp. 1538-1545, 1978.

13. Weber, T. A., "Simulation of *n*-Butane Using a Skeletal Alkane Model," *Journal of Chemical Physics*, Vol. 69, No. 6, pp. 2347-2354, 1978.

14. Weber, T., "Relaxation of a *n*-Octane Fluid," *Journal of Chemical Physics*, Vol. 70, No. 9, pp. 4277-4284, 1979.

15. Helfand, E., Z. R. Wasserman, and T. A. Weber, "Brownian Dynamics Study of Polymer Conformational Transitions," *Macromolecules*, Vol. 13, No. 3, pp. 526-533, 1980.

16. Zuniga, I., I. Bahar, R. Dodge, and W. L. Mattice, "Molecular Dynamics Analysis of Transitions Between Rotational Isomers in Polymethylene," *Journal of Chemical Physics*, Vol. 95, No. 7, pp. 5348-5354, 1991.

17. Rigby, D., and R.-J. Roe, "Molecular Dynamics Simulation of Polymer Liquid and Glass. III. Chain Conformation," *Macromolecules*, Vol. 22, No. 5, pp. 2259-2264, 1989.

18. Takeuchi, H., and R.-J. Roe, "Molecular Dynamics Simulation of Local Chain Motion in Bulk Amorphous Polymers. I. Dynamics Above Glass Transition," *Journal of Chemical Physics*, Vol. 94, No. 11, pp. 7446-7457, 1991.

19. Doruker, P., and I. Bahar, "Effect of Intrachain Constraints and Polymer-Solvent Interactions on Chain Statistics and Dynamics," *Computational Polymer Science*, Vol. 3, No. 3, pp. 87-99, 1993.

20. Rigby, D., and R.-J. Roe, "Molecular Dynamics Simulation of Polymer Liquid and Glass. I. Glass Transition," *Journal of Chemical Physics*, Vol. 87, No. 12, pp. 7285-7292, 1987.

21. Rigby, D., and R.-J. Roe, "Molecular Dynamics Simulation of Polymer Liquid and Glass. II. Short Range Order and Orientation Correlation," *Journal of Chemical Physics*, Vol. 89, No. 8, pp. 5280-5290, 1988.

22. Haliloglu, T., I. Bahar, and B. Erman, "Orientational and Conformational Correlations in Deformed Polymer Chains with Fixed End-to-end Separation: A Brownian Dynamics Simulation Study," *Journal of Chemical Physics*, Vol. 97, No. 6, pp. 4428-4437, 1992.

23. Haliloglu, T., I. Bahar, and B. Erman, "Time-Dependent Probability Distribution Functions for Orientational Motions of Segments in Polymer Chains," *Journal of Chemical Physics*, Vol. 97, No. 6, pp. 4438-4444, 1992.

24. Adolf, D. B., and M. D. Ediger, "Brownian Dynamics Simulations of Local Motions in Polyisoprene," *Macromolecules*, Vol. 24, No. 21, pp. 5834-5842, 1991.

25. Moe, N. E., and M. D. Ediger, "Molecular Dynamics Computer Simulation of Polyisoprene Local Dynamics in Dilute Toluene Solution," *Macromolecules*, Vol. 28, No. 7, pp. 2329-2338, 1995.

26. Bahar, I., B. Erman, and L. Monnerie, "Effect of Molecular Structure on Local Chain Dynamics: Analytical Approaches and Computational Methods," *Advances in Polymer Science*, Vol. 116, pp. 145-206, 1994.

27. Moro, G., "The Coupling between Librational Motions and Conformational Transitions in Chain Molecules. A Phenomenological Analysis," *Journal of Chemical Physics*, Vol. 94, No. 12, pp. 8577-8591, 1991.

28. Moro, G., "The Coupling between Librational Motions and Conformational Transitions in Chain Molecules. II. The Rotor Chain Represented by the Master Equation for Site Distributions," *Journal of Chemical Physics*, Vol. 97, No. 8, pp. 5749-5765, 1992.

29. Bahar, I., and B. Erman, "Investigation of Local Motions in Polymers by the Dynamic Rotational Isomeric State Model," *Macromolecules*, Vol. 20, No. 6, pp. 1368-1376, 1987.

30. Bahar, I., and B. Erman, "Anisotropy of Static and Dynamic Orientational Correlations in *n*-Alkanes," *Journal of Chemical Physics*, Vol. 88, No. 2, pp. 1228-1233, 1988.

31. Bahar, I., B. Erman, and L. Monnerie, "A New Approach to the Relationship between Chemical Structure and Local Dynamics Nuclear Magnetic Resonance Measurements in Dilute Polymer Solutions," *Polymer Communications*, Vol. 29, pp. 349-351, 1988.

32. Bahar, I., B. Erman, and L. Monnerie, "Comparison of Dynamic Rotational Isomeric State Results with Previous Expressions for Local Chain Motion," *Macromolecules*, Vol. 22, No. 1, pp. 431-437, 1989.

33. Bahar, I., B. Erman, and L. Monnerie, "Application of the Dynamic Rotational Isomeric States Model to Polyethyleneoxide and Comparison with Nuclear Magnetic Relaxation Data," *Macromolecules*, Vol. 22, No. 5, pp. 2396-2403, 1989.

34. Bahar, I., B. Erman, and L. Monnerie, "Local Orientational Motions in Flexible Polymeric Chains," *Macromolecules*, Vol. 23, No. 4, pp. 1174-1180, 1990.

35. Bahar, I., and W. L. Mattice, "Efficient Calculation of the Intramolecular Contribution to Orientational Autocorrelation Functions Using Dynamic Rotational Isomeric State Theory," *Macromolecules*, Vol. 23, No. 10, pp. 2719-2733, 1990.

36. Bahar, I., B. Erman, and L. Monnerie, "Stochastic Treatment of Conformational Transitions of Polymer Chains in the Sub-Rouse Regime," *Macromolecules*, Vol. 24, No. 12, pp. 3618-3626, 1991.

37. Bahar, I., B. Erman, F. Kremer, and E. W. Fischer, "Dynamic Rotational Isomeric State Approach for Segmental Motions of *cis*-Polyisoprene in the Bulk State," *Progress in Colloid and Polymer Science*, Vol. 91, pp. 1-4, 1993.

38. Bahar, I., B. Erman, and L. Monnerie, "Kinematics of Polymer Chains with Freely Rotating Bonds in a Restrictive Environment. I. Theory," *Macromolecules*, Vol. 25, No. 23, pp. 6309-6314, 1992.

39. Bahar, I., B. Erman, and L. Monnerie, "Kinematics of Polymer Chains with Freely Rotating Bonds in a Restrictive Environment. 2. Conformational and Orientational Correlations," *Macromolecules*, Vol. 25, No. 23, pp. 6314-6321, 1992.

40. Erman, B., and I. Bahar, "Local Dynamics of Freely Rotating Polymer Chains in Dense Systems," *Progress in Colloid and Polymer Science*, Vol. 91, pp. 16-19, 1993.

41. Bahar, I., N. Baysal, B. Erman, and L. Monnerie, "Kinematics of Polymer Chains in Dense Media. III. Influence of Intramolecular Conformational Potentials," *Macromolecules*, Vol. 28, No. 4, pp. 1038-1048, 1995.

42. Flory, P. J., *Statistical Mechanics of Chain Molecules*, New York: Oxford University Press, 1969.

43. Swope, W. C., H. C. Anderson, P. H. Berens, and K. R. Wilson, "A Computer Simulation Method for the Calculation of Equilibrium Constants for the Formation of Physical Clusters of Molecules: Application to Small Water Clusters," *Journal of Chemical Physics*, Vol. 76, pp. 637-649, 1982.

44. Berendsen, H. J. C., J. P. M. Postma, W. F. van Gunsteren, A. DiNola, and J. R. Haak, "Molecular Dynamics with Coupling to an External Bath," *Journal of Chemical Physics*, Vol. 81, pp. 3384-3390, 1981.

45. Rey, A., A. Kolinski, J. Skolnick, "Effect of Double Bonds on the Dynamics of Hydrocarbon Chains," *Journal of Chemical Physics*, Vol. 97, No. 2, pp. 1240-1249, 1992.

46. Helfand, E., "Numerical Integration of Stochastic Differential Equations," *The Bell System Technical Journal*, Vol. 58, No. 10, pp. 2289-2299, 1979.

47. Ediger, M. D., and D. B. Adolf, "Brownian Dynamics Simulations of Local Polymer Dynamics," *Advances in Polymer Science*, Vol. 116, pp. 73-109, 1994.

48. Glowinkowski, S., D. J. Gisser, and M. D. Ediger, "Carbon-13 Nuclear Magnetic Resonance Measurements of Local Segmental Dynamics of Polyisoprene in Dilute Solution: Nonlinear Viscosity Dependence," *Macromolecules*, Vol. 23, No. 14, pp. 3520-3530, 1990.

49. Dejean de la Batie, R., F. Laupretre, and L. Monnerie, "Carbon-13 NMR Investigation of Local Dynamics in Bulk Polymers at Temperatures Well above the Glass-Transition Temperature. III. *cis*-1,4-Polybutadiene and *cis*-1,4-Polyisoprene," *Macromolecules*, Vol. 22, No. 1, pp. 122-129, 1989.

50. Waldow, D. A., B. S. Johnson, P. D. Hyde, M. D. Ediger, T. Kitano, and K. Ito, "Local Segmental Dynamics of Polyisoprene in Dilute Solution: Solvent and Molecular Weight Effects," *Macromolecules*, Vol. 22, No. 3, pp. 1345-1351, 1989.

51. Adolf, D. B., and M. D. Ediger, "Brownian Dynamics Simulations of Local Polymer Motions in Polyisoprene: Comparison to NMR Experiments," in R. J. Roe (Ed.), *Computer Simulation of Polymers*, pp. 154-166, New Jersey: Prentice Hall, 1991.

52. Ryckaert, J.-P., G. Ciccotti, and H. J. C. Berendsen, "Numerical Integration of the Cartesian Equations of Motion of a System with Constraints: Molecular Dynamics of *n*-Alkanes," *Journal of Computational Physics*, Vol. 23, pp. 327-341, 1977.

53. van Gunsteren, W. F., and M. Karplus, "Effect of Constraints on the Dynamics of Macromolecules," *Macromolecules*, Vol. 15, pp. 1528-1544, 1982.

54. van Gunsteren, W. F., and H. J. C. Berendsen, "Computer Simulation of Molecular Dynamics: Methodology, Applications, and Perspectives in Chemistry," *Angewandte Chemie, International Edition in English*, Vol. 29, pp. 992-1023, 1990.

55. Ryckaert, J.-P., "Special Geometrical Constraints in the Molecular Dynamics of Chain Molecules," *Molecular Physics*, Vol. 55, No. 3, pp. 549-556, 1985.

56. Ryckaert, J.-P., and M. L. Klein, "Translational and Rotational Disorder in Solid *n*-Alkanes: Constant Temperature-Constant Pressure Molecular Dynamics Calculations Using Infinitely Long Flexible Chains," *Journal of Chemical Physics*, Vol. 85, No. 3, pp. 1613-1620, 1986.

57. Ermak, D. L., "A Computer Simulation of Charged Particles in Solution. I. Technique and Equilibrium Properties," *Journal of Chemical Physics*, Vol. 62, No. 10, pp. 4189-4196, 1975.

58. Bahar, I., I. Zuniga, R. Dodge, and W. L. Mattice, "Conformational Statistics of Poly(dimethylsiloxane). I. Probability Distribution of Rotational Isomers from Molecular Dynamics Simulations," *Macromolecules*, Vol. 24, No. 10, pp. 2986-2992, 1991.

59. Bahar, I., N. Neuburger, and W. L. Mattice, "Mechanism of Local Conformational Transitions in Poly(dialkylsiloxanes). Molecular Dynamics Simulations and Dynamic Rotational Isomeric States Approach," *Macromolecules*, Vol. 25, No. 18, pp. 4619-4625, 1992.

60. Kloczkowski, A., and J. E. Mark, "A Closed Form Solution for the Internal Dynamics of Polymer Chains. I. Bonds with Independent Rotational Potentials," *Journal of Chemical Physics*, Vol. 92, No. 7, pp. 4513-4518, 1990.

61. Weber, T., and E. Helfand, "Time-Correlation Functions from Computer Simulations of Polymers," *Journal of Physical Chemistry*, Vol. 87, No. 15, pp. 2881-2889, 1983.

62. Helfand, E., Z. R. Wasserman, and T. A. Weber, "Brownian Dynamics Study of Polymer Conformational Dynamics," *Journal of Chemical Physics*, Vol. 70, No. 4, pp. 2016-2017, 1979.

63. Adolf, D. B., and M. D. Ediger, "Cooperativity of Local Conformational Dynamics in Simulations of Polyisoprene and Polyethylene," *Macromolecules*, Vol. 25, No. 3, pp.

1074-1078, 1992.

64. Rigby, D., and R. J. Roe, "Local Chain Motion Studied by Molecular Dynamics Simulation of Polymer Liquid and Glass," in R. J. Roe (Ed.), *Computer Simulation of Polymers*, pp. 79-93, New Jersey: Prentice Hall, 1991.

65. Mattice, W. L., R. Dodge, I. Zuniga, and I. Bahar, "Use of Molecular Dynamics Trajectories for the Formulation of Statistical Weight Matrices for Chains of Bonds with Symmetric Threefold Rotation Potentials," *Computational Polymer Science*, Vol. 1, No. 1, pp. 35-40, 1991.

66. Abe, A., R. L. Jernigan, P. J. Flory, "Conformational Energies of *n*-Alkanes and the Random Configuration of Higher Homologs Including Polymethylene," *Journal of the American Chemical Society*, Vol. 88, pp. 631-639, 1966.

67. Monnerie, L., "Local Dynamics in Polybutadiene Melts," *Gazzetta Chimica Italiana*, Vol. 117, pp. 139-147, 1987.

68. Kim, E.-G., and W. L. Mattice, "Local Chain Dynamics of Bulk Amorphous Polybutadienes: A Molecular Dynamics Study," *Journal of Chemical Physics*, Vol. 101, No. 7, pp. 6242-6254, 1994.

69. Gee, R. H., and R. H. Boyd, "Conformational Dynamics and Relaxation in Bulk Polybutadienes: A Molecular Dynamics Simulation Study," *Journal of Chemical Physics*, Vol. 101, No. 9, pp. 8028-8038, 1994.

70. Abe, Y., and P. J. Flory, "Configurational Statistics of 1,4-Polybutadiene Chains," *Macromolecules*, Vol. 4, No. 2, pp. 219-229, 1971.

71. Li. Y., and W. L. Mattice, "Atom-Based Modeling of Amorphous 1,4-*cis*-Polybutadiene," *Macromolecules*, Vol. 25, No. 19, pp. 49-42-4947, 1992.

72. Kim, E.-G., S. Misra, and W. L. Mattice, "Atomistic Models of Amorphous Polybutadienes. II. Poly(1,4-*trans*-butadiene), Poly(1,2-butadiene), and a Random Copolymer of 1,4-*trans*-butadiene, 1,4-*cis*-butadiene, and 1,2-butadiene,"

Macromolecules, Vol. 26, No. 13, pp. 3424-3431, 1993.

73. Chen, S. P., and J. D. Ferry, "The Diffusion of Radioactively Tagged *n*-Hexadecane and *n*-Dodecane through Rubbery Polymers. Effects of Temperature, Cross-Linking, and Chemical Structure," *Macromolecules*, Vol. 1, No. 3, pp. 270-278, 1990.

74. Case, D. A., "Normal Mode Analysis of Protein Dynamics," *Current Opinion in Structural Biology*, Vol. 4, pp. 285-290, 1994.

75. Durand, P., G. Trinquier, and Y.-H. Sanejouand, "A New Approach for Determining Low-Frequency Normal Modes in Macromolecules," *Biopolymers*, Vol. 34, pp. 759-771, 1994.

76. Kitao, A., and N. Go, "Conformational Dynamics of Polypeptides and Proteins in the Dihedral Angle Space and in the Cartesian Coordinate Space: Normal Mode Analysis of Deca-Alanine," *Journal of Computational Chemistry*, Vol. 12, No. 3, pp. 359-368, 1991.

77. Dauber-Osguthorpe, P., and D. J. Osguthorpe, "Partitioning the Motion in Molecular Dynamics Simulations into Characteristic Modes of Motion," *Journal of Computational Chemistry*, Vol. 14, No. 11, pp. 1259-1271, 1993.

78. Sessions, R. B., P. Dauber-Osguthorpe, and D. J. Osguthorpe, "Filtering Molecular Dynamics Trajectories to Reveal Low-frequency Collective Motions: Phospholipase A_2," *Journal of Molecular Biology*, Vol. 209, pp. 617-633, 1989.

79. Dauber-Osguthorpe, P., and D. J. Osguthorpe, "Analysis of Intramolecular Motions by Filtering Molecular Dynamics Trajectories," *Journal of the American Chemical Society*, Vol. 112, No. 22, pp. 7921-7935, 1990.

80. Dauber-Osguthorpe, P., and D. J. Osguthorpe, "Extraction of the Energetics of Selected Types of Motion from Molecular Dynamics Trajectories by Filtering," *Biochemistry*, Vol. 29, pp. 8223-8228, 1990.

81. Levitt, M., "Real-time Interactive Frequency Filtering of Molecular Dynamics

Trajectories," *Journal of Molecular Biology*, Vol. 22, pp. 1-4, 1991.

82. Horiuchi, T., and N. Go, "Projection of Monte Carlo and Molecular Dynamics Trajectories Onto the Normal Mode Axes: Human Lysozyme," *Proteins: Structure, Function, and Genetics*, Vol. 10, pp. 106-116, 1991.

83. Fermi, E., J. Pasta, S. Ulam, and M. Tsingou, "Ordered and Chaotic Motions in Dynamical Systems with Many Degrees of Freedom," *Studies of Nonlinear Problems I*, Los Alamos Laboratory, 1955.

84. Benettin, G., in G. Ciccotti and W. G. Hoover (Eds.), *Molecular Dynamics Simulation of Statistical Mechanical Systems*, pp. 15-37, North Holland: Varenna, 1985.

85. Ford, J., "The Fermi-Pasta-Ulam Problem: Paradox Turns Discovery," *Physics Reports*, Vol. 213, pp. 271-310, 1992.

86. Noda, I., "Two-Dimensional Infrared Spectroscopy," *Journal of the American Chemical Society*, Vol. 111, No. 21, pp. 8116-8118, 1989.

87. Noda, I., "Two-Dimensional Correlation Approach to the Dynamic Rheo-optical Characterization of Polymers," *Chemtracts-Macromolecular Chemistry*, Vol. 1, pp. 89-105, 1990.

88. Noda, I., "Generalized Two-Dimensional Correlation Method Applicable to Infrared, Raman, and Other Types of Spectroscopy," *Applied Spectroscopy*, Vol. 47, No. 9, pp. 1329-1336, 1993.

89. Press, W. H., S. A. Teukolsky, W. T. Vetterling, and B. P. Flannery, *Numerical Recipes in FORTRAN*, Cambridge: Oxford University Press, 1992.

90. Amadei, A., A. B. M. Linssen, and H. J. C. Berendsen, "Essential Dynamics of Proteins," *Proteins: Structure, Function, and Genetics*, Vol. 117, pp. 412-425, 1995.

91. Jones, A. A., and W. H. Stockmayer, "Models for Spin Relaxation in Dilute Solutions

of Randomly Coiled Polymers," *Journal of Polymer Science: Polymer Physics Edition*, Vol. 15, pp. 847-861, 1977.

92. Bendler, J. T., and R. Yaris, "A Solvable Model of Polymer Main-Chain Dynamics with Applications to Spin Relaxation," *Macromolecules*, Vol., No. 4, pp. 650-658, 1978.

93. Hall, C. K., and E. Helfand, "Conformational State Relaxation in Polymers: Time Correlation Functions," *Journal of Chemical Physics*, Vol. 77, No. 6, pp. 3275-3282, 1982.

94. Howarth, O. W., "Effect of Internal Librational Motions on the ^{13}C Nuclear Magnetic Resonance Relaxation Times of Proteins and Peptides," *Journal of Chemical Society: Faraday II*, Vol. 74, pp. 1031-1041, 1978.

95. Howarth, O. W., "Effect of Internal Librational Motions on the ^{13}C Nuclear Magnetic Resonance Relaxation Times of Polymers and Peptides," *Journal of Chemical Society: Faraday II*, Vol. 75, pp. 863-873, 1979.

96. Howarth, O. W., "^{13}C Nuclear Magnetic Resonance Study of Molecular Motions in Natural Rubber," *Journal of Chemical Society: Faraday II*, Vol. 76, pp. 1219-1223, 1980.

97. Cook, R., and E. Helfand, "Time-Correlation Functions for a One-Dimensional Polymer Model," *Journal of Chemical Physics*, Vol. 82, No. 3, pp. 1599-1605, 1985.

98. Moro, G. J., "About the Coupling between Librational Motions and Conformational Transitions in Chain Molecules," *Chemical Physics Letters*, Vol. 173, No. 5,6, pp. 503-509, 1990.

99. Helfand, E., Z. R. Wasserman, and T. A. Weber, "The Kinetics of Conformational Transitions: Effect of Variation of Bond Angle Bending and Bond Stretching Force Constants," *Journal of Chemical Physics*, Vol. 75, No. 9, pp. 4441-4445, 1981.

100. Aue, W. P., E. Bartholdi, and R. R. Ernst, "Two-Dimensional Spectroscopy.

Application to Nuclear Magnetic Resonance," *Journal of Chemical Physics*, Vol. 64, No. 5, pp. 2229-2246, 1976.

101. Wefing, S., and H. W. Spiess, "Two-Dimensional Exchange NMR of Powder Samples. I. Two-Time Distribution Functions," *Journal of Chemical Physics*, Vol. 89, No. 3. pp. 1219-1233, 1988.

102. Wefing, S., S. Kaufmann, and H. W. Spiess, "Two-Dimensional Exchange NMR of Powder Samples. II. The Dynamic Evolution of Two-Time Distribution Functions," *Journal of Chemical Physics*, Vol. 89, No. 3, pp. 1234-1244, 1988.

103. Blumich, B., and H. W. Spiess, "Two-Dimensional Solid-State NMR Spectroscopy: New Possibilities for the Investigation of the Structure and Dynamics of Solid Polymers," *Angewandte Chemie, International Edition in English*, Vol. 27, pp. 1655-1672, 1988.

104. Ryckaert, J.-P., and A. Bellemans, "Molecular Dynamics of *n*-Butane near Its Boiling Point," *Chemical Physics Letters*, Vol. 30, No. 1, pp. 123-125, 1975.